UNIVERSITY of the
WESTERN CAPE

GEOCHEMICAL CONTROLS OF PLATINUM-GROUP ELEMENTS DISTRIBUTION PATTERNS IN THE PLATREEF, BUSHVELD COMPLEX, SOUTH AFRICA: A CASE STUDY AT ZWARTFONTEIN FARM, AKANANI PROSPECT AREA.

A thesis

Submitted to the Faculty of Science at University of the Western Cape

By

Ratshalingwa Patience Mudanalwo

In partial fulfilment of the requirements for a Master's degree in Applied Geology

Supervisor: Prof. C. Okujeni

Co-supervisor: Dr. A-M. Siad

Declaration

I declare that "Geochemical control of platinum group elements distribution patterns in the Platreef, Bushveld Complex, South Africa: a case study at Zwartfontein farm, Akanani prospect area" is my own work, that it has not been submitted before for any degree or examination in any other University, and that all the sources I have used or quoted have been indicated and acknowledge ed by means of complete references.

Ratshalingwa Patience Mudanalwo

_____

Signature

Abstract

The Platreef, is a contact-type pyroxenitic reef in the Northern Limb of the Bushveld Complex, enriched in platinum group elements (PGE) and base metal sulfides (BMS). Relatively subdued mining in the Platreef, compared to RLS, has been attributed to limited knowledge regarding irregular distribution, complex style and genesis of PGE mineralisation in the Platreef. This study was, therefore, aimed at investigating the petrogenesis of the Platreef, particularly to evaluate whether the formation of the ore reefs resulted from a single or multiple sill-like magma intrusions. The study also sought to unveil the interplay of fractional crystallisation, hydrothermal fluid activities, floor rock and crustal contamination on the formation of Platreef types, PGE mineralisation and the magma source. The study used petrography, geochemistry and core logging of borehole ZF044, ZF048 and ZF057 from Zwartfontein farm within Akanani Prospect area, in order to understand lithology and mineralogical variations with stratigraphy. A combination of Sr-Nd isotope data and whole-rock major and trace elements data were used to decipher the timing and source of magma emplacement.

Petrography and core logging revealed a series of rock layers that comprise of sill-like feldspathic pyroxenites, orthopyroxenites and harzburgite interlayered with norites and metasomatic rocks such as parapyroxenites and serpentinite. The feldspathic pyroxenites were further classified into feldspathic pyroxenite I (FP I), feldspathic pyroxenite II (FP II) and feldspathic pyroxenite III (FP III) based on mineralogical, textural and geochemical variations. The mineralised FP I and FP II sills contain high BMS and PGE compared to barren FP III sills. Geochemically, the feldspathic pyroxenites are characterized by high MgO, Fe_2O_3 and low CaO, Al_2O_3, in contrast to norites, with high CaO, Al_2O_3, SiO_2 and low MgO and Fe_2O_3. Whereas metasomatic rocks are characterized by high MgO and LOI with low SiO_2 snd Al_2O_3. The overall major elements and trace elements distributions patterns in the Platreef rocks suggest a normal fractionation trend.

The spider diagrams have shown high LREE fractionation and low HREE fractionation in Platreef rocks to indicate crustal contamination signature. FP III, pyroxenites and norite located in the upper Platreef contain higher $(La/Lu)_N$ and $(Eu/Eu^*)_N$ ratios in consonance with higher degree of fractionation and high feldspar content compared to rocks in the lower Platreef. Whole-rock major and trace elements plots show Mg# reversals and compositional breaks between the Platreef rocks which indicate multiple sill-like intrusions. The effects of hydrothermal fluids within Platreef zone, evidenced by vast occurrence of quartz, sericite,

serpentine and the high LOI, have variably redistributed PGE and BMS mineralisation. These effects are clearly noted in borehole ZF044 and ZF057 underlain by dolomite compared to borehole ZF048, underlain by Archean granite gneiss.

Rb-Sr isotopic data for the Platreef rocks constrained a crystallization age of 1.5 Ga, which is much less than previously suggested 2.06 Ga. In contrast, consistent results by Sm-Nd isotopic data have yielded a crystallization age of 2.05 Ga. The high susceptibility of Rb-Sr to metamorphic-hydrothermal alteration relative to Sm-Nd may explain the inconsistency in ages. The Platreef rocks at Zwartfontein are characterized by variably high initial $^{87}Sr/^{86}Sr$ ranging from 0.701017 to 0.714398 and moderately low initial $^{143}Nd/^{144}Nd$ ranging from 0.509096 to 0.509907 suggesting contamination by felsic melt derived from footwall rocks. The variations in $(^{87}Sr/^{86}Sr)_i$ and $(^{143}Nd/^{144}Nd)_i$ suggested replenishment of magma indicated by contrasting isotope signatures. High measured $(^{87}Sr/^{86}Sr)_m$ ranging from 0.709929 to 0.881729 and negative εNd (-1.23 to -17.14) indicate high post-crystallization contamination of the Platreef rocks by crustal material. Based on the initial $^{87}Sr/^{86}Sr$, $^{143}Nd/^{144}Nd$, εNd, steep REE patterns and high Mg# values the Platreef was formed from primitive mantle magma with high contribution of crustal materials.

In conclusion, the formation of the Platreef resulted from multiple sill-like intrusions of magma in an open system rather than single intrusion of magma with homogeneous Sr isotope. The redistribution of PGE and BMS mineralisation was predominantly controlled by sulfides related to hydrothermal fluids as a result of floor rock interaction.

Keywords: Platreef, PGE-BMS mineralisation, Petrogenesis, Sr-Nd isotope geochemistry, Multiple-staged magma, Crustal contamination.

Acknowledgement

I would like to give special thanks to my supervisor Prof. C. Okujeni and co-supervisor Dr A-M. Siad for squeezing out time and energy to ensure that this work is done correctly despite the unlimited challenges that arose during this study. To Senzangakhona Ndumo and Dr. James Tshipeng, thanks for your endless support, advice, patience and encouraging me from the begging of this research. I would also like to thank my parents for their continued love and support throughout my lifetime of education, as well as my brothers for helping me keep things in perspective. I further extend my gratitude to my life partner Awelani Mphephu for his love, support and caring during this study.

I acknowledge the Council for Geoscience (CGS) and National Research Funding (NRF) for funding this research. I also acknowledge University of Cape Town and CGS for XRF and ICP-MS analysis.

Above all, I would also like to give thanks to the almighty God who gave me strength, knowledge and wisdom to complete this project. "Trust in the Lord with all your heart and do not depend on your own understanding; seek his will in all you do and he will show you which paths to take." Proverbs: 3: 5-6.

Abbreviations and Acronyms

PGE	Platinum group elements
BMS	Base metal sulfides
RLS	Rustenburg layered suites
MZ	Marginal Zone
LZ	Lower Zone
CZ	Critical Zone
MZ	Main Zone
UP	Upper Zone
FP I	Feldspathic pyroxenite I
FP II	Feldspathic pyroxenite II
FP III	Feldspathic pyroxenite III
REE	Rare earths elements
LREE	Light rare earths elements
HREE	Heavy rare earths elements
LFSE	Low field strength elements
HFSE	High field strength elements
LILE	Large ion lithophile elements
Pd	Palladium
Pt	Platinum
ppm	Parts per million
Wt. %	Weight percentage
Nd	Neodymium
Sr	Strontium

Dedication

This work is dedicated

To

My Late father Tshililo Simon Ratshalingwa

And

My mother Tshimangadzo Jane Ratshalingwa

TABLE OF CONTENT

LIST OF FIGURES

LIST OF TABLES

LIST OF PLATES

CHAPTER ONE

1. INTRODUCTION

1.1. Background

The Bushveld Igneous Complex (BIC) is known as the largest layered intrusion in the world with a total extent of approximately 65 000 km^2. The emplacement of the BIC is dated at 2.06 Ga (Eales et al., 1993). The intrusion covers an area of about 400 km East-West and 300 km North-South and it comprises three major limbs namely; the Northern Limb, Eastern Limb and Western Limb (Kinnard et al., 2005). The Northern Limb of the Bushveld Complex with a total extent of 110 km and a width of 15 km is bounded by the Melinda Fault in the north and by Zebediela Fault in the south (Armitage et al., 2002). The Northern Limb hosts a contact-type PGE mineralisation known as the Platreef, which contains high-grade Cu, Ni and PGE mineralisation. The Northern Limb also hosts the Main Zone PGE mineralisation, which are mostly concentrated within leucogabronorite and gabronorite (Kinnard et al., 2005). The Platreef is underlain by rocks of the Transvaal Supergroup in the south and Archean granites in the north (Holwell and McDonald, 2007).

According to Mungall and Naldrett (2008) sulfide immiscibility which occurs when the magma becomes S-saturated is responsible for PGE mineralisation. The factors that contribute towards the formation of immiscible sulfides have been widely studied. Crustal sulfur assimilation is often thought to initiate sulfide immiscibility. In addition, fractional crystallization of oxides and silicate cumulates, the increase in oxygen fugacity and mixing of compositionally variable S-undersaturated magmas are also known to trigger S-saturation in the magma. Ihlenfeld and keays (2011) suggested two stages of crustal contamination that played a role in PGE mineralisation in the Platreef: (1) crustal contamination prior to emplacement and (2) crustal contamination due to interaction between the Platreef magma and the footwall rocks.

However, recent studies argued that the formation of PGE mineralisation in the Platreef was not dominantly controlled by assimilation of footwall rocks. In contrast, high-grade mineralisation in the Platreef, which is underlain by dolomite rocks (Sandsloot), was suggested by Pronost et al. (2008) to be influenced by assimilation of dolomite rocks. However, the exact link between PGE mineralisation and dolomite rocks is not well understood. Several studies have been conducted in the Platreef to ascertain the model which explains the formation of the PGE mineralisation in the Platreef (Barton et al., 1986; Harris and Chaumba, 2001; Kruger, 2005; Holwell and McDonald, 2007; Pronost et al., 2008). However, the genesis of PGE

mineralisation in the Platreef remains controversial including the nature of emplacement and geochemical controls of PGE mineralisation (e.g. Kruger, 1994).

In terms of the nature of emplacement/sequence of intrusion, most authors (Cox et al., 1993; Kruger, 1994 and Marsh, 2006) have suggested that the Platreef was formed from multiple sill-like intrusion of magma with distinct compositions rather than single magma influx. The present study aims at improving the understanding of the genesis of the Platreef particularly to investigate whether the Platreef was emplaced as multiple sill-like intrusion or single magma influx.

Zwartfontein marks the change in the footwall rocks from dolomite to Archean granite. Therefore, the change in footwall lithology from Transvaal Supergroup to Archean gneisses does provide a good location to study contamination by local footwall rocks and its effect on the genesis of Platreef type PGE mineralisation. This, evidently, may contribute towards the understanding of the geochemical controls and spatial distribution pattern of PGE mineralisation in relation to the stratigraphic framework of the Platreef and underlying footwall rocks.

1.2. Previous work

Introduction

This section describes the previous work that has been done in the Platreef regarding the genesis of the Platreef type PGE mineralisation. This includes a review of the origin of the Platreef in relation to other parts of the Bushveld Complex, specifically the Merensky reef, Critical Zone and the Main Zone and further assesses the nature of emplacement of the Platreef. This section also addresses the effect of crustal and local footwall rock contamination in the genesis of PGE mineralisation in the Platreef. This section is outlined as follows:

- The origin of the Platreef in relation to other parts of the Bushveld Complex and the nature of its emplacement.
- Formation of PGE-Ni-Cu deposits in the Platreef.
- The formation of PGE mineralisation in the Platreef and the influence of crustal/footwall rocks assimilation processes.

1.2.1. The origin of the Platreef in relation to other parts of the Bushveld Complex and the nature of its emplacement.

Several authors have investigated the nature of emplacement of the Platreef and its relationship to other parts of the Bushveld Complex (Wagner, 1929; Kruger, 2005; Kinnard, 2005; Manyeruke et al., 2005; McDonald et al., 2005; Holwell et al., 2007; Pronost et al., 2008). Wagner (1929) proposed the Platreef as the equivalent to the Merensky Reef. Furthermore, based on the similarity in the initial Sr- and Nd- isotope composition between the Platreef, hanging wall norite and the Merensky Reef, Pronost et al., (2008) argued that the Platreef share a common origin with the Merensky Reef. However, in terms of the differences in the stratigraphy and sulfides content between the Platreef and the Merensky reef, the question remains as to whether the Platreef and the Merensky reef share a common origin. In terms of PGE mineralisation, Smith et al. (2013) explained that sulphide saturation in the Platreef occurred in the staging chamber prior to the emplacement, whereas in the Merensky reef sulfides saturation occurred during its emplacement. On the other hand, McDonald et al., (2005) noted that the Platreef represent a unique event in the Northern Limb.

Other authors (e.g. Kruger, 2005) have suggested that the Platreef was formed from the Main Zone type magma. Kruger (2005) considered the intrusion of Main Zone type magma as resulting from the assimilation of Lower Zone rocks and chromitites, which later crystallize to form the Platreef. Contrastingly, Gain and Mostert (1982) reported the compositional differences in pyroxenes between the Platreef and the hanging wall as evidence that the hanging wall was formed from a separate magma. The study of the development of the Platreef and the overlaying Main Zone layer by Holwell et al. (2007) reflect a time break between the intrusion of Platreef and the Main Zone. This view was corroborated by Kinnard (2005) in alluding to the occurrence of the Platreef pyroxenites xenoliths in the Main Zone.

The Platreef is composed of different lithologies such as pyroxenite, feldspathic pyroxenite, harzburgite, dunite, peridotite and norite (Kinnaird et al., 2005) which cannot be correlated along the strike; same applies to the nature of the mineralisation in these rock units, in particular, the pyroxenites. This has been interpreted as caused by significant contamination from various footwall rocks, infiltration of felsic melts and multiple sill-like intrusion of the Platreef. Several researchers (Cox et al., 1993; Kruger, 1994; Hutchison and Kinnard, 2005; Manyuruke, 2005; Marsh, 2006; Mitchell and Scoon, 2012; Mandende, 2014; Mangwegape et al., 2016) have debated on the intrusion of the Platreef as multiple sill-like intrusion or single magma intrusion. Kruger (1994) suggested that the Rustenburg Layered Suites (RLS) was

formed from multiple magma pulses based on the variations in Sr-Nd isotope data. The variations in $(^{87}Sr/^{86}Sr)_i$ and $(^{143}Nd/^{144}Nd)_i$ isotope with the stratigraphic height from Lower Zone to Upper Zone enabled Kruger (1994) to subdivide the RLS into an integration stage and a differentiation stage. The integration stage is associated with multiple sill-like intrusion of magma with contrasting composition occurring from the Lower Zone to the lower Main Zone. On the other hand, differentiation stage is associated with single magma intrusion or intrusions of magmas with similar compositions occurring from the lower Main Zone to the Upper Zone.

The compositional variations in the Platreef have led most authors to suggest the formation of the Platreef through integration stage rather than differentiation stage. Kinnard (2005), explained the formation of the Platreef as a result of multiphase emplacement reflected by succession of pyroxenite sills separated from each other by interlayers of serpentinite, clinopyroxenite or pegmatitic norite. Manyeruke et al. (2005) further considered the three geochemically distinct pyroxenites at Townlands to represent separate sill-like intrusions. Marsh (2006) also argued against the formation of the Platreef from single magma pulse by proposing that the stratigraphic variations in the Platreef sills have resulted from multiphase pulses of magma. Mandende (2014) noted the decrease in Fe_2O_3, increase in Mg# and Cr_2O_3 with the stratigraphic height and associated this with the multiple magma influx.

1.2.2. Formation of PGE-Ni-Cu deposits in the Platreef

The formation of platinum group elements has been widely studied by several authors who came up with various propositions (e.g. Pronost et al., 2008; Mitchell and Scoon, 2012; Keays and Lightfoot, 2010). It is widely accepted that the formation of PGE mineralisation are associated with Ni-Cu sulfides or chromite. Chromite veins are not well developed in the Platreef and occur disseminated (Yudovskaya and Kinnaird, 2010). Therefore, mineralisation in the Platreef is mostly associated with Ni-Cu sulfides contrasting the prevalent association of chromitite layers to PGE mineralisation for the Merensky and UG2 reefs reported by Cawthorn (2010). In order for certain magma to form PGE mineralisation it first has to precipitate immiscible sulfides liquid (Keays and Lightfoot, 2012). The immiscible sulfides liquid may form when the magma becomes S-saturated as a result of fractional crystallisation of silicate minerals or crustal/footwall assimilation or both (Ihlenfeld and Keays, 2011). Sulfur saturation may also be triggered by the addition of silica through assimilation of felsic country rocks,

which lowers the sulfur solubility of the magma (Irvine, 1975; Li and Naldrett, 1993). However, it is widely accepted that crustal contamination of mantle-derived magmas is the significant influence in the formation of magmatic Ni-Cu-PGE deposits (Lesher and Keays, 2002; Lightfoot and Keays, 2005; Wilson and Chunnett, 2006).

There are several suggestions regarding the formation of PGE mineralisation in the Platreef, as to whether the Platreef magma derived its sulfur from crustal contamination before emplacement or the magma became sulfur saturated as a result of local footwall rocks assimilation. Some of the suggestions regarding the formation of PGE mineralisation are summarized below.

1.2.3. The formation of PGE mineralisation in the Platreef and the influence of crustal/footwall rocks assimilation process.

The sulfur and strontium isotopes have been previously used as tracers to determine the extent of interaction between the Platreef magma and the footwall rocks and their influence in the precipitation of sulfides. According to Mungall and Naldrett (2008), immiscible sulfide liquids are a critical component of the standard model for the formation of magmatic base metal sulfides (BMS) and platinum group elements (PGE) deposits. Crustal sulfur assimilation is often thought to initiate the ore-forming process by producing immiscible sulfides melt that can collect base metal sulfides and PGEs (Mungall and Naldrett, 2008). Mass-independent fractionation of sulfur isotopes is a chemically conservative tracer that indicates the involvement of crustal sulfur in marginal Ni-Cu-(PGE) deposits. Sharman-Harris et al. (2005) used mass-independent fractionation of sulfur isotope to evaluate sulfur budget in the Platreef. He postulated that sulfur in the Platreef is not purely of magmatic origin, but assimilation of crustal rocks also added sulfur to the Platreef magma.

Furthermore, Penniston et al. (2010) also used mass-independent sulfur isotope to test the hypothesis that the Platreef owes its sulfides to the underlying footwall rocks. In their study they found that Platreef rocks that are in contact with the footwall rocks have elevated mass-independent sulfur isotope ($\Delta^{33}S = 0.55‰$) which correspond to that of the underlying footwall rocks. Based on these results it was concluded that there was an addition of sulfur from the footwall rocks through advective-diffusion exchange of sulfur during the interaction between the Platreef magma and the footwall rocks. However, their final suggestion was that the

addition of sulfur from local footwall rocks has occurred but cannot be regarded as the primary trigger for PGE mineralisation in the Platreef.

Sulfur isotopes have been used by several authors (Manyeruke et al., 2005; Holwell et al., 2007; Penniston-Dorland et al., 2008; Ihlenfeld and Keays, 2011) to investigate the source of sulfur in the Platreef. On the bases of high ^{34}S values in the Platreef, Holwell et al. (2007) suggested that the enrichment of sulfur in the Platreef resulted from the interaction between the Platreef magma and local footwall rocks. In contrast, $\Delta^{33}S$ measurements from Sandloot and Tweenfontein mineralisation reveal that S in the Platreef is of magmatic origin (Ihlenfeld and Keays, 2011). Ihlenfeld and Keays (2011) further suggested two stages of crustal contamination in the Platreef: (1) crustal contamination before emplacement and (2) crustal contamination due to interaction between the Platreef magma and the local footwall rocks.

The first contamination event occurred before the emplacement of the Platreef magma, and it is thought to be responsible for the formation of PGE-rich sulfides through assimilation of crustal S. This is evidently supported by the inverse relationship between S/Se and PGE tenors. The second contamination event occurred as a result of interaction between the Platreef magma and the footwall rocks resulting in the dilution of metal tenors in the sulfides. Therefore, it was concluded that second contamination event by local footwall rocks cannot be considered as a significant trigger for PGE mineralisation in the Platreef (Ihlenfeld and Keays, 2011). This was further supported by uncontaminated magmatic isotope signature (^{34}S=0-2%) in the Platreef which indicate limited interaction with sedimentary sulfur during the emplacement. These results are consistent with the results reported by Penniston et al. (2010).

The study of mechanisms determining the distribution of PGE and base metal conducted by Holwell and McDonald (2006) emphasises the importance of floor rocks on the distribution of PGE. Holwell and McDonald (2006) suggested that areas underlain by Transvaal Supergroup sediments are highly controlled by fluid activities such as assimilation, metasomatic and transportation of PGE by hydrothermal fluid. However, in areas where the footwall rocks are Archean granite gneisses such as Overysel the distribution of PGE is controlled by the behaviour of sulphide liquid due to lack of fluid activities. McCutcheon (2012) conducted a study on platinum group minerals (PGM) assemblages at Tweenfontein farm and suggested that the assimilation of Duitschland footwall rocks by Platreef magma has played an important role in the formation of variable but predominantly bottom-loaded PGE mineralisation at Tweenfontein Hill.

Strontium (Sr) and neodymium (Nd) isotopes were previously used in the Platreef as tracers to determine the effect of local footwall contamination in the formation of Platreef-type PGE mineralisation (Barton et al., 1986). According to Kruger (1994), a primitive mantle magma that has not encountered crustal contamination is expected to have $(^{87}Sr/^{86}Sr)_i$ of approximately < 0.0704 and any deviation from this is associated with crustal contamination. Barton et al. (1986) conducted a study at Overysel using strontium (Sr) isotopes in order to quantify the extent of interaction between the footwall rocks and the Platreef magma. He noted that the Rb and Sr isotopes vary depending on the underlying footwall rocks. Barton et al., (1986) noted the occurrence of high initial $^{87}Sr/^{86}Sr$ isotopes (0.7107 – 0.7226) in areas where the footwall is granite (Overysel) compared to areas where the footwall is dolomite (Sandsloot). High $^{87}Sr/^{86}Sr$ isotopes in Overysel is in consonance with heterogeneous contamination by felsic melt derived from granite rocks.

1.3. Problem statement

The understanding of the genesis of PGE mineralisation is vital in mining and exploration. The mining industry requires information about the genesis of the PGE and host rocks, geological controls of mineralisation, geochemistry and spatial (vertical and lateral) distribution of mineralisation. Limited mining activities in the Northern Limb compared to the Western and Eastern Limbs is underpinned by the paucity of knowledge about the genesis and distribution of PGE mineralisation. PGE mineralisation in the Platreef is commonly hosted in feldspathic pyroxenite, pyroxenite, harzburgite and in places these mineralisation are also hosted in metasomatic rocks especially serpentinite and parapyroxenite. However, the stratigraphic positions of these rocks and the distribution of PGE mineralisation is complex and it is difficult to correlate them even on a local scale. The complexity of the Platreef owes its nature to morphology, variations in the footwall lithology, nature of emplacement and post-magmatic processes. Therefore, this makes it difficult to understand the style of PGE mineralisation, the spatial distribution of PGE mineralisation and to locate economically minable ore zones.

The extent of footwall/crustal contamination and the effect of fluid-rock interaction is poorly understood in the Platreef. Holwell and McDonald (2006) suggested that the distribution of PGE mineralisation within the Platreef pyroxenites are bottom and top-loaded and controlled by the nature of the footwall rocks. These authors observed that in areas where the footwall is

dolomite (e.g. Sandsloot) PGE mineralisation is controlled by base metal sulfides (BMS) and hydrothermal activities relative to areas where the footwall is granite (Turfspriut). Pronost et al. (2008) have demonstrated some effects of crustal contamination and fluid-rock interaction in the style of PGE mineralisation at Sandsloot.

The nature of emplacement and sequence of intrusive events in the Platreef remains controversial. Previously, there was a debate that the Platreef shares the same origin with the Main Zone. Kruger (2005) suggested that the Platreef was formed from the crystallization of the Main Zone magma that has assimilated some Lower Zone rocks and chromitites. In contrast, Holwell and Jodarn (2006) noted that rocks that form the hanging wall to the Platreef rocks at Zwartfontein farm postdate the cooling and deformation of the Platreef rocks. Furthermore, Holwell et al. (2007) suggested that there was a time break between the intrusion of the Platreef and the Main Zone as evidenced by discontinuity in textural, mineralogical and chemical compositions. There are also contradicting ideas regarding the emplacement of the Platreef as single magma intrusion or multiple magma intrusion. Manyeruke et al. (2005) and Kinnard et al. (2005) suggested that the Platreef intruded as multiple sill-like intrusions. Penniston et al. (2008) reported that the multiple magma pulses and variable degree of magmatic differentiation had played a role in the concentration of PGE in the Platreef.

The current study aims at improving the knowledge about the genesis of PGE mineralisation focusing on the nature of emplacement. The focus will be on two significant problems formulated as follows:

(1) The nature of emplacement as to whether the Platreef was formed as (a) multiple sill-like intrusion or (b) single body magma intrusion. If the former is true as suggested by most authors (e.g. Manyeruke et al., (2005) and Kinnard et al., (2005)), then the influence of multiple sill-like intrusion of the magma pulses on the nature and style of PGE mineralisation will be addressed.

(2) The extent and effect of crustal/footwall contamination and post-magmatic hydrothermal activities in the distribution of PGE mineralisation in the Platreef at Zwartfontein, Akanani Prospect area.

1.4. Aims and objectives

This study is aimed at improving the understanding of the genesis of the Platreef mainly to evaluate the formation of the Platreef, whether from multiple sill-like intrusion or single magma intrusion. The study could contribute towards understanding the geochemical controls and the effect of crustal contamination in the formation of PGE mineralisation in the Platreef.

- The first objective is to understand the types of Platreef lithology and their position in the stratigraphic height, including their relationship to PGE-BMS mineralisation. This objective will be achieved through detail modal analysis using petrography in order to ascertain the vertical and lateral distribution of primary minerals, texture as well as secondary alteration minerals that distinguish different types of pyroxenites in the Platreef.

- Geochemical classification and characterisation of the Platreef rocks using whole-rock major element chemistry to confirm and validate the results from petrography and identify the geochemical signatures of Platreef lithologies. This will be achieved through classifying major elements contents in Platreef lithologies using hierarchical cluster analysis (HCA) to identify the oxides elements controlling the lithologies with the aid of box and whisker plots. Further geochemical characterisation of Platreef rocks using scatter plots and spider diagrams will enable an understanding of major and trace elements fractionation between the Platreef lithologies.

- Identify the extent and nature of footwall/crustal contamination and their effect on both Platreef lithology and PGE mineralisation. A three-step approach will be adopted, firstly; identify the presence of minerals associated with felsic melts through petrography. Secondly, chondrite-normalised rare earth elements patterns to identify elemental fractionation between the Platreef rocks. Lastly, understand the extent of crustal contamination in the Platreef rocks using initial $(^{87}Sr/^{86}Sr)_i$, $(^{143}Nd/^{144}Nd)_i$ and εNd trends.

- Evaluate the effect of hydrothermal fluids activities in the Platreef rocks and their role in the distribution of PGE-BMS mineralisation in the Platreef. The approach is to evaluate the elemental exchange between the Platreef and footwall rocks.

Chemostratigraphic plots of BMS and PGE will aid in assessing the contribution of hydrothermal fluids in the decoupling of BMS from PGE mineralisation.

- Investigate the genesis of the Platreef, particularly the magma source and nature of emplacement in order to identify whether the Platreef formation relates to multiple sill-like intrusions and several magma influxes. Compositional changes in the Platreef rock sequence will be identified through evaluating the variation in major elements and initial $(^{87}Sr/^{86}Sr)_i$ and $(^{143}Nd/^{144}Nd)_i$ patterns with the stratigraphic height.

1.5. Study area

Samples were collected from three drillcores (ZF044, ZF048 and ZF057) across the Platreef at Zwartfontein farm within Akanani Prospect area. The footwall rocks in the Platreef varies along the strike from north to south with borehole ZF048 underlain by granite and borehole ZF044 and ZF057 underlain by dolomite. The succeeding chapters present a detailed description of the Platreef lithologies and the underlying footwall rocks.

CHAPTER TWO

2. GEOLOGY

2.1. Regional geology of the Bushveld Complex

The Bushveld Complex intruded into the Kaapvaal Craton at 2.06 Ga (Walvaren et al., 1990) and is located on the northern part of South Africa hosting over half of the world's platinum, chromium, vanadium, etc. reserves (Cawthorn et al., 2002). The Bushveld Complex comprises the intrusive Rustenburg Layered Suite (RLS), Rashoop Granophyre Suite, and Lebowa Granite Suite and extrusive Rooiberg Group. The Bushveld Complex comprises three major limbs known as the Northern Limb, Eastern Limb and the Western Limb (Figure 2.1). The current study focuses on the Rustenburg Layered Suite (RLS), which host a variety of economic mineralised reefs including the Merensky reef, UG-2 chromitite layers and the Platreef.

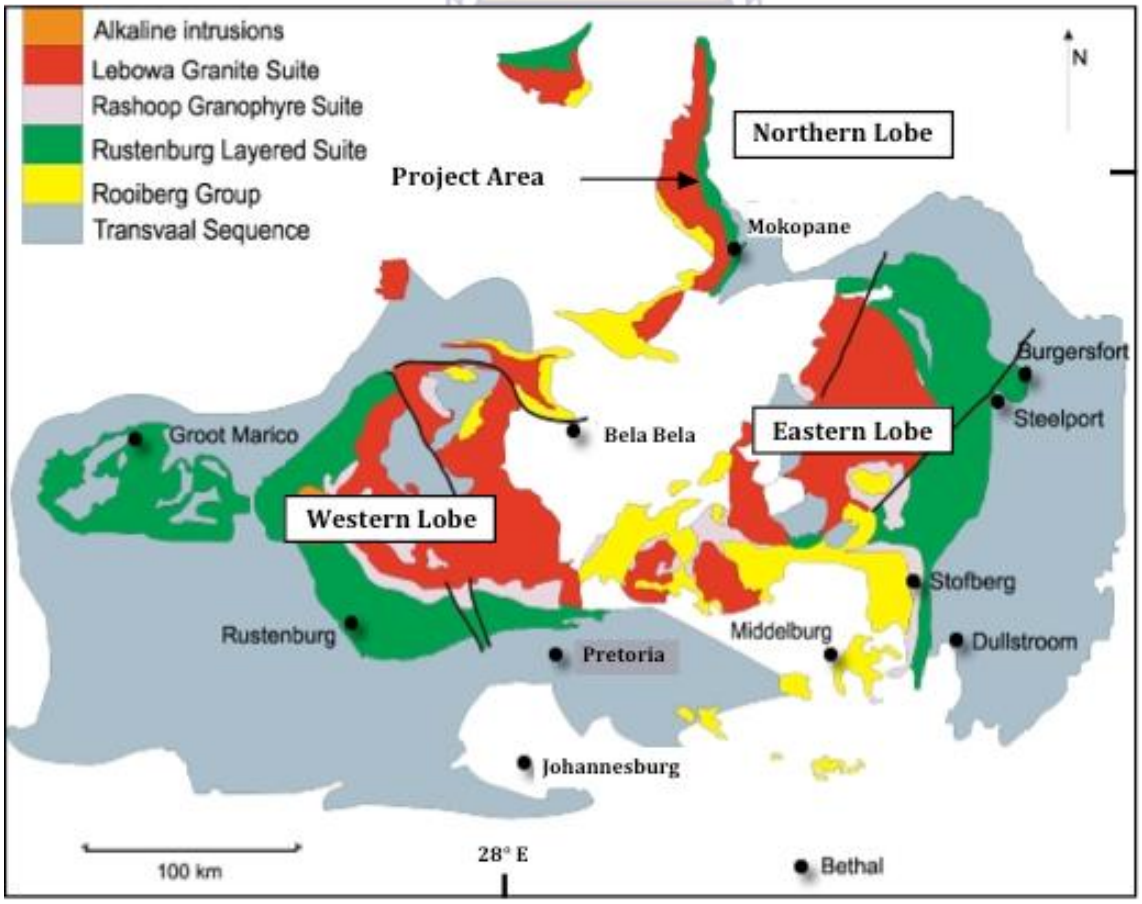

Figure 2.1: Simplified geological map of the Bushveld Complex showing the location of the Northern, Eastern and Western Limbs (After Kinnaird et al., 2005).

The RLS which intruded into the Transvaal Supergroup rocks at 2054.4 ± 1.3 Ma has a thickness of 7-9 Km is divided into five major zones; Marginal Zone (MZ), Lower Zone (LZ),

Critical Zone (CZ), Main Zone (MZ) and Upper Zone (UZ) in an upwards succession (Figure 2.2) (McCandless and Ruiz, 1991). However, there is still much debate regarding the exact boundaries between these zones. The Critical Zone is subdivided into the Lower Critical Zone and the Upper Critical Zone. The Main Zone is subdivided into the lower Main Zone and the Upper Main Zone (Kinnard et al., 2005).

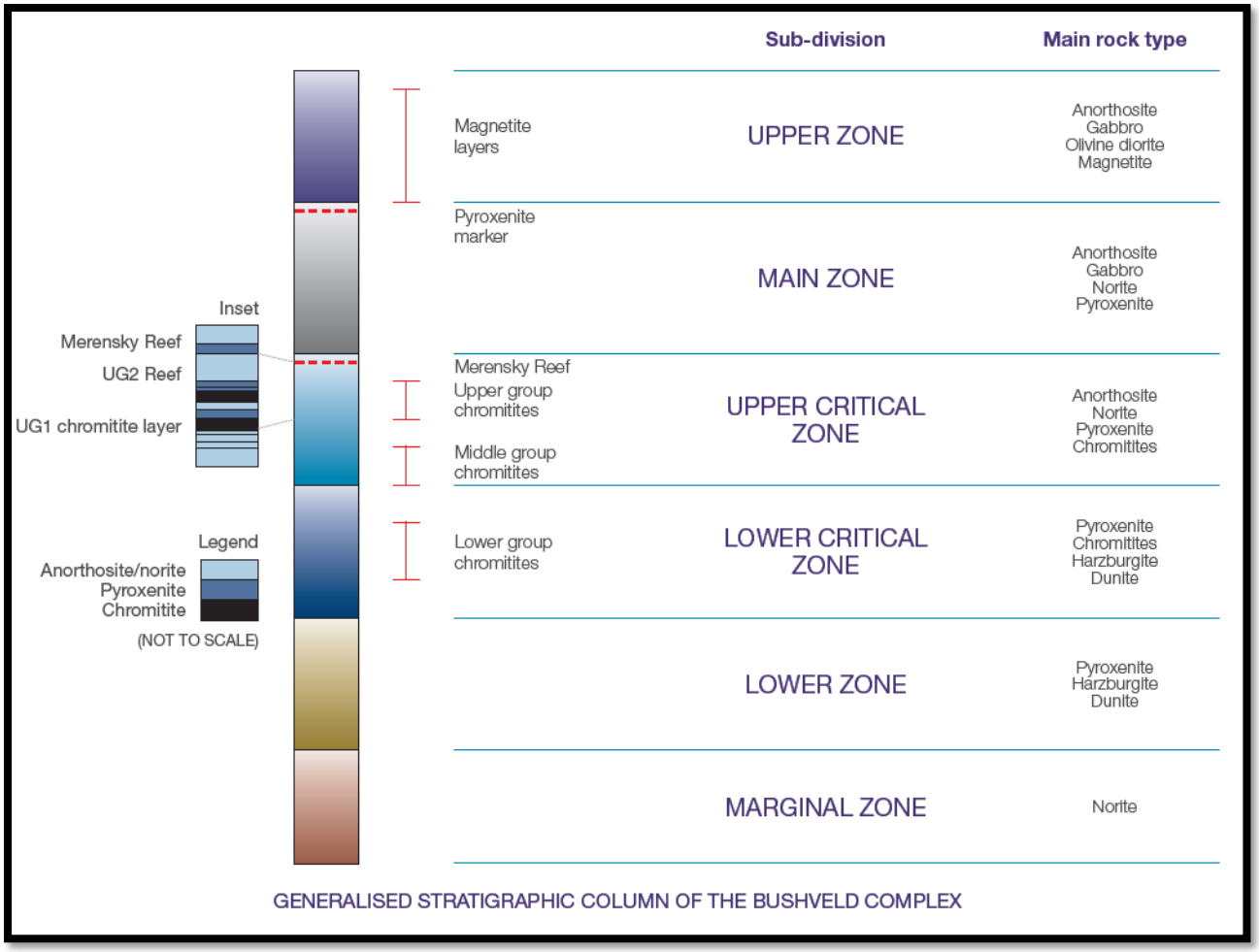

Figure 2. 2: Generalized stratigraphic column of the Rustenburg Layered Suite: Bushveld Complex (After Kinnaird et al., 2005).

2.2. Evolution of the Rustenburg Layered Suite (RLS)

The RLS according to Nell (1985) was formed by multiphase emplacement, which involves two stages; 1) the first event relates to the intrusion of the Lower Zone (LZ) magma and 2) the second event is underpinned by the intrusion of the Main Zone (MZ) and Upper Zone (MZ) magma. The LZ and the CZ formed from crystallization of olivine/orthopyroxene-rich magma with chromitite layers dominating the CZ (Cameron, 1978). The progressive mixing of the residual LZ magma and MZ magma resulted in the formation of feldspathic orthopyroxenite dominated Lower Critical Zone (C_LZ) and norite/anorthosite dominated Upper Critical Zone (C_UZ) (Kruger et al., 1990). After the deposition of the Merensky pegmatoids and pyroxenites, the MZ magma continued to flow into the chamber; resulting in the formation of the Lower Main Zone (LMZ) and the Upper Main Zone (UMZ) (Yudovskaya et al., 2011). The Upper Zone (UZ) crystallized from the largest influx of the Bushveld Complex initiated just below the Pyroxenite Marker (Armitage et al., 2005).

Marginal Zone (MaZ)

The MaZ with a thickness of approximately 800m marks the base of the Rustenburg Layered Suite of the Bushveld Complex. This zone is dominated by heterogeneous norite rocks (Barnes and Maier, 2002).

Lower Zone (LZ)

The LZ of the RLS is underlain by MaZ and overlain by Lower Critical Zone (C_LZ). This zone consists of pyroxenites and harzburgite (olivine-rich rocks) rocks. The LZ is lithologically subdivided into three subzones; the lower pyroxenites subzone, harzburgite subzone and upper pyroxenites subzone in an upwards succession (Cameron, 1978). The exact boundary between the LZ and the C_LZ is not well defined, and there are several views regarding this matter. Overall, the boundary between the LZ and the C_LZ, the position of the uppermost harzburgite is accepted as the most reliable boundary (Yudovskaya and Kinnard, 2010). The thickness of the LZ varies from one location to another and is defined by the topography of the floor rocks with maximum thickness occurring along the troughs (Mangwegape et al., 2016).

Critical Zone (CZ)

The CZ is up to 1500m thick and referred to as the most economic valuable zone which hosts major chromitite layers within the Merensky reef and the UG-2 chromitite layers (Kinnard et al., 2005). The CZ is lithologically subdivided into Lower Critical Zone (C_LZ) characterised by the dominance of pyroxenite and Upper Critical Zone (C_UZ) characterised by the dominance of norite and anorthosite (Kruger et al., 1990). The transition from the C_LZ to the C_UZ is marked by the occurrence of thin layer of anorthosite (Kinnard et al., 2005).

Main Zone (MZ)

The MZ is the thickest zone (~3940m) of the RLS dominated by gabbronorite. The MZ is further subdivided into the Lower Main Zone (LMZ) and the Upper Main Zone (UMZ) (Molyneaux, 1974). Mangwegape et al. (2016) proposed a model for the formation of the LMZ, as formed from the magma derived from the mantle that become contaminated by mixtures of upper and lower crustal mushes. In the northern limb the MZ overlies the Platreef whereby the boundary between the MZ and the Platreef is mostly marked by gabbronorite. The Main Zone contains a troctolite horizon.

Upper Zone (UZ)

The UZ is characterised by the dominant of magnetite layers and contains rocks such as anorthosite, leucogabbros and olivine diorite (Molyneaux, 1974). The UZ overlies the MZ, and the transition between the UZ and MZ is marked by the occurrence of magnetite cumulates (Kruger et al., 1990).

2.3. The Northern Limb

The northern limb of the Bushveld Complex with a total strike length of 110km and a width of 15km is marked by the Melinda Fault in the north and by Zebediela Fault in the south (Armitage et al., 2002). Based on modelling of gravity data, Van der Merwe (1976) estimated that the northern limb has a total areal extent of 7275 km^2. The northern limb shows a unique stratigraphy along the Thabazimbi Murchison Lineament (Kruger, 2005). However, the stratigraphy of the northern limb is subdivided into MaZ, LZ, CZ, MZ and UZ based on the lithological variation throughout the succession. The MaZ, LZ and the CZ are not always developed in the northern limb compared to the western and eastern limbs (Kinnard, 2005).

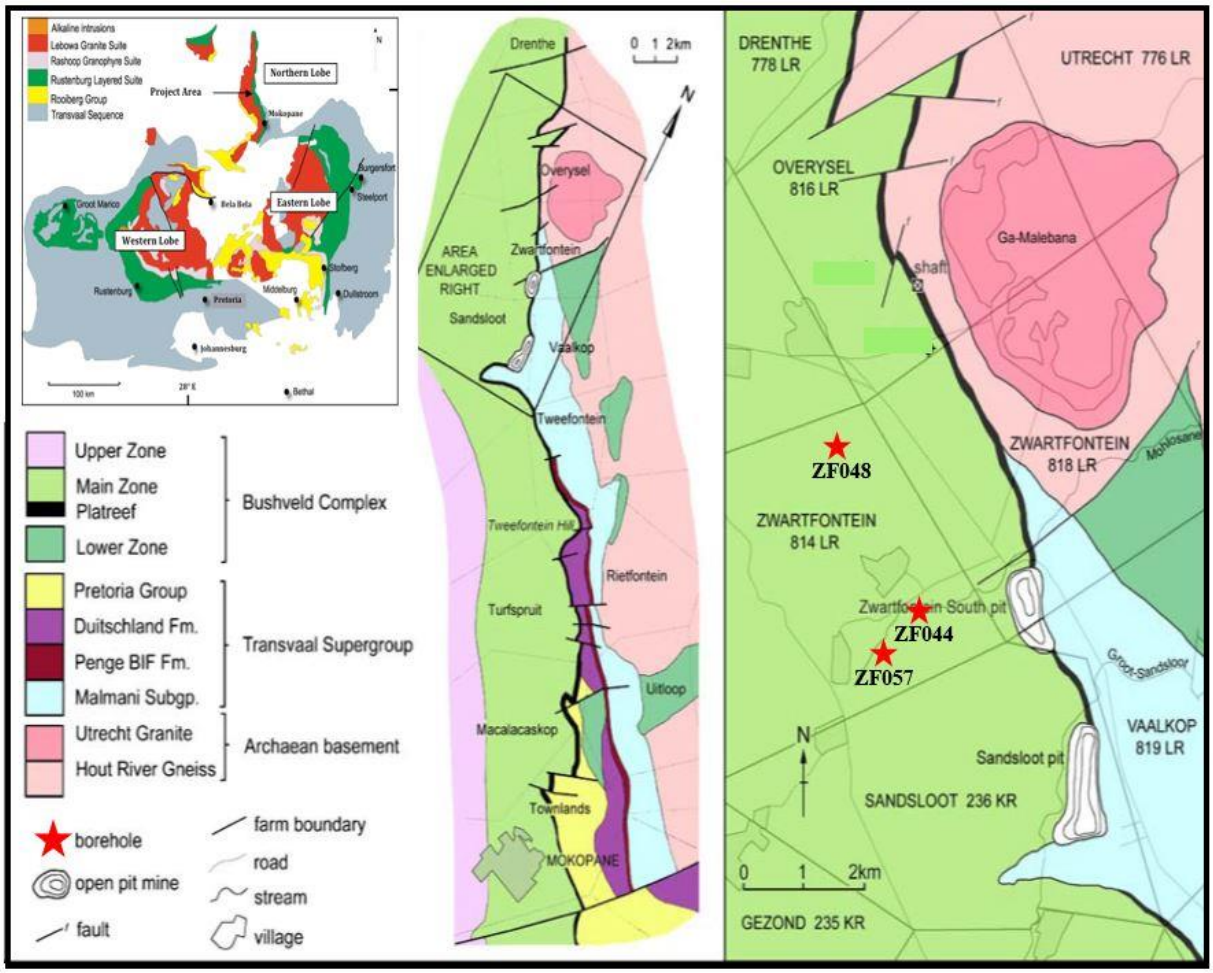

Figure 2.3: Geological map of the Platreef, showing a detailed map of the Zwartfontein area and the locality of borehole ZF044, ZF048 and ZF057 utilized in the current study. Modified after Holwell and McDonald (2006).

2.4. The Platreef

The Platreef is well known as the major host of Ni-Cu-(PGE) mineralisation in the Northern Limb, previously known as Potgietersrus limb (Van der Merwe, 1976). Several authors (e.g. McDonald et al., 2005; Manyeruke, 2005; Holwell and McDonald, 2007) have previously investigated the geology of the Platreef. However, there is still contradicting ideas regarding the origin of Ni-Cu-(PGE) mineralisation and the age of the Platreef. The Platreef is located at the base of the Northern Limb and it is underlain by Transvaal Supergroup and Archean granite rocks in the southern sector and northern sector respectively (McDonald et al., 2005) (Figure 2.3). The thickness of the Platreef reaches approximately 400 m in the southern sector and becomes thinner towards the northern sector where the thickness is approximately 250 m

(Winch, 2011). The variation in the thickness of the Platreef, according to Kinnaird et al. (2005) is defined by the irregular topography of the footwall and faulting which occurred before the intrusion of the Bushveld Complex. However, the origin of basement highs on the footwall lithology is not yet clear as to whether they were formed as a result of faulting, antiforms or diapiric domes (Kinnaird et al., 2005).

The lithologies of the Platreef are more heterogeneous than those of the Merensky reef on the Western and the Eastern Limbs (Armitage et al., 2002). The heterogeneity of the Platreef was due to the interaction between the footwall rocks and the Platreef magma (Armitage et al. 2002). According to Gain and Mostert (1982), this is evident by the presence of xenoliths from the footwall rocks of the Transvaal Supergroup and Archean Granite. The rock types in the Platreef are mafic to ultramafic and contain xenoliths, which are derived from the footwall rocks (Armitage et al., 2002). The rock types include variably layered sills of pyroxenite, feldspathic pyroxenite, norite and gabbro, whereby the pyroxenite is the dominant rock type in the Platreef (Kinnard et al., 2005). According to Kinnard et al. (2005) the occurrence of variable layers of sills indicate multiple influxes of magma. Kruger (2005) reported the occurrence of only two discontinuous chromitite horizon in the Platreef. Yudovskaya and Kinnaird (2010) noted that chromitite are not well developed in the Platreef and they occur erratically. A recent study by Mitchell and Scoon (2012) emphasized the occurrence and importance of harzburgite rock as part of the Platreef lithology. Besides the occurrence of primary magmatic rocks in the Platreef, most studies (Wagner, 1929; Holwell, 2006) have reported the presence of metasomatic rocks such parapyroxenite and serpentinite.

The Platreef is a magmatic Ni-Cu-(PGE) deposit and is subdivided into three layers; the lower, middle and the upper layer (Armitage et al., 2002). The source of sulfur (S) which triggered PGE mineralisation in the Platreef has been widely investigated and researchers came up with different suggestions. According to the study conducted by Tawanda et al, (2005) the PGE mineralisation in three layers of the Platreef was influenced by crustal contamination before the emplacement of Platreef magma which was revealed by the enrichment of heavy sulfur ($\delta^{34}S$ of 2.6 to 9.1 ‰). Mungall et al. (2005) suggested that the assimilation of sulfur from the footwall during the interaction between the Platreef magma and the footwall has triggered PGE mineralisation in the Platreef. However, Ihlefeld and Keays (2011) noted that the local contamination of Platreef magma was not a trigger for driving the Platreef magma to S-saturated and PGE mineralisation.

In contrast, Ihlefeld and Keays (2011) support that S-saturation in the Platreef magma was triggered by crustal contamination prior to the emplacement. Previous studies suggest that mineralisation in the Platreef was not formed as a result of one process, but due to interaction between different processes which include magmatic process, contamination of magma by footwall and hydrothermal activities (Buchanan et al., 1981; Armitage et al., 2002). The recent studies show that magmatic process and hydrothermal fluids played a vital role in the formation of Platreef type PGE mineralisation. The PGE mineralisation at Overysel was controlled by magmatic process with less contribution of assimilation and metamorphism (Pronost et al., 2008).

The Platreef shows high PGE mineralisation (4 g t^{-1}) in the central sector where the footwall is dolomitic (e.g. Sandsloot) (Holwell and McDonald, 2006). The PGE mineralisation in the Platreef is lower than the Merensky and the UG2 chromitite reefs which have an average grade of 4–6 g t^{-1} (Armitage et al., 2005).

CHAPTER THREE

3. METHODOLOGY

3.1. Introduction

This chapter presents the methods followed in order to achieve the aims and objectives of the current study. The methodology includes fieldwork, core logging, sample selection, sample preparation, petrography and geochemical analysis. Petrography involves preparation of thin section and analysing the thin section under the microscope. The geochemical analysis consists of bulk chemistry analysis by XRF and isotope geochemistry by ICP-MS. Bulk chemistry analysis involves major and trace elements data by XRF and semi-quantitative mineralogy by X-ray diffraction (XRD).

3.2. Fieldwork

Samples used in the present study were collected from Zwartfontein 814LR at Akanani Prospect area. Samples were taken from three boreholes namely; ZF044, ZF048 and ZF057 with the depths 1330 m, 1571 m and 1520 m respectively. The footwall to the Platreef in boreholes ZF044 and ZF057 is Malmani dolomite of Transvaal Supergroup, whereas in borehole ZF048 the reef is underlain by Archean granite rocks. The length of core samples varies between 20 and 30 cm.

3.3. Core logging

In the current study, core logging was carried out using eighty core samples collected from borehole ZF044, ZF048 and ZF057 in order to construct a detailed vertical lithology profile. The descriptions of lithology included mineralogy, texture, colour and grain size. The descriptions of lithology from core logging will be associated with petrographic studies in order ascertain to detail the understanding the stratigraphy of the study area and identify zones of high PGE-BMS mineralisation.

The core samples from selected intervals in borehole ZF044, ZF048 and ZF057 were analysed and described from the bottom upwards using the following procedure.

• Firstly, the location of the core, the core number and the drill-hole name were recorded to avoid confusion.

• Identify mineral abundance, the grain size in mm, grain shape and degree of mineral alteration.

• The presence of veins and fractures, including their abundance, width, mineral fillings or coatings and orientation were also recorded.

• The type and distribution of mineral alteration in altered rocks were recorded.

• The boundaries and geological contacts (i.e. sharp or gradational) of each core section were noted.

• Lithology in each interval was identified based on the mineralogy, grain size and texture.

• Rock names were assigned using IUGS classification in figure 3.1, based on essential primary minerals in mafic and ultramafic phaneritic igneous rocks.

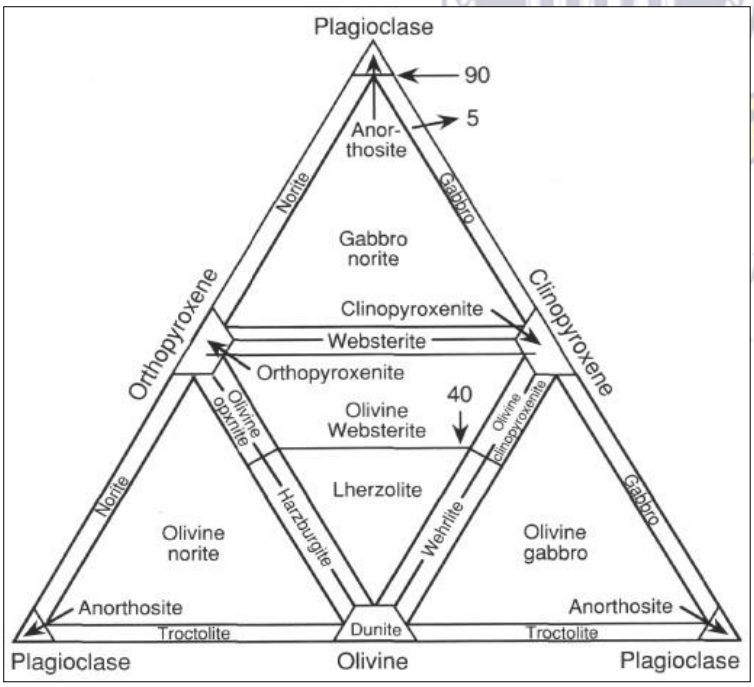

Figure 3.1: IUGS classification used for rock classification based on mineralogical composition.

3.4. Sample selection

Samples used in the current study were collected from Zwartfontein farm located in the central sector of the Northern Limb. Fifteen core samples were selected from each borehole (ZF044,

ZF048 and ZF057) to carry out the petrographic studies. Samples were selected based on the lithological changes and mineralisation occurrence along with the core. 3 cm of the selected core samples were cut for thin section preparation at University of the Western Cape laboratory. For geochemical and isotope analysis, 5 core samples of about 20 cm long were selected from each borehole. The selected cores were then cut into three pieces; 10 cm core for geochemical and isotope, 3 cm for thin section and 7 cm for hand specimen analysis. The 10 cm cores were milled at University of the Western Cape. Twenty grams of each core sample was sent to Council for Geoscience for geochemical analysis (major and trace elements data) and another 20 g was sent to University of Cape Town for isotope analysis.

3.5. Petrography

The main objective of petrography is to understand the types of Platreef lithology and their position in the stratigraphic height, including their relationship to PGE-BMS mineralisation. This objective will be achieved through detail modal analysis using petrographic methods in order to ascertain the vertical and lateral distributions of primary minerals, texture as well as secondary alteration minerals that distinguish different types of pyroxenites in the Platreef.

3.5.1. Thin section preparation

The thin sections were analysed at the University of the Western Cape using binocular microscope under both reflected and transparent light. The mineral and modal compositions, textures, alterations and ore mineralogy (mainly the base metal sulfides) of the various rock types of interest were determined using a binocular microscope. The mineralogy, textures, base metal sulfides (BMS) and alterations that distinguish different types of Platreef feldspathic pyroxenites rocks were also identified during petrography.

3.6. Geochemical sample preparation

Sample preparation for major and trace elements which include splitting, jaw-crushing and milling of rock samples was done at the University of the Western Cape Laboratory. The procedure followed during bulk chemistry analysis by XRF for major and trace elements is shown in appendix II. The core samples were crushed and milled using 5x3 inch Dickie & Stockler® jaw crusher machine and Dickie & Stockler® T-S 250 mill respectively. Samples were milled to <50 µm. During the process of grinding and milling, two quartz run were done

after each sample and the milling pot was always washed with distilled water and cleaned to dryness after every single milling in order to avoid contamination.

3.6.1. Bulk chemistry by XRF

3.6.1.1. Laboratory analysis of major elements

(a) Fusing

Fusing is the process which is taken during major elements analysis in which the glass-like fuse bead is produced and it is a valuable means of eliminating errors with materials which exhibit varying mineralogical composition or are difficult to present in other forms. In order to make the fuse beads, the first step is to determine the Loss On Ignition (LOI) for all the samples.

(b) Determining the Loss On Ignition (LOI)

Determining the Loss On Ignition (LOI) of the samples involves three steps: Pre-ignition weighing, Ignition and Post-ignition weighing.

(i) Pre-ignition weighing:

During major elements analysis, the first step was to weigh the clean crucible and then weigh the milled samples. The mass of the samples weighed was approximately between 3g to 5g for all the samples. The internal standard and external standard (SARM-46) were weighed to a mass of 5g-10g.

(ii) Ignition:

After weighing, the samples were then placed in the oven for 2 hours at a temperature of 1000 °C, and the purpose of doing this was to remove all the excess water from the samples. The dried samples were then weighed again in order to determine the mass of the samples without any moisture/water. The dried samples were then placed in the oxidizing machine overnight in order to remove volatiles and oxidize the samples. After oxidizing, the samples, initially whitish changed to light brown, and the samples that were initially grey-black changed to dark brown.

(iii) Post-ignition weighing:

The oxidized/ignited samples were weighed immediately after removing them from the oxidizing machine to avoid rehydrating of the samples and the Loss On Ignition (LOI) was automatically calculated using "LOI Short Calc" worksheet. The Loss On Ignition (LOI) calculated were used to determine which flux to use between A flux (34.83% $Li_2B_4O_7$ – 64.67% $LiBO_2$ – 0.50% LiBr), B flux (49.50% $Li_2B_4O_7$ – 49.50% $LiBO_2$ – 1.00% LiBr) and C flux (66.67% $Li_2B_4O_7$ – 32.83% $LiBO_2$ – 0.50% LiBr). The B flux (Lithium Tetraborate with Lithium Mataborate and Lithium Bromide fused, Anhydrous: 49.50% $Li_2B_4O_7$ – 49.50% $LiBO_2$ – 1.00% LiBr) was used to fuse all the samples with LOI less than 5 except for external standard (SARM-46) in which C flux (66.67% $Li_2B_4O_7$ – 32.83% $LiBO_2$ – 0.50% LiBr) was used because it has high LOI (17.94).

(c) Preparation of fuse beads:

1g of each sample was fused with 10g of B flux (49.50% $Li_2B_4O_7$ – 49.50% $LiBO_2$ – 1.00% LiBr). The sample to flux ratio (1:10) is important in analysis and affect both the speed of the reaction and the way the sample is absorbed by the flux. The mixture of the sample and the flux was placed in the platinum crucible and then in the OX fusing machine at a temperature of 800°C to 1000°C for 20 minutes in order to produce the fuse beads. The samples that were originally whitish changed to light brown, and the ones that were grey-black changed to light green after fusing (Plate 3.1). The fused beads were analysed in the XRF machine and the results were recorded.

Plate 3.1: Fuse beads produced after heating the mixture of the sample and the flux at a temperature of 800°C to 1000°C for 20 minutes in the OX fusing machine.

3.6.1.2. Mathematical corrections

The results recorded by the detector include 90% concentration of the flux and 10% concentration of the sample because during the fusing process 10g of the flux was mixed with 1g of the sample. Therefore, the factor was calculated in order to identify the exact concentration of the major elements in the sample without flux. The formula used to calculate the factor is shown below. The calculated factor was then multiplied by the concentration of each major element in order to identify the initial concentration in the sample.

$$\text{Factor} = \frac{\text{Total concentration} - \text{Loss On Ignition (LOI)}}{\text{Total concentration} - \text{flux } (B_2O_3 + Li_2O)}$$

Original Concentration = factor *concentration of the element

3.6.1.3. Laboratory analysis of trace elements

Trace element were also analysed using XRF instrument at Council for Geoscience Laboratory, and they were measured in parts per million (ppm). The first step during trace elements analysis was to weigh 12 g of powdered sample. The measured 12 g of powdered samples were mixed with 3 g of wax and placed in the shaker overnight for homogeneity purpose. The purpose of mixing the sample with wax was to ensure that the sample materials remain intact and to avoid expansion during pressing. After shaking, the mixture of the sample and wax was transferred into aluminium dish. The aluminium dish was then pressed under high pressure using the pressing machine in order to produce the pressed pellets (Plate 3.2). The pressed pellets were then weighed and the average mass was 17 g which is the accepted mass for pellets. The pellets were analysed for trace elements in the XRF machine for about 12 hours. The results were recorded in the detector computer.

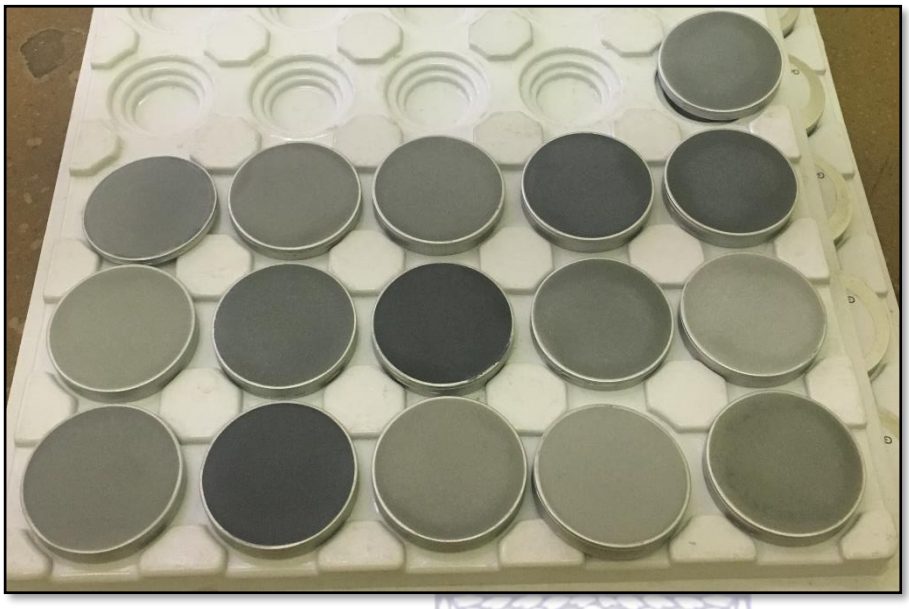

Plate 3.2: Press pellets produced by pressing the aluminium dish containing the mixture of the sample and the wax using the pressing machine.

3.7. Bulk chemistry by XRD analysis

The X-ray Diffraction (XRD) is a standard primary procedure used by mineralogist to examine the physical and chemical make-up of unknown solids. The XRD was done at Council for Geoscience Laboratory using D8 advanced machine. About 15 of powdered samples were analysed in order to determine the mineralogy of the rocks. The powdered samples were placed in the sample holders. The sample holders were placed on the magazine tray and then placed in the D8 advanced machine. During analysis, the samples were illuminated with X-rays of a fixed wavelength and the intensity of the reflected radiation was recorded using a goniometer. The analysis took about 30 minutes to 1 hour per sample of which the total time for 15 samples was approximately 15 to 20 hours. After running the samples in the D8 advanced machine the difractogram was produced (Figure 3.2). The peaks on the difractogram were classified into main peaks and secondary peaks, where the secondary peaks are used as reference during identification of minerals. The minerals were identified depending on different peaks of the diffractogram.

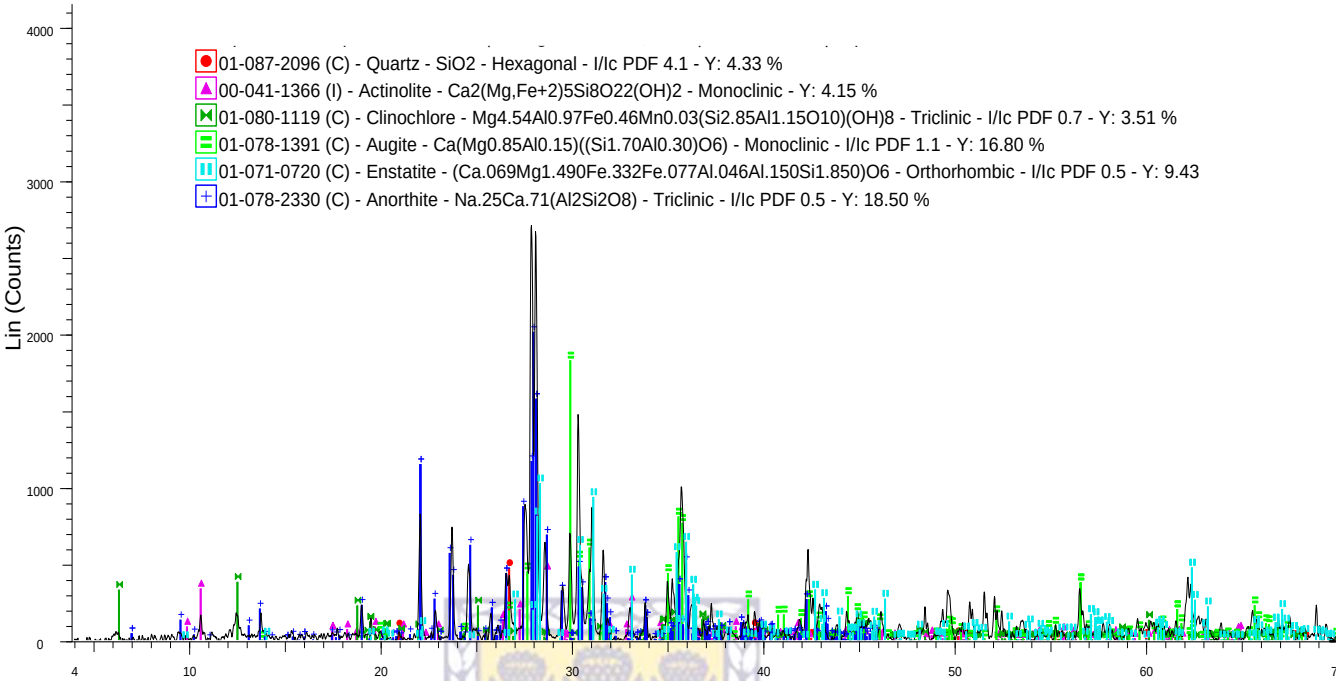

Figure 3.2: The diffractogram of sample ZF044-19 showing the main peaks and secondary peaks.

3.8. Isotope geochemistry

3.8.1. Introduction

$^{87}Sr/^{86}Sr$ and $^{143}Nd/^{144}Nd$ are routinely used in geochemistry as petrogenetic tracers, yielding information on time-integrated elemental fractionation through processes of melting, crystallization, metasomatism and contamination (Barton et al., 1986). The aim of doing Sr-Nd isotope analysis in the current study is to investigate the petrogenesis of the Platreef pyroxenite rocks. In particular, to determine the age, the parental magma source and further constraining the role of crustal contamination in the formation of both the Platreef pyroxenites and PGE mineralisation. Besides, Sr-Nd isotope data from the Platreef pyroxenites will be compared to those of the Merensky reef, UG2 and the Main Zone in order to identify if they share the common parental magma source.

Sr – Nd isotope analysis involves three processes; (1) sample digestion, (2) sequential separation of Sr – Nd from LREE and (3) isotope determination using TIMS and MC-ICP-MS. Sr – Nd isotope analyses were performed using Nu Instruments NuPlasma HR in the MC-ICP-MS (multiple-collector inductively coupled plasma mass spectrometry) facility, housed in the Department of Geological Sciences, University of Cape Town, Rondebosch, South Africa. MC-ICP-MS together with TIMS (Thermal ionization source mass spectrometry) is known as benchmark technique for Sr – Nd isotope ratios since they both provide accurate results with excellent sensitivity.

The rock samples were first crushed and milled, digested using concentrated HF: HNO3 and simultaneous separation of Sr and Nd by extraction chromatography before isotope ratios determination by TIMS and MC-ICP-MS. The rock samples were crushed and milled using5x3 inch Dickie & Stockler® jaw crusher machine and Dickie & Stockler® T-S 250 mill respectively at University of Western Cape.

3.8.2. Sample digestion

About 100mg – 250mg of each milled sample was wetted with 1 mL of concentrated 7M HNO3, then digested with 1 to 2 mL of concentrated 29M HF for 48 hours at 140 ºC in closed Teflon beakers. The solution was further evaporated to dryness. After evaporation, the sample residue was treated with concentrated HNO_3, in order to convert the sample to nitrates. The sample residue was then taken up with 2 mL of concentrated 1M HNO_3 enamel digestion at

140 ºC in closed Teflon beakers for 1 hour. Any visible whitish compound at this stage was treated with a few hundred µL of 1M HNO3 solution saturated in boric acid. Therefore, the dissolution process was complete when all the compounds were completely dissolved and the resulting solution is combined with the bulk sample solution. Lastly, the amount of Fe (III) in the sample was reduced to Fe (II) by adding 100g – 200g of the reducing agent. For the purpose of this study, ascorbic acid ($C_6H_8O_6$) was used as a reducing agent, and the amount used depends on the amount of Fe (III) in each sample. The initially colourless sample solution becomes pale yellow after allowing *ca*. 10 minutes for the dissolution and reducing action of ascorbic acid, and was ready for the column work.

3.8.3. Sequential separation of Sr and Nd

The process of sequential separation of Sr and Nd elements from sample matrices is important and must be done prior to TIMS and MC-ICP-MS measurements. This is to ensure that stable and high intensity of ion signals are obtained. Sr and Nd separation is done after complete digestion process of the samples and reduction of Fe (III) to Fe (II) in samples. Sr is separated first and Nd is separated after Sr and hence is called sequential separation. During Sr separation, the digested sample solution is passed through two tandem columns containing 250 µL of Sr Spec and TRU Spec extraction chromatography resins, respectively. The upper Sr Spec column extracts Sr, while the lower TRU Spec column extracts the LREE. The LREE are eluted directly onto a longer column containing 300 mg of the HDEHP-based EXC material Ln Spec to obtain Nd fraction through sequential elution with 0.25M HCl.

3.8.4. Sr analysis by MC-ICP-MS

The separated Sr was analysed as 200ppb 0.2% HNO3 solution using NIST SRM987 as standard reference. All Sr isotope data were corrected for (1) Rb interference using the measured signal for ^{85}Rb and the natural ^{85}Rb/^{87}Rb ratio and (2) instrumental mass fractionation using the exponential law and an ^{86}Sr/^{88}Sr value of 0.1194. The samples were analyzed with international rock standards (NIST SRM987) in order to compare the data for accuracy and precision. The time-dependent fractionation of ^{87}Sr/^{86}Sr ratios during the analyses was corrected by normalisation to ^{86}Sr/^{88}Sr = 0.710255, using an exponential law. The external

reproducibility of a BHVO-2 standard sample used by Weis et al., (2006) was ± 0.000011 for $^{87}Sr/^{86}Sr$ = 0.703474. However, in the present study the external reproducibility of a BHVO-2 standard used was ± 0.000018 for $^{87}Sr/^{86}Sr$ = 0.703510 which is a long term UCT average with n=124.

3.8.5. Nd analysis by MC-ICP-MS

Nd isotopes were analyzed as 50ppb 2% HNO_3 solutions using Nu Instruments DSN-100 desolvating nebulizer. JNdi-1 was used as a standard reference and the normalizing value for $^{143}Nd/^{144}Nd$ was 0.512115 (Tanaka et al., 2000). The samples were analyzed with international rock standards in order to compare the data for accuracy and precision. All Nd isotope data were corrected for (1) Sm and Ce interference using the measured signal for ^{147}Sm and ^{140}Ce, and natural Sm and Ce isotope abundances and (2) instrumental mass fractionation using the exponential law and a $^{146}Nd/^{144}Nd$ value of 0.7219.

3.9. Quality Control and Quality Assurance

Quality Assurance/Quality Control (QA/QC) procedures are essential in all aspects of mineral deposit evaluation processes. QA/QC provides quantitative information on the quality of the analytical results. To ensure high accuracy and precision of the data used in the current study, all samples analysed for bulk geochemistry and isotope geochemistry were analysed with certified international standards. Five samples were duplicated during bulk geochemistry analysis and the precision between the samples was calculated. The purpose of duplicating the samples was to account for any outside influences and offer insight into potential analytical errors. The graphical representation of the correlation between original and duplicate sample is shown in figure 3.3. A good correlation between original and duplicate sample with a precision of 10 % in figure 3.3 indicate good sample homogenization and analytical precision.

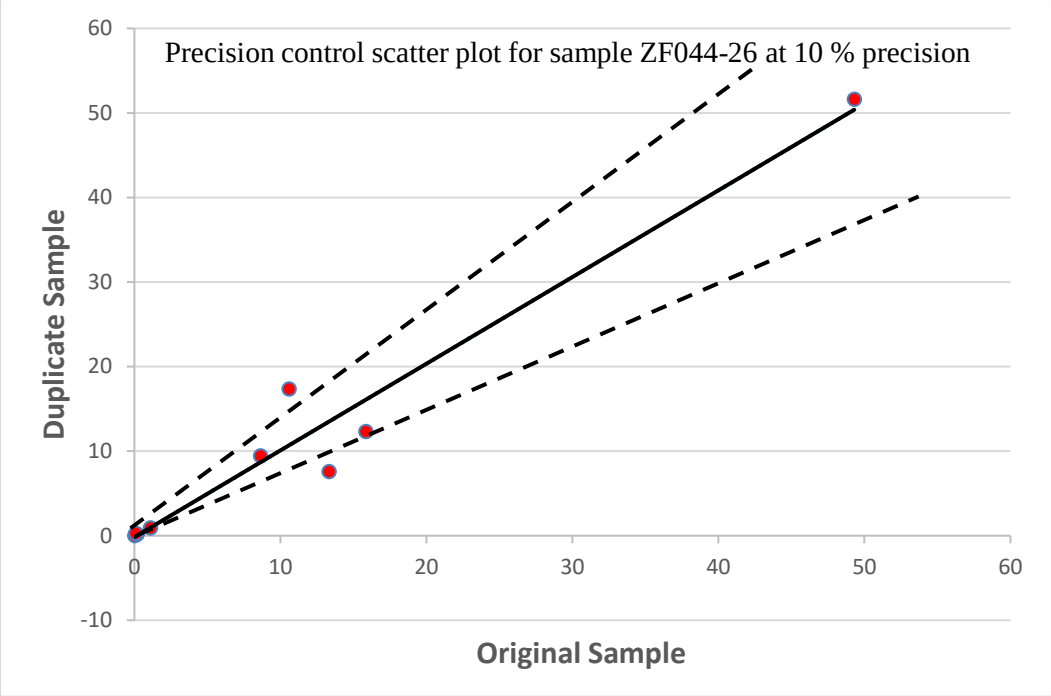

Figure 3.3: Precision scatter plot for sample ZF044-26.

3.10. Data evaluation

Data evaluation methodology

(i) Cluster Analysis

The first step of geochemical data analysis involved geochemical classification of the Platreef rocks using cluster analysis in to validate the lithology results from the petrographic studies. Cluster analysis in the present study was employed with the purpose of (1) detecting geochemical relations between the rock samples and (2) assigning the samples into specific rock types based on the clusters/groups formed during HCA. Finch (2005) defined cluster analysis as an analytical method which is used to classify and group together samples that are homogeneous. Hierarchical cluster analysis (HCA) is one of the cluster analysis methods that have been widely applied in geochemical data analysis and was described by Templ et al. (2008) as the best method in handling geochemical data. In the current study, HCA was applied to major element data using Geochemical Data Toolkit (GCDkit), and the results were displayed in the form of a dendrogram.

(ii) Descriptive statistics

The second step involved the use of descriptive statistics in order to describe the underlying distribution of elements amongst different rock types. In descriptive statistics, the sample data are first described with its different statistics presented in the summary tables and after that the describing figures are added for each parameter. The statistical parameters presented in the summary tables include mean values, variance, covariance and quartiles with minimum and maximum values. The describing figures that are usually used in descriptive statistics are histograms, box-whisker plots and quartile-quartile plots. The main objective of the descriptive statistic is to use box-whisker plots to understand the elements distribution and the major elements that characterize each rock type identified during petrographic studies and cluster analysis.

(iii) Scatter plots

The third step involved the use of scatter plots to show the relationship/correlation between two elements (e.g. MgO vs FeO). The main objective of using Binary Harker diagrams (scatter plots) is to assess the co-genetic nature of the mafic-ultramafic rocks, mineral distributions in the Platreef rocks and the sequence of mineral fractionation during the emplacement. Friendly and Denis (2005) defined scatter plots as plots of two variables measured independently to produce bivariate pairs and are designed to show the relationship/correlation between two variables. In scatter plot, the relationship between two variables can be defined as a positive or negative relationship. A positive relationship exists when one variable decreases as the other variable decreases or one variable increases while the other variable increases. Negative relationship exists when one variable increases as the other variable decreases, and vice versa. In correlation coefficient, perfect positive relationship is represented by +1 and perfect negative relationship is represented by -1. In some cases, scatter plots may show no correlation between two variables and this is known as zero correlation (Figure 3.4).

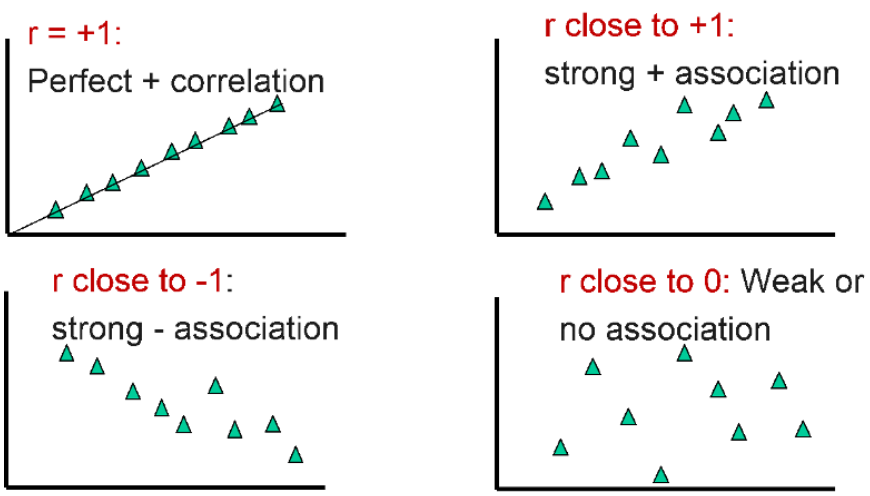

Figure 3.4: Sctter plots correlation coefficient showing positive, negative and zero correlation between two variables.

(iv) Spider diagrams

Incompatible trace elements ratios (ITE) was used to fingerprint the possible sources of parental magma. Crustal and mantle sources have very different trace element ratios, and these, combined with isotopic data, can be used to ascertain the relative contributions of these disparate sources to Platreef magmas.

(v) Mass balance

The fourth step involves the use of mass balance in order to evaluate element exchange between the Platreef magma and crustal rocks. Firstly, between the Platreef pyroxenites and the dolomite footwall in borehole ZF044 and ZF057. Secondly, between the Platreef pyroxenites and Archean granite footwall in borehole ZF048. The understanding of elemental exchange will aid in identifying the effect of crustal contamination in the formation of PGE mineralisation in the Platreef. Mass balance calculations will be done using EASYGRESGRANT considering all possible reference frames between the unaltered rocks and their altered counterpart.

(vi) Sr-Nd isotope data analysis

The firth step involved the use of Sr-Nd isotope data to investigate the petrogenesis of the Platreef pyroxenites rocks. Isotope geochemistry (Sr-Nd) will be used to (1) identify the age of the Platreef rocks, (2) constrain understanding about the parental magma source that gave rise to the formation of the Platreef and (3) identify the effect of crustal contamination in the Platreef rocks. Sr-Nd isotopes were analysed at the University of Cape Town using Nu

Instruments NuPlasma HR in the MC-ICP-MS facility. The Sr-Nd isotopes measured at UCT represent the isotope of the rocks in the present day. Therefore, the initial Sr-Nd isotope of the rock is calculated using Sr-Nd isotope data, Rb and Sm data using GCDkit software. The initial Sr-Nd isotope data are essential in understanding the parental magma source, the time of crustal contamination as to whether contamination occurred prior to crystallization or after crystallization and the degree/effect of crustal contamination. Sr-Nd isotope data will be presented on isochron diagram using GCDkit software. Firstly, Rb-Sr and Sm-Nd dating methods will be employed to identify the age of the Platreef rocks. Secondly, a graph of εNd versus initial 87Sr/86Sr calculated at 2.06 Ga will be plotted in order to identify the parental magma source and the effect of crustal contamination in the Platreef rocks.

CHAPTER FOUR

4. PETROGRAPHY RESULTS

4.1. Introduction

This chapter focuses on modal mineralogical analysis of rocks using core logging and petrography in order to ascertain the vertical and lateral distribution of primary minerals as well as alteration in minerals. A detailed petrography studies was also used to understand the Platreef lithology, distribution of PGE-BMS mineralisation in the Platreef lithology, the extent of hydrothermal alteration and the stratigraphy of the Platreef. The lithology and stratigraphy of Platreef will be explained using cores and thin sections cut from three boreholes, namely: ZF044, ZF048 and ZF057. Since the lithology of Platreef according to Kinnaird et al. (2005) is heterogeneous and stratigraphy cannot be correlated, the petrography will be used as the baseline, and the results will be complemented by whole-rock geochemical data analysis. This chapter explains the lithology and stratigraphy intersected by each borehole individually; this will provide better understanding of variations in the Platreef lithology of the study area.

The description of the Platreef lithology and the stratigraphy encompasses two stages, first through macroscopy using cores and secondly through microscopy using thin-section evaluation under the microscope. The macroscopic evaluation of cores helped in classifying rocks into ultra-mafic, mafic and felsic based on the colour of the rocks, and identify the presence of hydrothermal alteration. On the other hand, microscopic evaluation of thin-section was used to identify the grain size, texture, crystal habit and mineral compositions expressed in modal percentage using the count method.

Core samples were collected from three boreholes, namely; ZF044, ZF048 and ZF057 drilled to depths of 1334.11 m, 1564.52 m and 1521.28 m respectively.

4.1.1. Introduction to Platreef lithology

The Platreef rocks are medium- to coarse-grained, mafic- to ultramafic rocks, comprising orthopyroxene and clinopyroxene cumulates with minor intercumulus plagioclase; olivine and interstitial sulfides. Secondary minerals include amphibole (tremolite and actinolite), serpentine and sericite. Accessory minerals are biotite, magnetite and quartz. The Platreef lithology according to the previous studies (e.g. Hutchison and Kinnaird, 2005; Kinnaird et al., 2005; Holwell and McDonald, 2006; Kinnaird and Yudovskaya, 2010) comprises feldspathic pyroxenite, pyroxenite, harzburgite, peridotites, serpentinite, gabbronorites and norite.

Kinnaird and Yudovskaya (2010) described the Platreef lithology at Zwartfontein farm to be dominantly coarse-grained feldspathic pyroxenites with minor feldspathic harzburgite, norite and parapyroxenites.

The classification of rocks in the current study was based on the major cumulus and intercumulus minerals following Kinnaird et al. (2005). The Platreef lithology intersected by borehole ZF044, ZF048 and ZF057 at Zwartfontein farm is consistence with the Platreef lithology from previous studies (e.g. Kinnaird and Yudovskaya, 2010). The Platreef consist variably of fine-grained feldspathic pyroxenite, harzburgite, parapyroxenites, calc-silicate xenolith, coarse-grained feldspathic pyroxenite and overlain by gabbronorite, norite, mottled anorthosite and leuconorite of the Main Zone. The Platreef at Zwartfontein is dominated by feldspathic pyroxenite that occurs as sill-like intrusions separated by variety of rock types including calcsilicate xenoliths, granite xenoliths and parapyroxenite.

Parapyroxenite is a term normally used by field geologist to explain an intermediate rock type between calc-silicate and pyroxenite or feldspathic pyroxenite. Parapyroxenite contain low calcium content than calc-silicate but have significantly high iron content (Schouwstra et al., 2013). Parapyroxenite were formed from modified pyroxenites as a result of contact metamorphism with Malmani dolomite-calcsilicates. According to Harris and Chaumba (2001), parapyroxenites are rocks that seem to be a 'mélange of variably recrystallised pyroxenites and calc-silicates rocks'. Parapyroxenite was intersected by borehole ZF044 and ZF057 at various depths and contained massive and disseminated sulphildes mineralisation such as chalcopyrite, pentlandite and pyrite. Harris and Chaumba (2001) explained the economic occurrence of sulfides mineralisation in parapyroxenite rocks as evidence of high degree of fluid-rock interaction in the Platreef.

Orthopyroxenites rocks, which occurs as thin layers in the Platreef occur in borehole ZF048 and consist of >90% cumulus orthopyroxene, minor plagioclase and clinopyroxene with fibrous amphibole. Serpentinisation, as noted to be dominant towards the south in the Platreef by Holwell and McDonald (2006), were intersected by borehole ZF044 and ZF057 and occurs in rocks referred to as harzburgite in the current study.

Feldspathic pyroxenite is regarded as one of the major lithologies of the Platreef package and occurs throughout the Platreef. According to the Bushveld nomenclature the feldspathic pyroxenite is referred to the rock which consists of cumulus orthopyroxene and significant intercumulus plagioclase (>10%). According to IUGS, this rock is referred to as norite. In the

current study, however, norite refers to a rock that contains cumulus as opposed to intercumulus plagioclase in feldspathic pyroxenite. The texture of feldspathic pyroxenite varies throughout the Platreef package. Fine-grained feldspathic pyroxenite generally occurs at the base of the Platreef, while the medium to pegmatoidal feldspathic pyroxenite occurs below the Platreef-Main Zone boundary. In the current study, feldspathic pyroxenite will be classified into three groups namely; feldspathic pyroxenite I (FP II), feldspathic pyroxenite II (FP II) and feldspathic pyroxenite III (FP III) based on their grain size, colour, texture and PGE mineralisation. FP I are fine-grained, FP II are medium- to coarse-grained and FP III are medium- to fine-grained.

In terms of BMS/PGE mineralisation and grain size, feldspathic pyroxenite I (FP II), feldspathic pyroxenite II (FP II) and feldspathic pyroxenite III (FP III) can be correlated to A-reef, B-reef and C-reef described by White (1994) respectively. Where A-reef contains little mineralisation, B-reef is extensively mineralised, and C-reef is barren. The subdivision and succession of the Platreef sequence into A-reef, B-reef and C-reef is not clearly developed at Zwartfontein. For example, in borehole ZF044 the rocks, which are referred to A-reef are found to be intercalated in-between the B-reef rocks. Besides, in borehole ZF048, only A-reef and B-reef occur. Therefore, the subdivision of the Platreef into A-, B- and C-reef may not be applicable at Zwartfontein. Instead, the subdivision into lower Platreef, middle Platreef and upper Platreef consisting of feldspathic pyroxenite I (FP I), feldspathic pyroxenite II (FP II) and feldspathic pyroxenite III (FP III) are adopted.

Petrography was done at the University of the Western Cape using microscope under 4X magnification and the studied samples are indicated in the logs (Figure 4.1, 4.2 and 4.3). Thin sections were analysed under crossed-polarised (XPL) and plane-polarised light (PPL). Minerals were abbreviated as follows: plagioclase (Plag), orthopyroxene (Opx), olivine (Ol), clinopyroxene (Cpx), sulfides (Sulp), tremolie (Trem), actinolite (Act), sericite (Ser), quartz (Qtz), serpentine (Serp), biotite (Bio), chromite (Cr).

4.2. Borehole ZF044

4.2.1. Lithostratigraphy of the Platreef in borehole ZF044

Borehole ZF044 intersected the Platreef at a depth of 910.90 m and have the thickest Platreef package (~450m) compared to other boreholes utilised in the current study. The thickness of the Platreef intersected by Borehole ZF044 is consistent with the Platreef thickness (200m-500m) in the central sector (Sandsloot, Vaalkop and Zwartfontein) reported by Yudovskaya and Kinnaird (2010). The Plareef package in borehole ZF044 consists of coarse-grained feldspathic pyroxenite II, fine-grained feldspathic pyroxenite I, harzburgite and medium- to coarse-grained feldspathic pyroxenite III with intercalated calc-silicate xenoliths, parapyroxenite and serpentinite (Figure 4.1). The simplified lithostratigraphy in borehole ZF044 from bottom to top consist of ~5 m thick Calc-silicate overlain by feldspathic pyroxenite II occurring in four sills of varying thickness separated by calcsilicate xenoliths. Following this is the feldspathic pyroxenite I with the thickness of ~8 m underlain by ~4 m calcsilicate, which is overlain by ~3 m harzburgite. Overlying the harzburgite is another sill of feldspathic pyroxenite II with a thickness of ~50 m. The upper Platreef consists of feldspathic pyroxenite III, which occurs as discreet sills of varying thickness intercalated by layers of calcsilicate and quartzo-feldspathic pyroxenites. The thickness of calcsilicate xenoliths varies between 0.4 – 7.4 m throughout the Platreef succession in borehole ZF044. Chromitite also occurs as thin layers intercalated between feldspathic pyroxenites. Calc-silicate form part of the footwall rocks in borehole ZF044. Serpentinite mostly occurs towards the upper Platreef package together with parapyroxenite.

The detailed description of the footwall rocks, the Platreef rocks and the comparison between the different types of the Platreef feldspathic pyroxenites is presented in section 4.2.2.

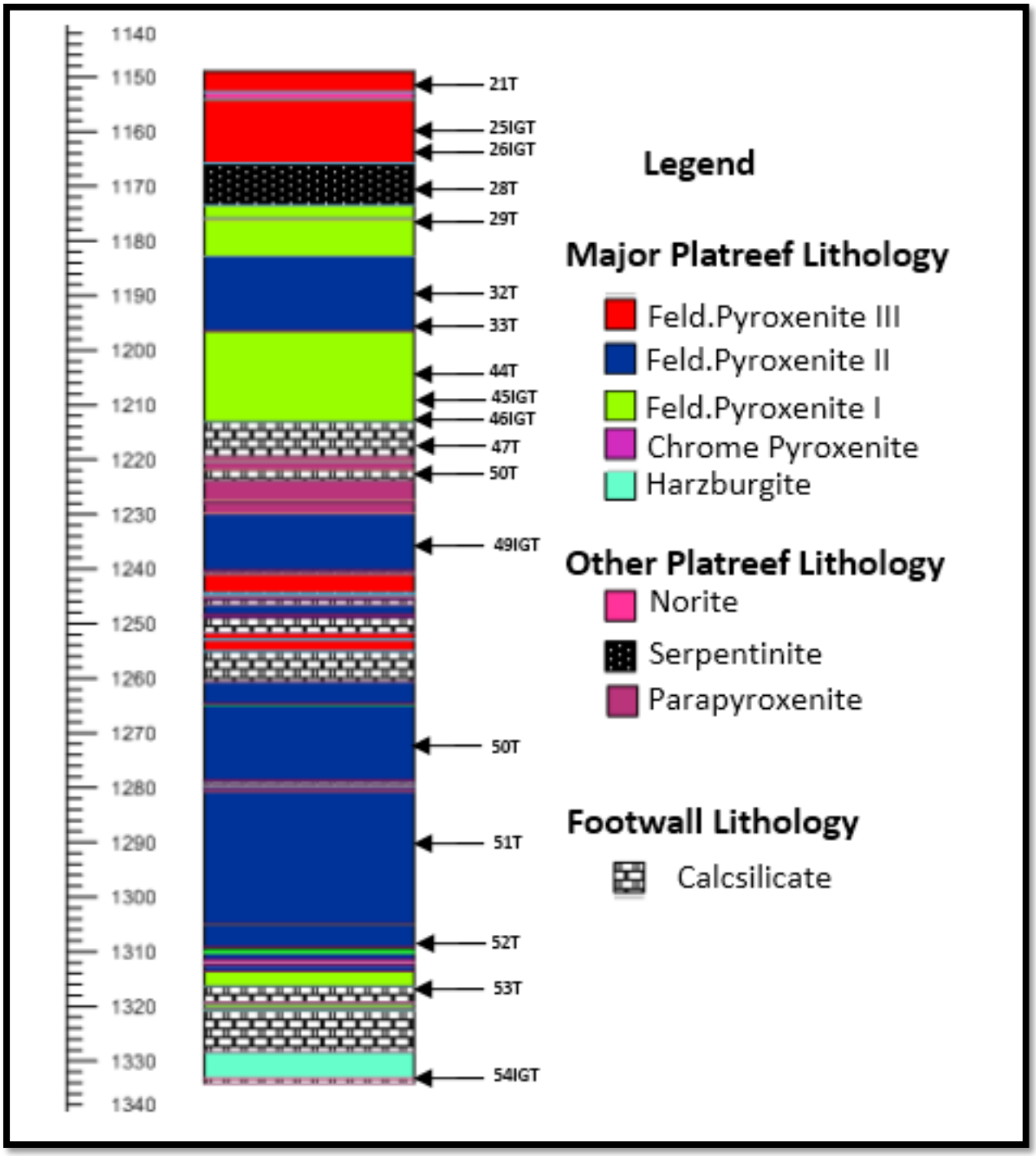

Figure 4.1: Lithostratigraphic log for borehole ZF044 with sample numbers labelled IGT and T, where IGT represent samples that were used for isotope, geochemistry and thin-section analysis respectively. And samples labelled T only were used for thin-section analysis.

4.2.2. Description of the Platreef lithologies in borehole ZF044

This section focuses mainly on the petrographic description of the major Platreef rocks, which include various types of feldspathic pyroxenite such as FP I, FP II and FP III identified in the current study. The feldspathic pyroxenite I, II and III are also defined as Lower Platreef, Middle Platreef and Upper Platreef respectively.

Feldspathic pyroxenite I (Lower Platreef) consist of cumulus orthopyroxene, clinopyroxenite and significant cumulus olivine relative to FP II (Middle Platreef) and FP III (Upper Platreef). Feldspathic pyroxenite II contain significantly high orthopyroxene with varying amount of clinopyroxene and plagioclase. Feldspathic pyroxenite III differs from FP I and FP II mostly because of high plagioclase and a varying amount of orthopyroxene and clinopyroxene. The similarity between these three feldspathic pyroxenite types lies in their cumulus orthopyroxene and clinopyroxene contents, although their relative volume varies. Harzburgite referred to serpentine harzburgite in the current study have intensively serpentinised olivine and minor amount of orthopyroxene, which are altered to amphibole (tremolite and actinolite).

4.2.2.1. Platreef feldspathic pyroxenites

The Platreef in borehole ZF044 consists of three feldspathic pyroxenite that differs in terms of mineral modal composition, texture, grain size and sulfides mineralisation. Plate 4.1 shows the photomicrographs of feldspathic pyroxenites.

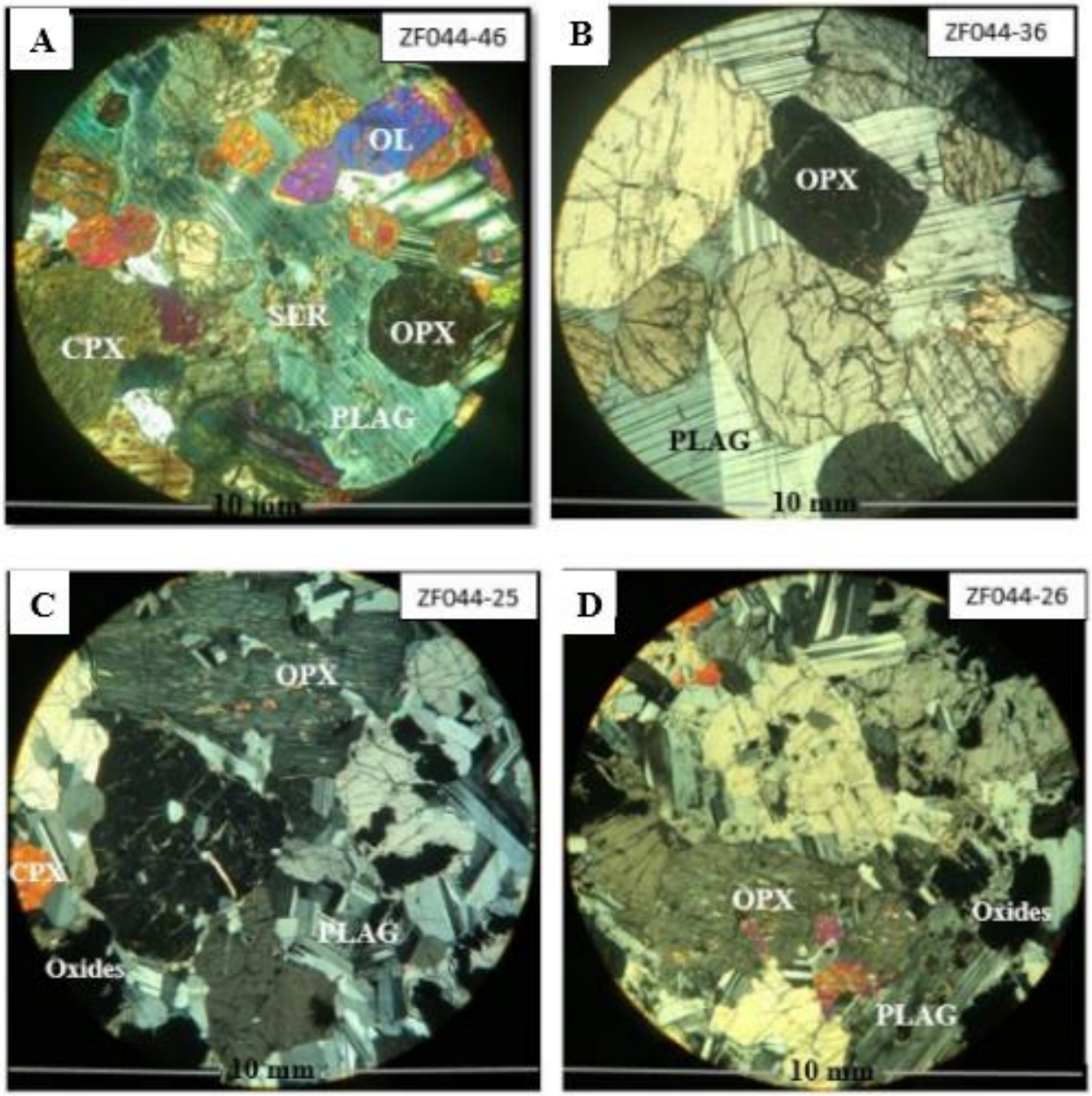

Plate 4.1:(**a**) Feldspathic pyroxenite I (Lower Platreef) consisting of plagioclase oikocryst enclosing cumulus orthopyroxene, olivine and clinopyroxene. Orthopyroxene and olivine exhibit euhedral habit. Clinopyroxene occurs as anhedral crystals. Plagioclase occurs as anhedral crystals and is moderately altered to sericite. (**b**) Feldspathic pyroxenite II (Middle Platreef) consist of euhedral cumulus orthopyroxene (3-5mm) enclosed within plagioclase oikocryst. Orthopyroxene phenocrysts are moderately fractured and exhibit glomeporphyritic texture.

(**c-d**) Feldspathic pyroxenite III (Upper Platreef) consist of cumulus orthopyroxene surrounded by groundmass plagioclase and interstitial clinopyroxene.

(i) Feldspathic pyroxenites I (Lower Platreef)

Feldspathic pyroxenites I consist of orthopyroxene (70-60 vol. %), clinopyroxene (10-15 vol. %), olivine (15-10 vol. %) and plagioclase (5-10 vol. %). Accessory minerals include sulfides (pyrite, chalcopyrite and pentlandite), biotite and quartz (3-5 vol. %). Feldspathic pyroxenite I (FP I) are medium- to fine-grained (~4 mm grain size) with poikilitic texture and are melanocratic in colour. Orthopyroxene (~4 mm) and olivine (~3 mm) is euhedral whereas clinopyroxene (~3 mm) occurs as anhedral crystals (Plate 4.1-a). Plagioclase occurs as anhedral crystals and is moderately altered to sericite (Plate 4.1-a). Olivine is slightly fractured and shows an overgrowth texture. The alteration features include sericitization of plagioclase to sericite. Sulfides minerals (pyrite, chalcopyrite and pentlandite) occur as interstitial phase between cumulus orthopyroxene and clinopyroxene.

(ii) Feldspathic pyroxenites II (Middle Platreef)

Feldspathic pyroxenites II consists of orthopyroxene (85-70 vol. %), clinopyroxene (5-25 vol. %) and plagioclase (10-5 vol. %). Accessory minerals include sulfides (pyrite, chalcopyrite and pentlandite) and biotite (~3 vol. %). Feldspathic pyroxenite II are coarse-grained rocks (5-10 mm), with a poikilitic texture and are melanocratic due to high mafic mineral content. Orthopyroxene occurs as cumulus phase (8-10 mm), euhedral phenocrysts enclosed within plagioclase oikocryst. Orthopyroxene phenocrysts are moderately fractured and exhibit glomeporphyritic texture (Plate 4.1-b). In some samples, euhedral orthopyroxene phenocrysts contain small lamellae of exsolved clinopyroxene crystals. The alteration features include imphibole which is alteration of orthopyroxene to tremolite/actinolite and sericitization of plagioclase. Accessory minerals including sulfides occurs as irregularly-shaped minerals in between orthopyroxene and clinopyroxene crystals.

(iii) Feldspathic pyroxenites III (Upper Platreef)

Feldspathic pyroxenites III consists of orthopyroxene (65-60 vol. %), clinopyroxene (15 -25 vol. %) and plagioclase (20-15 vol. %). Accessory minerals include quartz, illmanite and hematite (2 vol. %). Orthopyroxene (3mm) and clinopyroxene (2 mm) occur as cumulus phase within plagioclase (2 mm) matrix preserving a poikilitic texture. Some plagioclase and clinopyroxene occur as inclusions within cumulus orthopyroxene. Plagioclase inclusions are relatively small (<0.5 mm) and well-rounded compared to the randomly oriented groundmass plagioclase which is elongated and is subhedral to anhedral (Plate 4.1-d). The randomly

oriented lath-shaped groundmass plagioclase exhibit an ophitic texture. Most of the groundmass plagioclase shows fewer extinction angles on the rim than in the core and some have been altered to sericite. Accessory minerals occurs as interstitial phase between orthopyroxene and clinopyroxene. Alteration features include sericitization of plagioclase to sericite. No sulfides minerals were identified in feldspathic pyroxenite III.

4.2.2.2. Serpentinised harzburgite

Harzburgite contain olivine (75-65 vol. %), orthopyroxene (25-30 vol. %) and clinopyroxene (< 5 vol. %). Accessory minerals are sulfides, hematite and ilmanite (5 vol. %). Although harzburgite originally contains a high volume of olivine, almost 90% of this olivine have been altered to serpentine, and hence this rock is called serpentinised harzburgite. Olivine (2-3 mm) occurs as cumulus phase within the orthopyroxene (3mm) oikocrysts preserving a poikilitic texture. Accessory minerals occurs as interstitial phase between olivine and orthopyroxene minerals. Extensive serpentinisation in harzburgite is depicted by occurrence of dark black veins of serpentinised olivine representing the effect of hydrothermal fluid/activity (Plate 4.2 a-b). Serpentine veins filled with sulfides extend from serpentinised olivine through adjacent orthopyroxene oikocryst (Plate 4.2a). Sulfides minerals (chalcopyrite, pentlandite and pyrrhotite) occurs as irregularly-shaped disseminated minerals mostly concentrated on the rim of serpentinized olivine and within serpentine veins (Plate 4.2a).

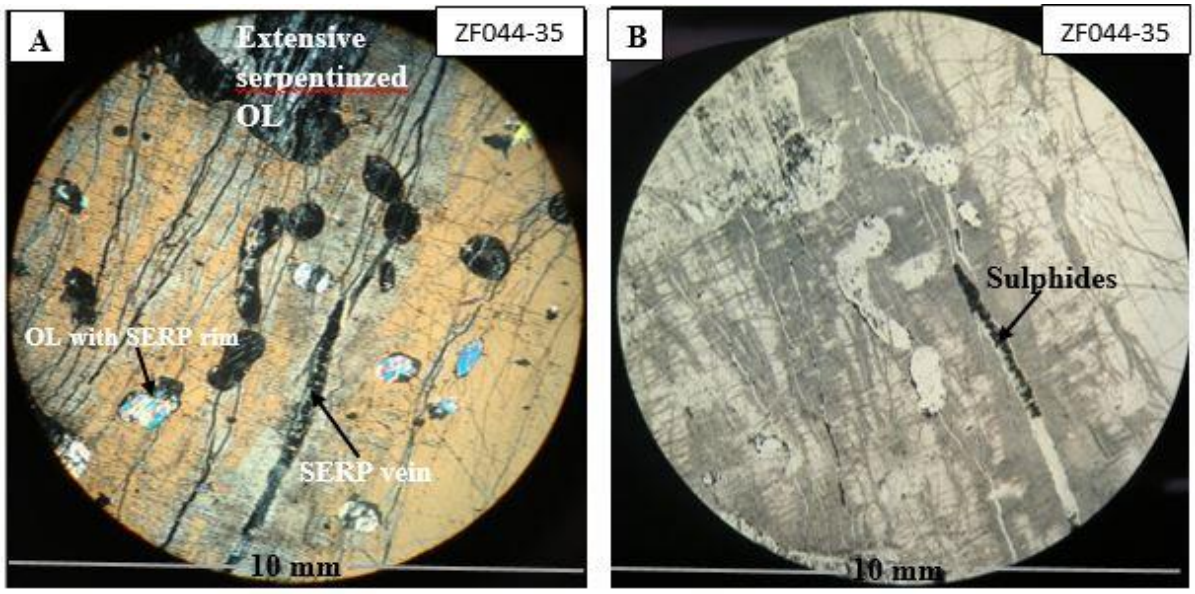

Plate 4.2: **(a)** Seperntinised harzburgite *under cross-polar light shows the occurrence of euhedral olivine within orthopyroxene oikocrysts. Most of the olivine is completely altered to serpentine. Serpentine veins extend from serpentinized olivine through adjacent orthopyroxene oikocryst. Sulfides mineralisation are mostly concentrated on the rim of serpentinized olivine and within serpentine veins. The thickness of serpentine veins ranges between <1mm to 2mm.* **(b)** Seperntinized harzburgite *under plane-polarized light shows the concentration of sulfides on the rim of olivine and within serperntine vein.*

4.2.2.3. Footwall calc-silicate

Calc-silicate can be defined as rocks that were formed from the metamorphism of impure dolomite or limestone. Calc-silicate consists of dolomitic/calcitic minerals (75 vol. %), orthopyroxene (20 vol. %) and plagioclase (5 vol. %). Accessory minerals are sulfides minerals (2 vol. %). Calc-silicate is known to be yellow or pale; however, the calc-silicate xenolith encountered in borehole ZF044 appears to be dark black due to high degree of alteration (Plate 4.3). Serpentinite footwall rock mostly shows a transitional boundary with unaltered rocks, but in rare cases sharp contact may occur (Armitage et al. 2002). At Zwartfontein, calc-silicate was found to be in a transitional contact with mineralised feldspathic pyroxenite II in borehole ZF044 (Plate 4.3). Microveins in calc-silicate was previously explained by Armitage (2002) to resemble high degree of hydrothermal fluid infiltration.

Alteration features include sericitization of plagioclase and amphibole which is alteration of orthopyroxene to tremolite/actinolite.

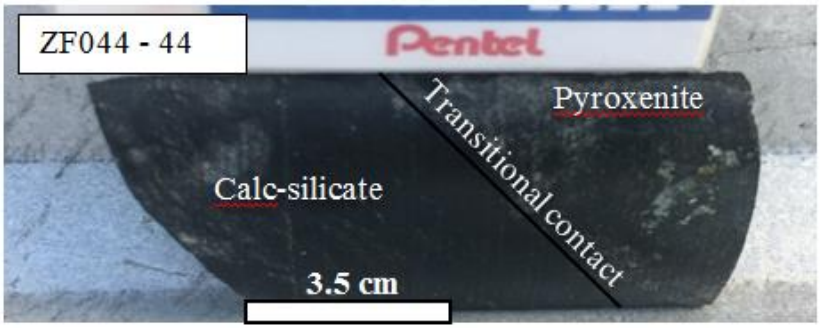

Plate 4.3: Calc-silicate pyroxenite rock intersected by borehole ZF044 at a depth of 1221.58m.

4.3. Borehole ZF048

4.3.1. Lithostratigraphy of the Platreef in borehole ZF048

Borehole ZF048 intersected the Platreef package with a thickness of 147.79 m at the depth of 1416.53 m. Borehole ZF048, in contrast to borehole ZF044, consist of feldspathic pyroxenite I, feldspathic pyroxenite II and a thin layer of Harzburgite at the base of the Platreef. The Platreef in borehole ZF048 is underlain by coarse-grained granite. This is overlain by sills of fine-grained feldspathic pyroxenite I that forms the base of the Platreef package. Overlaying feldspathic pyroxenite I is a series of sills of coarse-grained feldspathic pyroxenite II separated by norite rocks and granite xenoliths (Figure 4.2). Calc-silicate xenoliths and serpentinite rocks are absent in borehole ZF048.

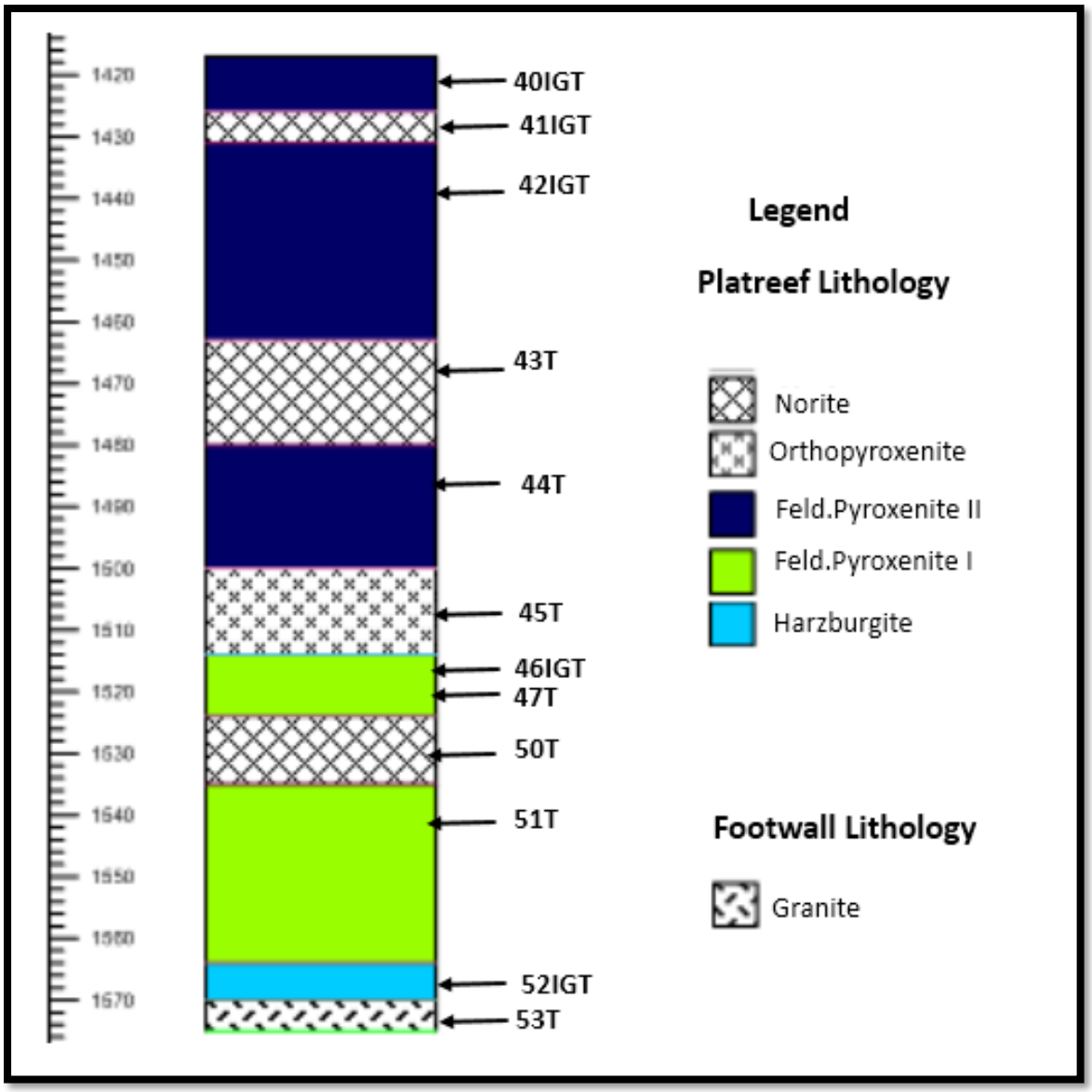

Figure 4.2: Lithology log for borehole ZF048 with sample numbers labelled IGT and T, where IGT represent samples that were used for isotope, geochemistry and thin-section respectively. Samples labelled T only were used for thin-section analysis.

4.3.2. Description of the Platreef lithologies in borehole ZF048

4.3.1.1. Platreef feldspathic pyroxenites

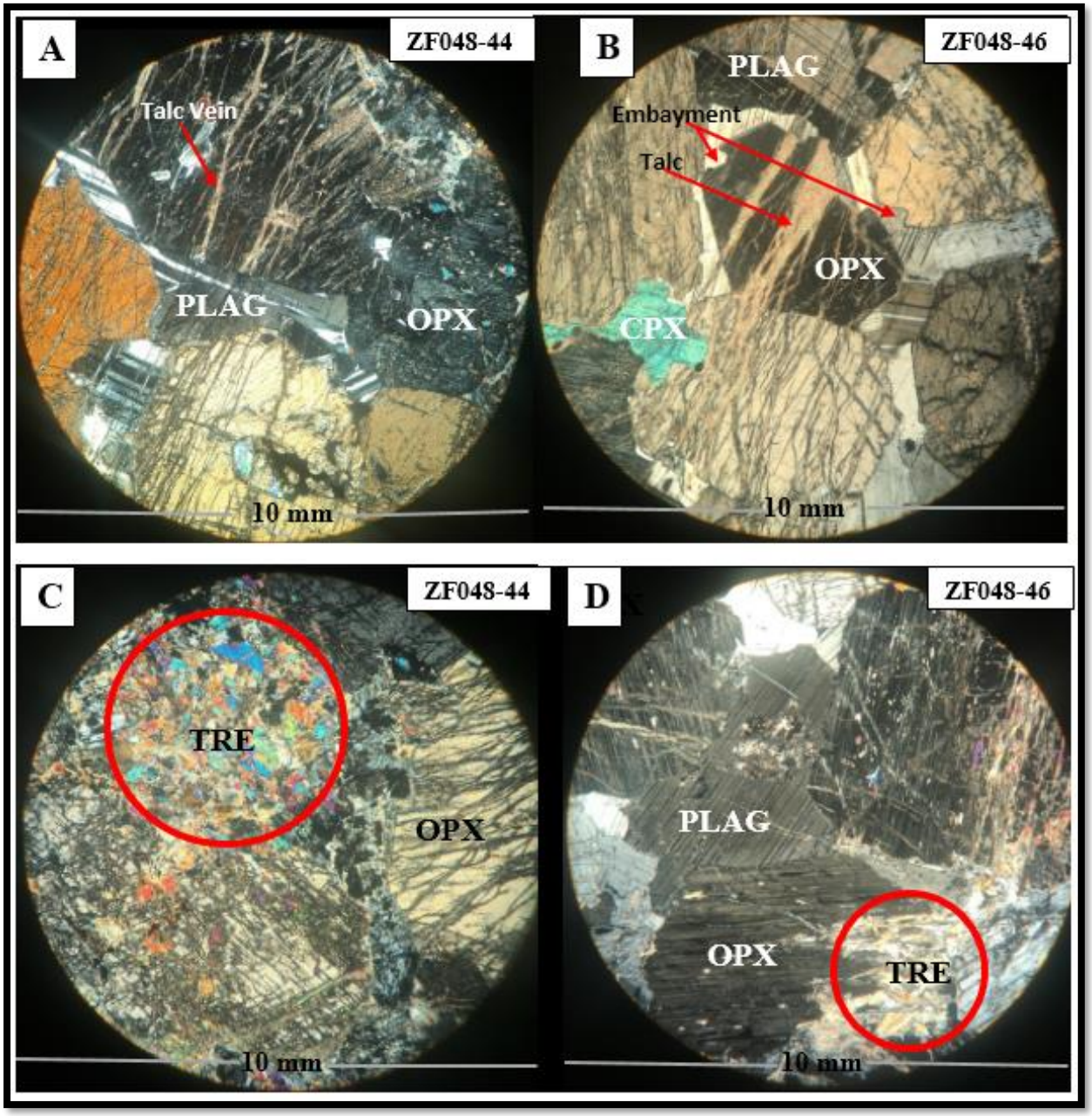

Plate 4. 4: Coarse-grained feldspathic pyroxenite II (FP II) *intersected by borehole ZF048 shows high hydrothermal fluid activity.* ***(a)*** *Cumulus orthopyroxene and clinopyroxene with intercumulus plagioclase. Orthopyroxene crystals are fractured and contain small plagioclase and clinopyroxene inclusions.* **(b)** *Anhedral plagioclase crystals showing extensive alteration to sericite. Subhedral orthopyroxene crystals are extensively fractured.* **(c)** *Orthopyroxene occurs as cumulus phase with interstitial plagioclase and clinopyroxene. Euhedral orthopyroxene crystals are extensively fractured and cut through by talc veins (1mm-2 mm).Orthopyroxene is altered to tremolitte.* **(d)** *Cumulus orthopyroxene crystals with intercumulus plagioclase. Orthopyroxene is moderately altered to tremolite and contains some small lamellae of exsolved clinopyroxene. Intercumulus plagioclase has an altered core to sericite.*

4.3.2.1.1. Feldspathic pyroxenites I

Feldspathic pyroxenites I consist of orthopyroxene (70-60 vol. %), clinopyroxene (10-15 vol. %), olivine (15-10 vol. %) and plagioclase (5-10 vol. %). Accessory minerals are sulfides and hematite (1 vol. %). Feldspathic pyroxenite I (FP I) are medium- to fine-grained (1-3 mm grain size) and are melanocratic rocks dominated by mafic minerals. Most of the feldspathic pyroxenite I exhibit poikilitic texture where some crystals cannot be easily distinguished from the hand specimen. Feldspathic pyroxenite I intersected by borehole ZF048 is similar to that intersected by borehole ZF044 in terms of accessory minerals and sulfides mineralisation. However, feldspathic pyroxenite I in borehole ZF048 is extensively altered due to metasomatism/hydrothermal fluid activities. The alteration features include sericitization of plagioclase to sericite. Sulfides minerals (pyrite, chalcopyrite and pentlandite) occur as interstitial phase between cumulus orthopyroxene and clinopyroxene.

4.3.2.1.2. Feldspathic pyroxenites II

A coarse-grained feldspathic pyroxenite II (FP II) with interlocking texture is the dominant rock in the Platreef package in borehole ZF048. Feldspathic pyroxenite II contain primary minerals such as orthopyroxene (85-70 vol. %), clinopyroxene (5-25 vol. %) and plagioclase (10-5 vol. %). Accessory minerals are sulfides, quartz, hematite and ilmanite (5 vol. %). Orthopyroxene (5-10 mm) occurs as phenocryst in plagioclase (< 1 mm) groundmass giving rise to poikilitic texture with subhedral to anhedral grains (Plate 4.4 a and c). Feldspathic pyroxenite II intersected by borehole ZF048 shows extensive effect of hydrothermal fluids evidenced by the presence of serpentine and talc veins (Plate 4.4a-c). Similar results were previously reported by Armitage et al. (2002) where the presence of seperntine microveins was attributed to intense infiltration of hydrothermal fluids in Sandsloot. The difference between feldspathic pyroxenite II intersected by borehole ZF044 and by ZF048 is that FP II in the later shows interlocking texture, extensively fractured and large orthopyroxene crystals (5-10 mm). Orthopyroxene crystals in borehole ZF048 also show some small disequilibrium texture such as embayed texture as a result of resorption (Plate 4.4c). Secondary minerals include sericite, amphibole, talc and chlorite. The alteration of orthopyroxene to amphibole (tremolite and actinolite) by hydrothermal fluid is well preserved in sample ZF048-46 (Plate 4.4d). FP II is extensively mineralised with sulfides mineralisation such as chalcopyrite, pentlandite and

pyrrhotite which occurs as dissiminated irregulary-shaped minerals between orthopyroxene and clinopyroxene minerals.

4.3.3.2. Orthopyroxenite

Orthopyroxenite consists of orthopyroxene (90 vol. %), clinopyroxene (5 vol. %) and plagioclase (5 vol. %). Accessory minerals include biotite and quartz (<1 vol. %). Medium-grained orthopyroxenite with equigranular texture intersected at 1514 m forms a boundary between FP I and FP II sills (Figure 4.2). Orthopyroxene (3-5 mm) occurs as cumulus subhedral crystals with interstitial clinopyroxene (< 1mm) and plagioclase (< 0.5 mm). Orthopyroxene shows an interlocking texture with some of actinolite occurring as interstitial around the margins of cumulus orthopyroxene (Plate 4.5a-b). Secondary minerals are actinolite and tremolite resulted from alteration of orthopyroxene. Actinolite is randomly oriented and exhibit a lath-like shape between orthopyroxene crystals (Plate 4.5b). No sulfides minerals were noted in orthopyroxenite rocks.

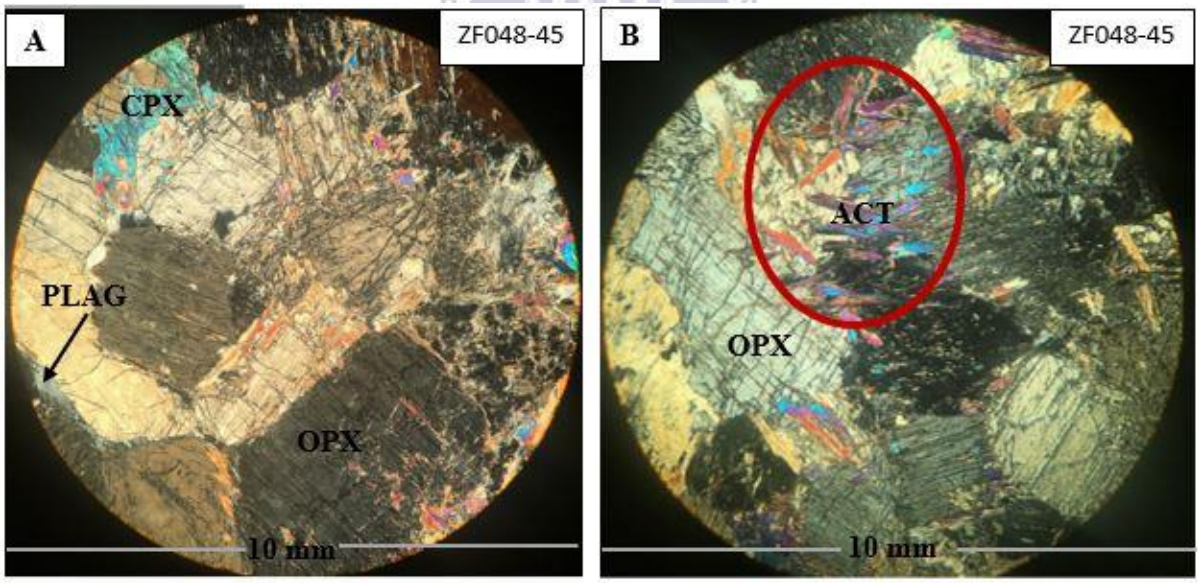

Plate 4.5: Medium grained orthopyroxenite **(a)** Subhedral orthopyroxene with interstitial clinopyroxene, plagioclase and actinolite. **(b)** Subhedral crystals of cumulus orthopyroxene with the inclusion of randomly oriented laths shaped actinolite.

4.3.3.3. Platreef Norite

The Platreef norite is medium- to coarse-grained with grain size ranging between 10mm to 20mm (Plate 4.6). Platreef norite contain plagioclase (75-60 vol. %), orthopyroxene (5-10 vol. %) and clinopyroxene (15-10 vol. %). Norite also contains minor sulfides mineralisation with

accessory minerals such as biotite, quartz and oxides (< 2 vol. %). Plagioclase is anhedral-subhedral, laths-shaped and occurs as both cumulus and intercumulus crystals with minor polysynthetic twinning (Plate 4.6a-b). Platreef norite occurs as intercalated layers between feldspathic pyroxenite II sills towards the upper Platreef succession. Secondary minerals are sericite which resulted from alteration of plagioclase during metasomatic processes.

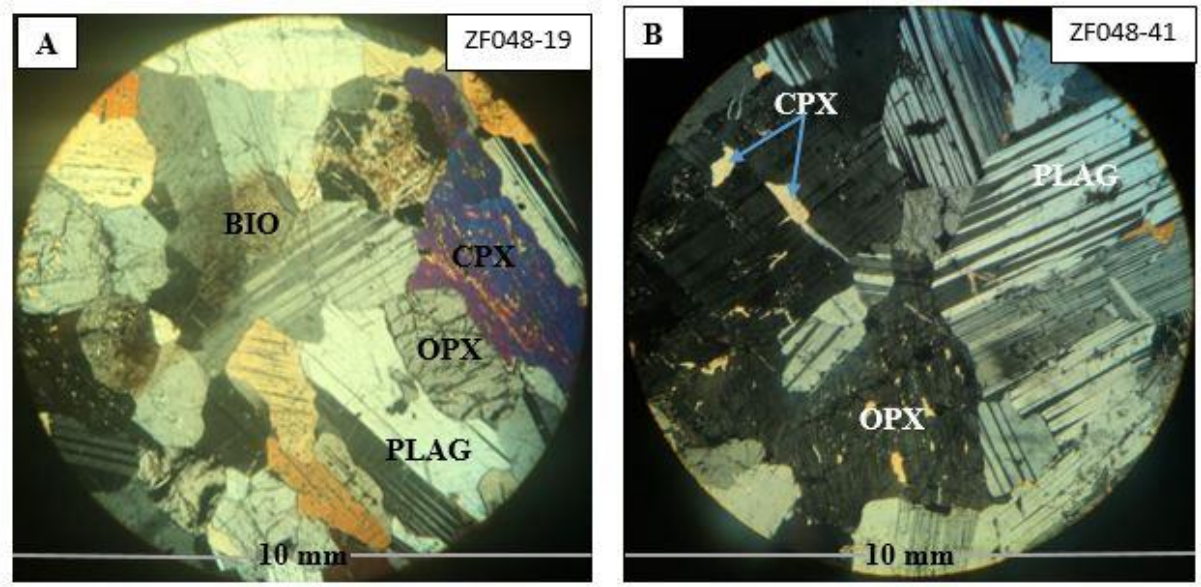

Plate 4. 6: Platreef norite showing interlocking texture (**a**) Cumulus plagioclase and orthopyroxene intergrown with interstitial clinopyroxene. Biotite occurs as a dusty band cross-cutting cumulus plagioclase and orthopyroxene. (**b**) Cumulus plagioclase and orthopyroxene interwined with interstitial clinopyroxene. Plagioclase is slightly altered to sericite. Orthopyroxene contains anhedral exsolved lamellae inclusion of clinopyroxene.

4.3.3.4. Footwall granite

The Platreef rocks in borehole ZF048 are underlain by coarse-grained footwall granite. Granite consists of quartz (60-30 vol. %), plagioclase (40-35 vol. %), orthoclase (~15 vol. %) and biotite (~10 vol. %). Plagiclase (3mm) and quartz (3-4 mm) occur as cumulus set in biotite, muscovite and microcline groundmass giving rise to porphyritic texure. Plagioclase is moderatly altered to sericite. No sulfides minerals were noted in granite rocks.

4.4. Borehole ZF057

4.4.1. Lithostratigraphy of the Platreef in borehole ZF057

Borehole ZF057 intersected the Platreef package at a depth of 1248.93 m with the average thickness of 272.35 m. The Platreef rocks intersected by borehole ZF057 varies from alternating sills of variable feldspathic pyroxenites, harzburgite, orthopyroxenites, and chromitites separated by calc-silicates xenoliths and parapyroxenites (Figure 4.3). The footwall consist of ~5 m medium- to coarse-grained granofels. Overlying granofels is a relatively thin sill (~0.5 m) of chromite-rich feldspathic pyroxenite I. Feldspathic pyroxenite I occur as two sills of variable thickness at the base and the top of the Platreef (Figure 4.3). Feldspathic pyroxenite I is overlain by four sills of feldspathic pyroxenite II with variable thickness (~20 – 150 m). FP II sills are separated by calc-silicates (~1.5 – 5 m), parapyroxenite (~0.5 – 10 m) and chromitite (< 1.5 m). Overlaying FPII is a ~20 m sill of medium to coarse-grained FP III. Parapyroxenite, calc-silicate, FP I and FP II are variably mineralised with disseminated sulfides (chalcopyrite, pentlandite and pyrrhotite).

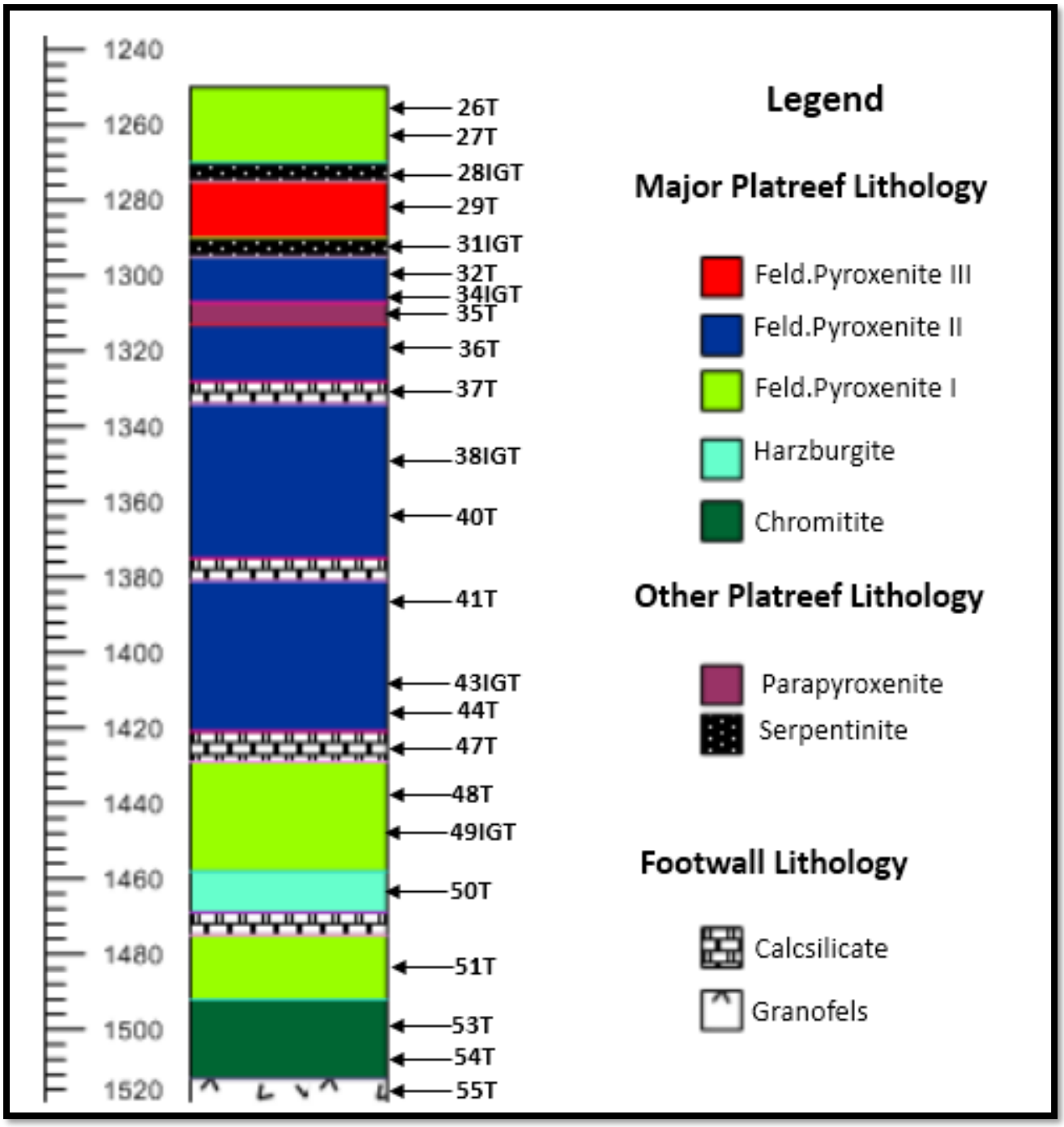

Figure 4.3: Lithology log for borehole ZF057 with sample numbers labelled IGT and T, where IGT represent samples that were used for isotope, geochemistry and thin-section respectively. And samples labelled T only were used for thin-section analysis.

4.4.2. Description of the Platreef lithologies in borehole ZF057

4.4.2.1. Platreef feldspathic pyroxenites

Feldspathic pyroxenite I and III intersected by borehole ZF057 is the same as the ones described in borehole ZF044 in section 3.2.2.2. Therefore, for this reason only feldspathic pyroxenite II will be described in this section for borehole ZF057.

4.4.2.1.1. Feldspathic pyroxenites II

Coarse-grained feldspathic pyroxenite II (FP II) exhibit a poikilitic texture and major minerals include orthopyroxene (85-70 vol. %), clinopyroxene (5-25 vol. %) and plagioclase (10-5 vol. %). Accessory minerals include sulfides, hematite, biotite and microcline (3 vol. %). Orthopyroxene (8-10 mm) and clinopyroxene (3-5 mm) occurs as cumulus in plagioclase oikocryst giving rise to poikilitic texture. Clinopyroxene also occurs as exsolved lamellae within cumulus orthopyroxene (Plate 4.7a). Some orthopyroxene when in contact with plagioclase reacts to form clinopyroxene coronas around orthopyroxene crystals (Plate 4.7b). In borehole ZF057, feldspathic pyroxenite II forms alternating layers with parapyroxenite and they are confined (top and bottom) by feldspathic pyroxenite I. Plagioclase and orthopyroxene were moderately altered to sericite and amphibole, respectively. FP II is extensively mineralised with disseminated sulfides mineralisation such as chalcopyrite, pentlandite and pyrrhotite (Plate 4.7a).

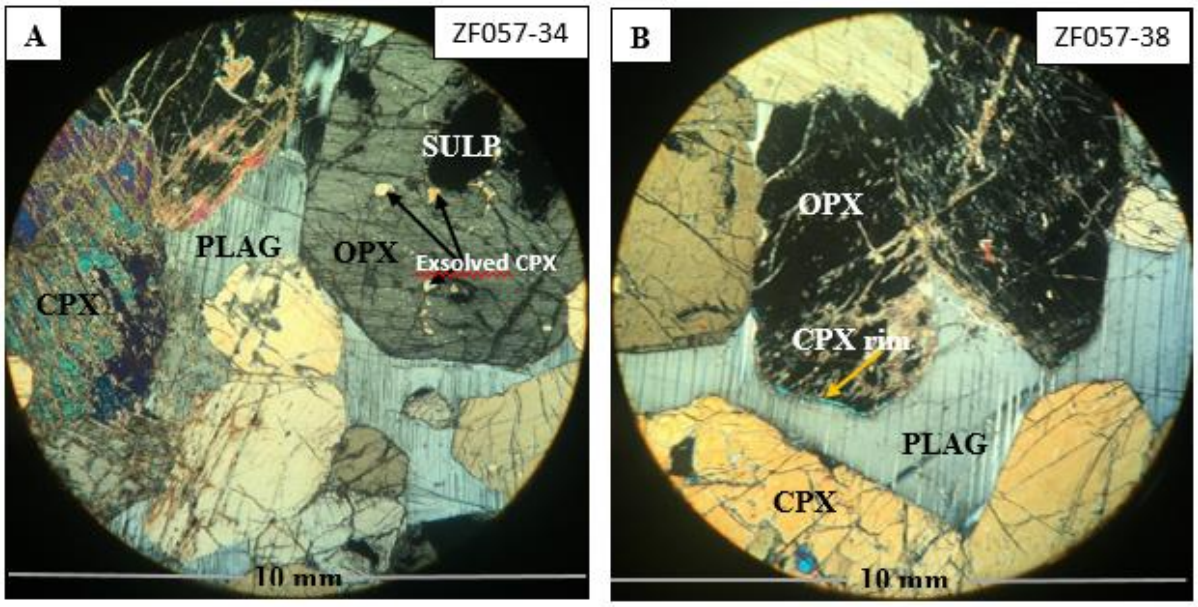

Plate 4.7: Feldspathic pyroxenite II (**a**) Cumulus orthopyroxene and clinopyroxene occurs as euhedral phenocrysts enclosed within plagioclase oikocryst. Orthopyroxenes contains sulfides and exsolved clinopyroxene. Sulfides occur as disseminated inclusions within euhedral orthopyroxene. (**b**) Euhedral orthopyroxene surrounded by a pure rim of clinopyroxene and other minerals include cumulus clinopyroxene with intercumulus plagioclase.

4.4.2.2. Chromitite

Chromitite layers extensively occur in the Critical Zone of the western and the eastern limbs of the Bushveld Complex, but their occurrence in the Platreef of the northern limb is very rare and erratic. Holwell and McDonald (2006) recognised the occurrence of erratic, relatively thick chromitites in the Sandsloot open pit mine. Chromitites at Zwartfontein farm were only intersected by borehole ZF057. According to Holwell and McDonald (2006), the erratic occurrence of chromitites in the Platreef is essential in identifying the mechanism that triggered the formation of mineralisation in the Platreef.

Chromitite is medium-to fine-grained, dark and contain sulfides minerals such as pentlandite, pyrrhotite and chalcopyrite. Chromitites identified in borehole ZF057 were hosted between feldspathic pyroxenite and pyroxenite ultramafic rocks of the Platreef package. The occurrence of chromites at Zwartfontein is associated with feldspathic pyroxenite I (Plate 4.8a-b) and olivine-rich rocks (Plate 3.15c-d) referred to as harzburgite in the present study. Chromite bearing feldspathic pyroxenite I is similar to the one intersected by borehole ZF044 explained in section 4.3.2.

Harzburgite consist of cumulus olivine (90 vol. %) with interstitial orthopyroxene (10 vol. %). Olivine in harzburgite are well rounded and moderately fractured (Plate 4.8c). Accessory minerals are chromite and sulfides (10 vol. %). Olivine (2-3mm) and orthopyroxene (2mm) show interlocking textures. Chromite occurs as dark green, euhedral-subhedral crystals enclosed within olivine in harzburgite and within plagioclase, orthopyroxene and clinopyroxene in feldspathic pyroxenite I (Plate 4.8a-d). Chromite bearing rocks show a slight alteration of plagioclase and olivine to sericite and serpentine, respectively. Sulfides (pyrrhotite, pentlandite and pyrite) minerals occurs as irregular-shaped disseminated minerals.

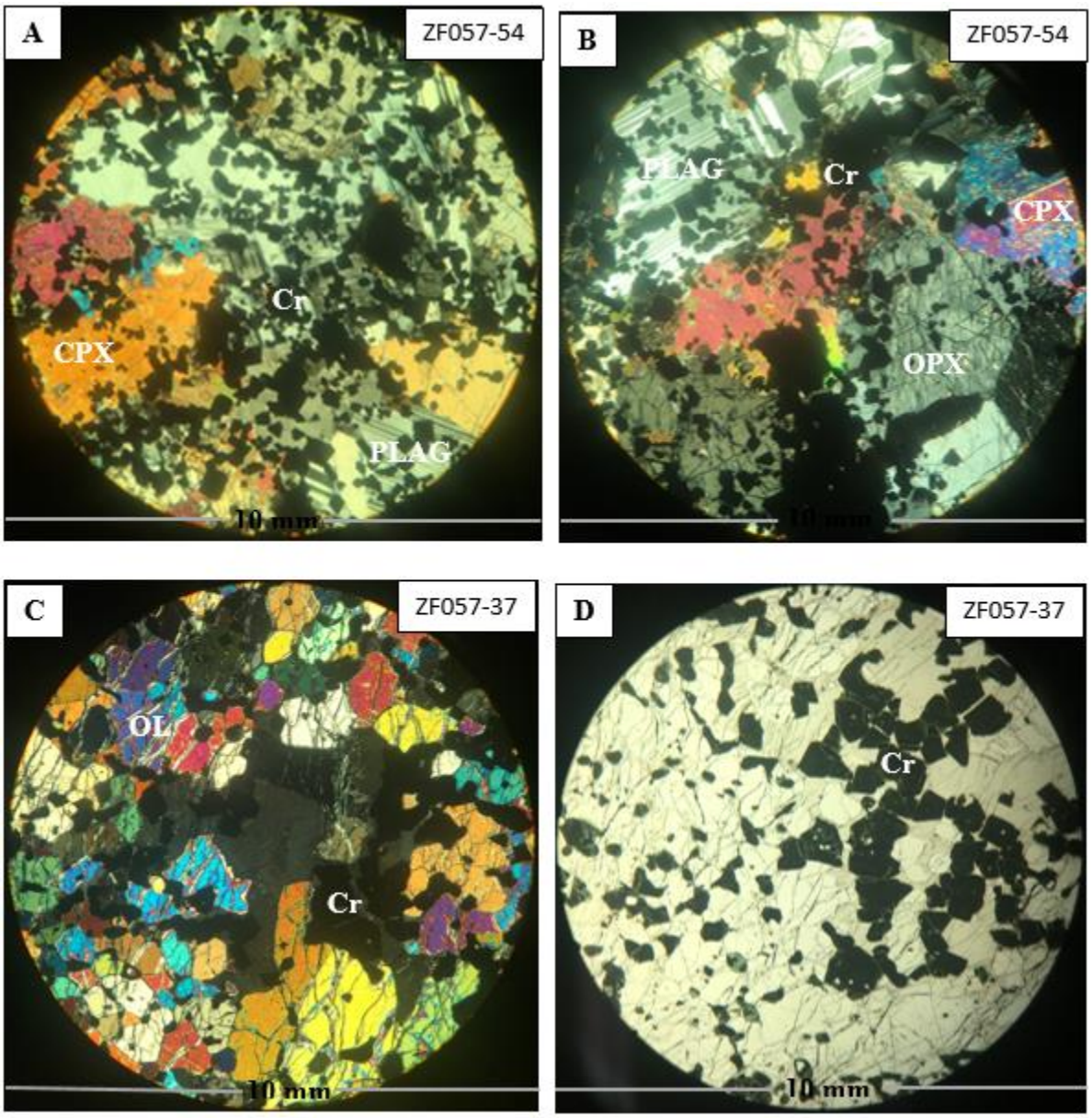

Plate 4.8: (**a-b**) Chromite-rich feldspathic pyroxenite I intersected by borehole ZF057 at the depth of 1513.10 m consists of cumulus orthopyroxene and clinopyroxene with intercumulus plagioclase and microcline. (**c-d**) Chromite-rich harzburgite intersected by borehole ZF057 at the depth of 1347.64 m consists of 90% olivine with interlocking texture.

4.4.2.3. Parapyroxenite

In the current study, parapyroxenite is referred to an intermediate rock type between Platreef pyroxenites and calc-silicates. Parapyroxenite consist of olivine (60-70 vol. %), clinopyroxene (25-20 vol. %) and orthopyroxene (15-10 vol. %). Accessory minerals include sulfides and biotite (3 vol. %). Olivine (5mm) and clinopyroxene (2-3mm) occurs as cumulus phase in orthopyroxene (2mm) oikocryst giving rise to poikilitic texture. Parapyroxenite intersected by borehole ZF057 is dark, medium- to fine-grained rock that forms a gradual contact with calc-silicate (Plate 4.9). Parapyroxenite was moderate to extensively metasomatised/altered and appears dark green due to chloritization (Plate 4.9-4.10). Parapyroxenite contains significant amount of disseminated sulfides mineralisation (chalcopyrite, pentlandite and pyrite) and thin veins of altered olivine to serpentine which indicate hydrothermal fluid activities (Plate 4.10).

Plate 4.9: Parapyroxenite intersected by borehole ZF057 at a depth of 1403m showing a gradational contact with calc-silicate and high sulfides mineralisation.

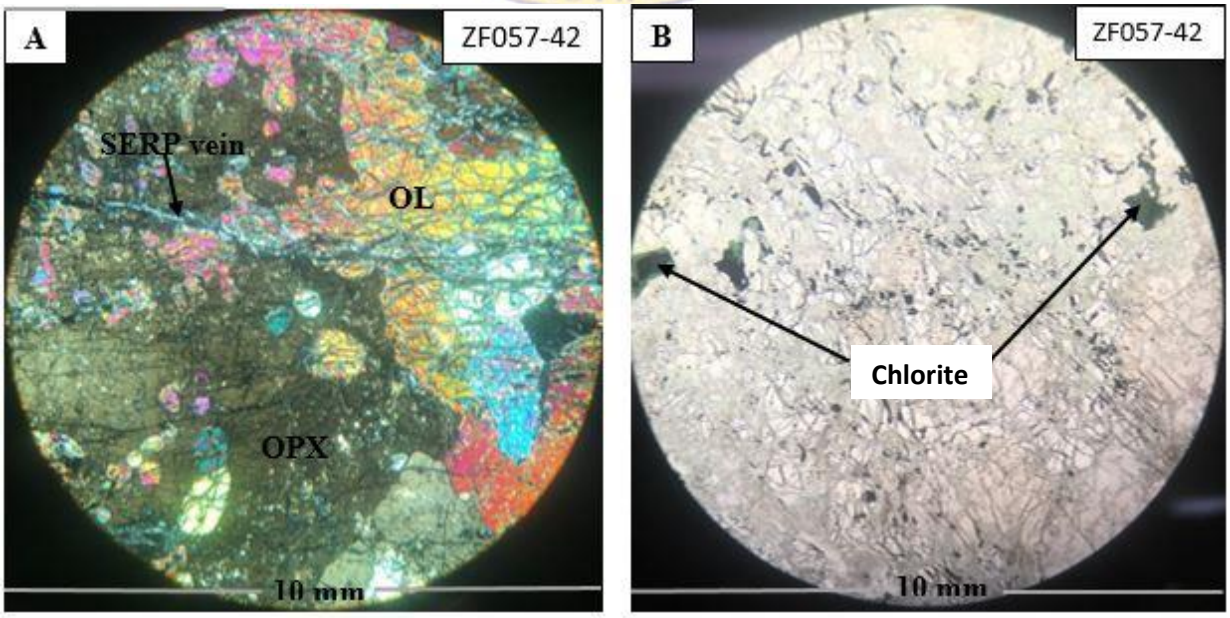

Plate 4.10: Parapyroxenite ***(a)*** Parapyroxenite under polarized light shows euhedral to subhedral olivine within orthopyroxene oikocryst. Olivine is cut through by serpentine veins. ***(b)*** Parapyroxenite under plane-polarized light, note the dark green chlorite crystals

Serpentinised harzburgite

Harzburgite is a dark black, coarse-grained rock consisting of olivine (75-65 vol. %), orthopyroxene (25-30 vol. %) and clinopyroxene (<5 vol. %). Accessory minerals include sulfides and hematite (3 vol. %). Olivine (10mm) is euhedral-subhedral occuring as a cumulus phase enclosed within orthopyroxene (5mm) and clinopyroxene (4mm) giving rise to poikilitic texture (Plate 4.11a). Harzburgite also contains veins of serpentinised olivine with the thickness that varies from 1 mm to 3 mm (Plate 4.11b). Harzburgite contain moderate to high sulfides minerals such as chalcopyrite, pentlandite and pyrhotite (1-2mm). Sulfides mineralisation are associated with serpentine veins and in places the serpentine forms rims around sulfides mineralisation. In less serpentised harzburgite, cumulus olivine minerals still maintain their euhedral shape (Plate 4.11a).

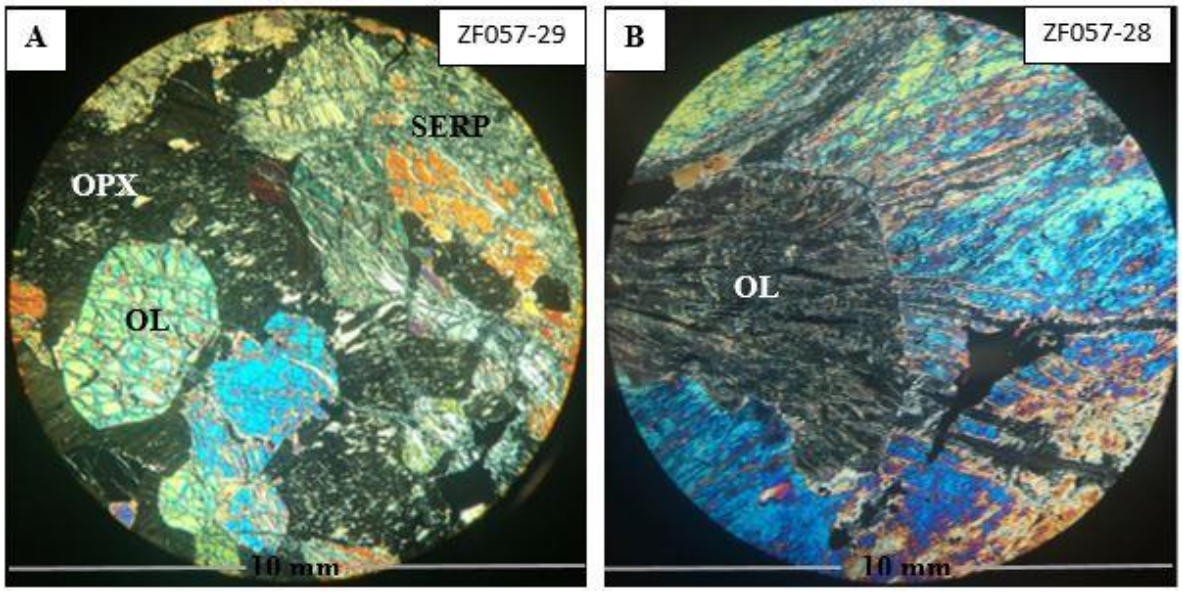

Plate 4.11: Harzburgite (**a**) Orthopyroxene occurs as a large oikocryst enclosing euhedral to subhedral olivine. Olivine is serpentinized and contains veins of serpentine of which some are filled with sulfides and oxides. Some olivine is completely altered to serpentine. (**b**) subhedral olivine cut through by several serpentine veins.

4.4.2.4. Footwall granofels

Granofels was formed through metamorphism during the interaction between the footwall rocks and the Platreef magma. Granofels are medium- to coarse-grained rocks that underlie the

Platreef rocks and were intersected by borehole ZF057. Granofels consist of Plagioclase (50 vol. %), Quartz (35 vol. %) and Orthopyroxene (15 vol. %). Accessory minerals include biotite and garnet (1 vol. %). Granofels consist dominantly of equant quartz grains (5mm) and plagioclase (3mm) with minor mafic minerals such as orthopyroxene (2mm) and garnet (2mm) and shows a granoblastic texture. Plagioclase was moderately altered/metasomatised to sericite. No sulfides minerals observed in granofels.

Summary

This section present the summary of the Platreef lithology based on the logs and petrography outlining the similarities and differences between the Platreef rocks.

The similarity between the three feldspathic pyroxenite types (FP I, FP II and FP III) lies in their cumulus orthopyroxene and clinopyroxene contents, although their relative volume varies (Table 4.1). Feldspathic pyroxenite I is a fine-grained rock which dominate the lower Platreef and is characterized by high orthopyroxene, moderate olivine, low clinopyroxene and plagioclase. Feldspathic pyroxenite II is a coarse-grained rock which dominate the middle Platreef and is characterized by high orthopyroxene and clinopyroxene with low plagioclase (Table 4.1). Feldspathic pyroxenite II is distinguished from feldspathic pyroxenite I because it is coarse-grained, contains high orthopyroxene and clinopyroxene and shows the absence of olivine. In terms of PGE and BMS mineralisation, both FPI and FPII contains moderate to high irregularly-shaped disseminated mineralisation. On the other hand, feldspathic pyroxenite III is a medium- to fine-grained rock characterized by orthopyroxene and clinopyroxene with significantly high plagioclase compared to FPI and FPII. FP III does not contain PGE and BMS mineralisation. Harzburgite is a medium- to fine-grained rock characterized by high olivine with orthopyroxene occurring as oikocryst phase. Harzburgite, when compared to FP I and FP II contains significantly high PGE and BMS mineralisation. Parapyroxenite is a medium- to fine-grained rock and it is distinguished from other Platreef rocks because it was formed through metasomatic processes and it contains significantly high dissiminated BMS mineralisation.

FP I and FP II are moderately to extensively affected by metasomatic processes especially those intersected by borehole ZF048. Both FP I and FP II shows alteration of orthopyroxene to amphibole (tremolite and actinolite) and plagioclase to sericite. On the contrary, FP III and norite shows low effect of metasomatic processes where plagioclase are slightly altered to

sericite. Harzburgite, when compared to FP I, FP II and FP III is extensively affected by metasomatic processes where olivine is completely altered to serpentine.

Table 4. 1: Petrographic summary of the Platreef rocks, including the footwall rocks intersected by borehole ZF044, ZF048 and ZF057 at Zwartfontein.

Lithologies		**Texture and Alterations**	**Mineral assemble and Abundance**
Major Plareef rocks (Felspathic pyroxenite)	**FP I**	Fine-grained Poikilitic texture Sericitization and chloritization	Primary: Orthopyroxene (65 vol. %), Olivine (10 vol. %), Clinopyroxene (15 vol. %) and Plagioclase (10 vol. %). Accessories: Sulfides, biotite, quartz and hematite Seconadry: Sericite
	FP II	Coarse-grained Poikilitic texture Sericitization, chloritization, serpentinization, amphibole	Primary: Orthopyroxene (70 vol. %), Clinopyroxene (25 vol. %) and Plagioclase (5 vol. %). Accessories: Biotite, sulfides, quartz, hematite and ilmanite. Secondary: Amphibole, chlorite and sericite.
	FP III	Medium- to coarse-grained Poikilitic texture Sericitization	Primary: Orthopyroxene (60 vol. %), Clinopyroxene (25 vol. %) and Plagioclase (15 vol. %). Accessories: Biotite and quartz Secondary: Sericite
Other Platreef rocks	**Harzburgite**	Medium- to fine-grained Porohyritic texture Serpentinization, Amphibole	Primary: Olivine (65 vol. %), Orthopyroxene (30 vol. %) and Clinopyroxene (< 5 vol. %). Accessory: Sulphide and hematite Secondary: Amphibole
	Orthopyroxenite	Medium-grained Interlocking texture Amphibole	Primary: Orthopyroxene (> 90 vol. %), Clinopyroxene (< 5 vol. %) and Plagioclase (< 5 vol. %). Accessories: Biotite Secondary: Tremolite and actinolite
	Norite	Medium- to coarse-grained Interlocking texture Sericitization	Primary: Plagioclase (75 vol. %), Clinopyroxene (15 vol. %) and Orthopyroxene (5 vol. %). Accessories: Quartz and biotite. Secondary: Sericite
	Parapyroxenite	Medium- to fine-grained Poikilitic texture Serpentinization Chloritization	Primary: Olivine (60 vol. %), Orthopyroxene (30 vol. %) and Clinopyroxene (10 vol. %). Accessories: Sulfides and biotite Secondary: Amphibole and chlorite
	Chromitite	Medium- to fine-grained Interlocking texture Serpentinization	Primary: Chromitite (70 vol. %), Olivine (20 vol. %) and Orthopyroxe (10 vol. %). Secondary: Serpentine and amphibole.
Footwall rocks	**Calc-silicate**	Medium- to fine-grained Intergranular texture Sericitization, chloritization and serpentinization.	Primary: Dolomitic/calcitic minerals (75 vol. %), Orthopyroxene (20 vol. %) and Plagioclase (5 vol. %). Accessories: Sulfides and biotite Secondary: Sericite
	Granofels	Medium- to coarse-grained Granoblastic Chloritization	Primary: Plagioclase (50 vol. %), Quartz (35 vol. %) and Orthopyroxene (15 vol. %) Accessories: Garnet

CHAPTER FIVE

5. WHOLE-ROCK GEOCHEMISTRY RESULTS

5.1. Introduction

This section covers the identification of petrogenesis of the Platreef and associated rocks through the use of whole-rock major and trace elements data and isotope geochemistry. Geochemical variations will be used to constrain the genesis of Platreef type PGE mineralisation by evaluating the magmatic history of the parental magma providing further knowledge about the nature of emplacement and effect of crustal/local footwall contamination. Whole-rock geochemistry results will also be used to confirm and validate the results from petrography in chapter four.

The main objective of this chapter is to (1) identify the lithological variations in the Platreef based on major and trace elements, (2) ascertain the effect of crustal contamination on both Platreef rocks and PGE mineralisation and (3) identify the isotopic variations (Sr-Nd isotope) in the Platreef rocks with the stratigraphic height. The above objectives are aimed at constraining whether the Platreef was formed from multiple sill-like intrusion or single magma intrusion and the effect of crustal contamination in the Platreef type PGE mineralisation.

The whole-rock major and trace elements were analysed using ICP-MS and XRF at Council for Geoscience and University of Cape Town respectively, and the data are presented in appendix 1.

Sr-Nd isotopes were analysed for 12 samples randomly selected from three boreholes (ZF044, ZF048 and ZF057) using Nu Instruments NuPlasma HR in the MC-ICP-MS facility at University of Cape Town and the data are documented in appendix 2. The data evaluation will be done using Geochemical Data Toolkit® (GCDkit) 3.00 software.

These data will be interpreted using the following methods:

- Geochemical classification and characterization of the Platreef rocks using whole-rock major elements was done to confirm and validate the results from petrography and identify the geochemical signatures of Platreef lithology. This objective was achieved through the classification of different types of Platreef lithology using hierarchical cluster analysis (HCA) and further identify the oxides elements controlling clustering of rocks using box and whisker plots. This was followed by geochemical

characterization of Platreef rocks using scatter plots and spider diagrams to understand major and trace elements fractionation between the Platreef lithology.

(1) Geochemical classification of the Platreef rocks

(i) Hierarchical cluster analysis

Firstly, hierarchical cluster analysis (HCA) was used to classify rocks depending on their geochemical compositions preferably major elements in this case. The compositional clustering of rocks was done to validate the rock identities from the petrographic studies. HCA is one of the cluster analysis technique which uses Euclidian distance to assign observations to a number of groups. Hierarchical cluster analysis groups together rocks that are geochemically similar and separate rocks that are geochemically heterogeneous. Hierarchical cluster analysis of the geochemical data would, therefore, enable identifying groupings with geochemical attributes that define the rock types identified in the Platreef through the use of petrographic studies in chapter four. The results from HCA are displayed as dendrograms.

(ii) Box and whisker plots

Following Hierarchical cluster analysis, is the box and whisker plots which were used to identify the oxides elements underpinning the different rock types. The use of box and whisker plots allows identification of major elements that define each rock type identified during petrography. Box and whisker plots also aid in establishing the compositional relationships between rock types.

(2) Geochemical characterisation of the Platreef rocks

(i) Scatter plots

Scatter plots, e.g. binary Harker diagrams, were employed, whereby MgO is a differentiation index (DI) plotted against the major elements. Binary Harker diagrams was used in assessing co-genetic nature of the mafic-ultramafic rocks, mineral distributions in the Platreef rocks and the sequence of mineral fractionation during the emplacement of the Platreef magma. Binary Harker diagrams also provided the information about the nature of magma emplacement, and to ascertain any underpinning cyclicity.

(ii) Spider diagrams

The main objective of spider diagrams was to use the trace elements (REE, LILE & HFSE) to validate the results given by the major elements in the characterization of the Platreef rocks.

The behaviour of LREE, HREE, LILE and HFSE will allow the comparison of elemental fractionation between the Platreef rocks. In particular, the understanding of elemental fractionation between the Platreef rocks gave insight into the nature and extent of contamination by footwall rocks.

(3) Mass balance

Mass balance analysis was employed to (1) evaluate the elemental exchange in rocks during hydrothermal activities to assess the effect and degree of hydrothermal alteration and (2) evaluate the degree of interaction between the footwall rocks and the Platreef magma at Zwartfontein. By applying mass balance analysis, elements added and removed during hydrothermal alteration were identified and the extent of hydrothermal alteration defined. The first step in mass balance analysis was to identify immobile elements that will be used to plot an isocon to distinguish between elements added and removed during alteration. Mass balance analysis was done by plotting altered rocks versus unaltered/least altered rocks. Elements that plot below and above the isocon represent those that were removed and added during alteration respectively. This analysis was done using GCDkit software which displays graphics that are easy to interpret.

(4) Chemostratigraphy

Chemostratigraphy was used to identify the relationship between base metal sulfides (Ni+Cu) and platinum group elements (Pt+Pd). The aim is to ascertain if the metasomatic/alteration processes identified during petrography and mass balance analysis have played a role in the redistribution of BMS and PGE mineralisation. The main objective of this section is to distinguish between mineralised rock layers from barren and to determine if the distribution of PGE mineralisation was primarily controlled by sulfides or by hydrothermal activities.

(5) Isotope geochemistry

Lastly, isotope geochemistry (Sr-Nd) was used to (1) identify the age of the Platreef rocks, (2) constrain better understanding about the parental magma source that gave rise to the formation of the Platreef (3) identify if the Platreef was formed from multiple sill-like intrusion or single intrusion and (4) identify the effect of crustal contamination in the Platreef rocks.

The above was done through evaluation of Sr-Nd isotope data using GCDkit software. Sr-Nd isotopes were analysed at the University of Cape Town using Nu Instruments NuPlasma HR

in the MC-ICP-MS facility. The Sr-Nd isotopes measured at UCT represent the isotope composition of the rocks on the present day. Therefore, the initial $^{87}Sr/^{86}Sr$ and $^{143}Nd/^{144}Nd$ isotope of the rocks is calculated from measured $^{87}Sr/^{86}Sr$ and $^{143}Nd/^{144}Nd$ data in conjunction with Rb and Sm rare earth elements using GCDkit software. The initial Sr-Nd isotope data are essential in understanding the parental magma source, the time of crustal contamination as to whether contamination occurred before crystallization or after that and also ascertain the degree/effect of crustal contamination.

5.2. Geochemical classification of the Platreef rocks

5.2.1. Cluster analysis

5.2.1.1. Hierarchical Cluster Analysis

The petrographic studies based on the mineralisation and texture have shown that the Platreef consist mainly of pyroxenites, feldspathic pyroxenites (FP I, FP II and FP III), harzburgite and norite. However, the distinct boundaries between these rocks could not be identified using petrography due to pervasive hydrothermal alteration. Therefore, the geochemical classification of rocks using the major elements is applied to identify the distinct boundaries between different rock types and to validate the results from petrography.

The HCA method using the major elements was selected as a suitable method for geochemical classification of rocks to group rock samples into clusters. This method involves grouping samples that are geochemically similar to one cluster and separate samples that are geochemically heterogeneous. There are two types of HCA methods known as agglomerative method and divisive method. The agglomerative method, in which each subject start as a single cluster and merges with closely related subjects sequentially until all subjects form one cluster. The divisive method is the opposite of agglomerative method, in which all subjects start in the same cluster and reverse until every subject is in a separate cluster (Everitt, 2001). According to Templ et al. (2008) a good outcome of cluster analysis result in several clusters where the observations within a cluster are as similar as possible while a significant difference exists between the different clusters. The similarity between observations is determined by the distances that exist between them in the multivariate data space. The most frequently used distances in clustering observations are Euclidean distance and the Manhattan distance. The later measures the distance parallel to the variable axes, rather than directly (Euclidean), and they both give more stable clusters compared to other distances (e.g. Gower distance and Canberra distance).

5.2.1.2. Hierarchical Cluster Analysis Results

Based on the HCA the Platreef rocks are divided into four main clusters using 1.4 as a cut-off Euclidean distance. From the dendrogram in figure 5.1, it can be seen that the primary Platreef rocks are feldspathic pyroxenite, pyroxenites, harzburgite and norite. The feldspathic pyroxenites group are subdivided into three subgroups namely FPI, FPII and FPIII. The results from HCA are in consistence with the results from petrography except for sample ZF044-34, which was misclassified as feldspathic pyroxenite in petrographic studies.

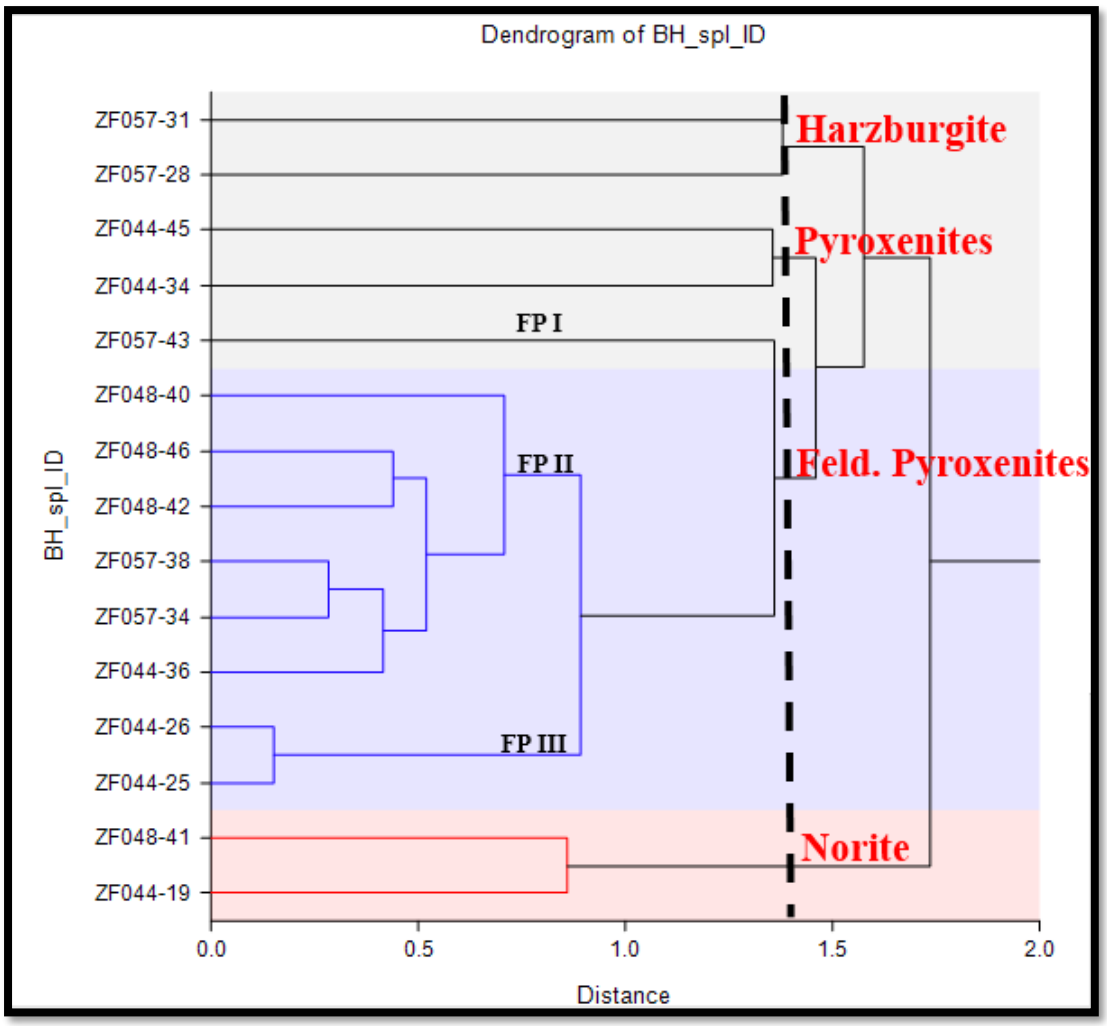

Figure 5. 1: Dendrogram showing the lithology of the Platreef at Zwartfontein, Akanani prospect.

5.2.2. Box and Whisker plots

The HCA was used in the previous section to classify the rock samples into different rock types, and the box and whisker plots will be used in this section to identify the oxides elements controlling the clustering distribution of samples into different rock types. The box and whisker plots of the major oxides versus rock types classified by HCA are shown in figure 5.2 and 5.3.

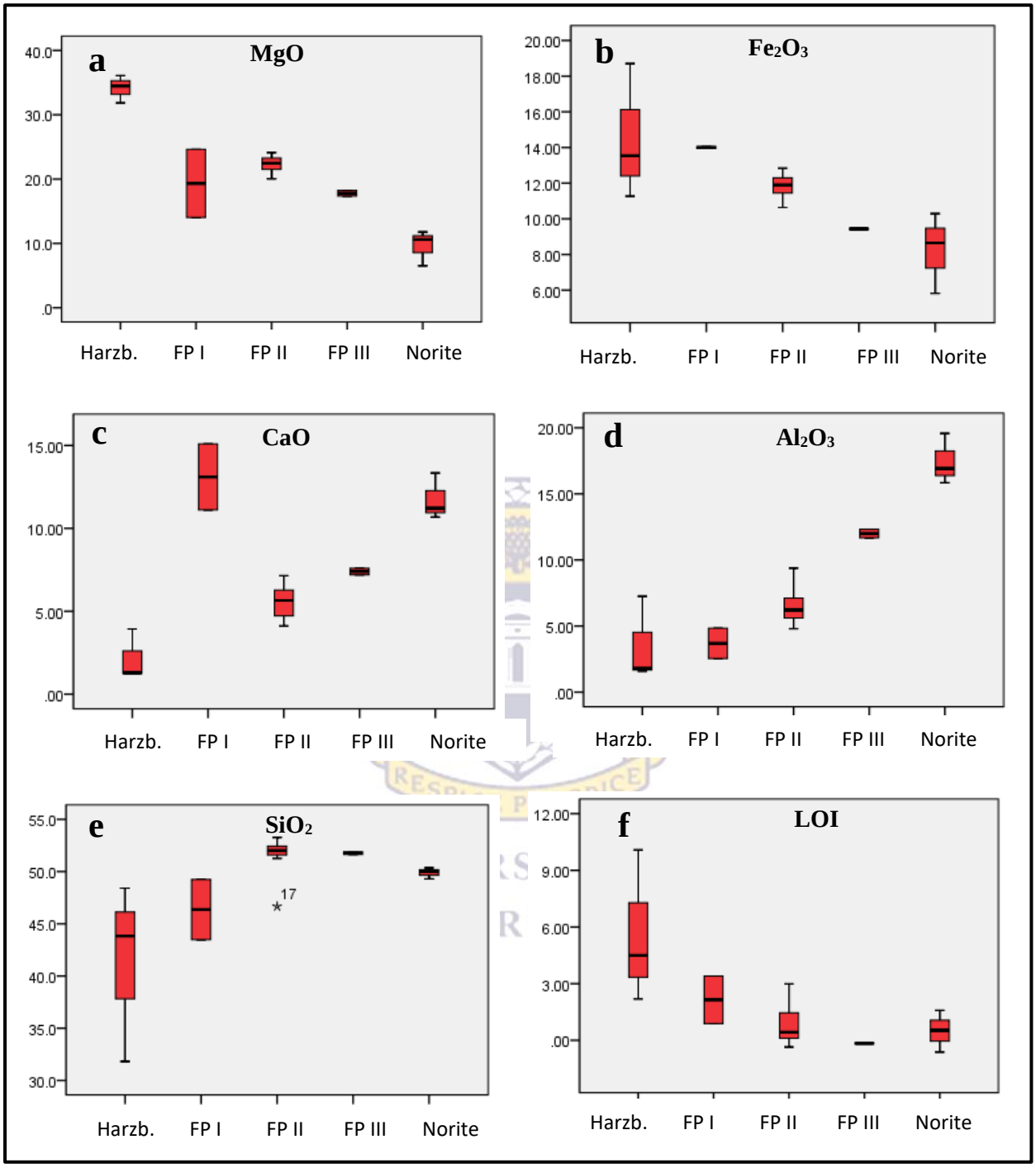

Figure 5. 2: Box and whisker plots showing major elements distribution in the Platreef rocks.

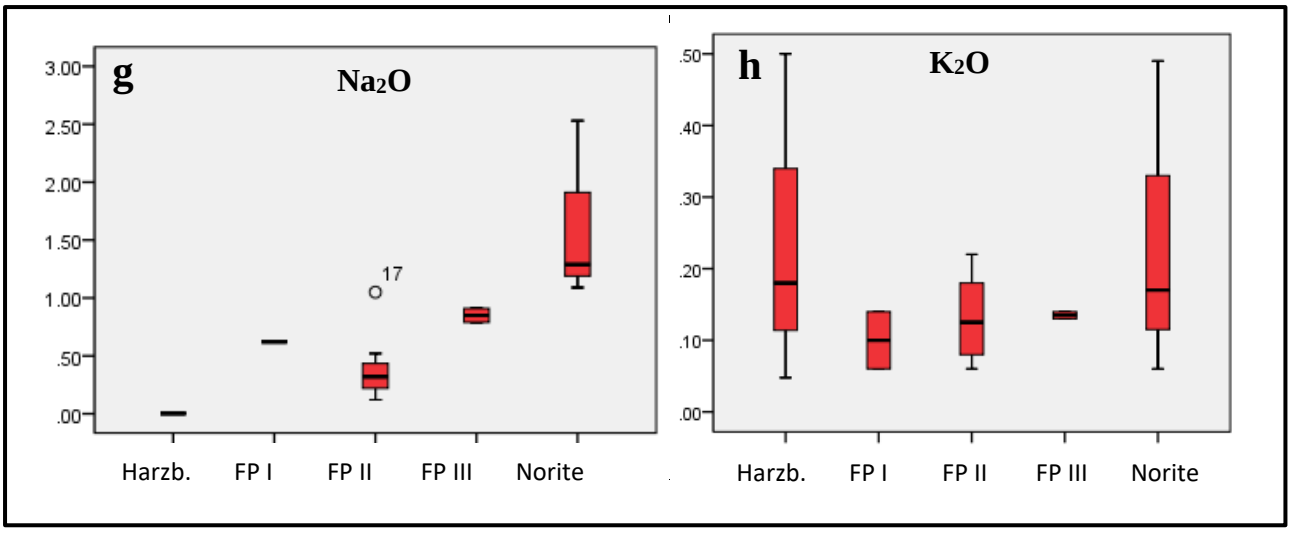

Figure 5.3: Box and whisker plots showing major elements distribution in the Platreef rocks.

The results from the box and whisker plots can be summarized as follows:

Feldspathic pyroxenite I

Box and whisker plots show high contents of MgO, Fe_2O_3, CaO and LOI in FP I (Figure 5.2 and 5.3). The high concentration of MgO and Fe_2O_3 results from early fractionation of ferromagnesian minerals such as olivine and pyroxenes. The high concentration of CaO in FP I is associated with both intercumulus plagioclase and Ca-rich pyroxene as noted in petrographic studies in chapter four. Besides, FP I is characterized by low contents of Al_2O_3, Si_2O, Na_2O and K_2O.

Feldspathic pyroxenite II

Feldspathic pyroxenite II is characterized by moderately high MgO, Fe_2O_3 and Si_2O with low CaO, Al_2O_3, Na_2O, K_2O and LOI (Figure 5.2 and 5.3). The moderately high concentration of MgO and Fe_2O_3 is also associated with fractionation of olivine and pyroxene minerals at the early stage of magma crystallization. FP II can be distinguished from FP I by low CaO content attributed to low concentration of plagioclase minerals. Low LOI in FP II compared to FP I represent low to moderate alteration of this rock type by hydrothermal alteration.

Feldspathic pyroxenite III

Feldspathic pyroxenite III contain low MgO and Fe_2O_3 compared to FP I and FP II, but it shows high Al_2O_3 and Si_2O. From the petrography, FP III consists of minor cumulus clinopyroxene and orthopyroxene with abundant intercumulus plagioclase, which in part occurs as cumulus phase. The above explains the low MgO, Fe_2O_3 and high Al_2O_3 in FP III.

The feldspathic pyroxenites subtypes, which is FP I, FP II and FP III, shows a decreasing trend of MgO, Fe_2O_3 and LOI from FP I, FP II and FP III respectively. Also, an increasing trend of Al_2O_3 and Si_2O occurs in the order; FP I, FP II to FP III respectively. The distribution of Na_2O and K_2O are relatively similar in all the subtypes of feldspathic pyroxenites.

Harzburgite

The box and whisker plots show that harzburgite contains relatively high MgO, Fe_2O_3 and LOI. High MgO and Fe_2O_3 are associated with significant occurrence of cumulus olivine, orthopyroxene and clinopyroxene minerals. High MgO and LOI in harzburgite are associated with hydrothermal alteration of olivine to serpentine. The above aligns with the occurrence of moderate to extremely altered olivine in harzburgite rocks (e.g. sample ZF057-28) as noted during petrographic studies. Harzburgite contains relatively low CaO, Al_2O_3, Na_2O and Si_2O as compared to FP I, FP II and FP II.

Norite

Norites are entirely different from FP I, FP II, FP III and harzburgite due to their relatively high CaO, Al_2O_3 and Si_2O with low MgO, Fe_2O_3 and LOI. High CaO and Al_2O_3 in norite is associated with the occurrence of felsic minerals such as cumulus plagioclase whereas low MgO and Fe_2O_3 is associated with the occurrence of intercumulus orthopyroxene and clinopyroxene. Besides, low LOI is associated with low hydrothermal alteration in norite.

5.3. Geochemical characterization of the Platreef rocks

5.3.1. Statistical summary

Table 5. 1: Statistical summary of major and trace elements of the Platreef rocks.

	FP I		FP II		FP III		Harzburgite		Norite	
	Mean	Std.Dev	Mean	Std.Dev	Mean	Std.Dev	Mean	Std.Dev	Mean	Std.Dev
SiO_2	46.36	4.07	51.50	2.04	51.76	0.18	41.36	8.57	49.89	0.54
Al_2O_3	3.69	1.63	6.51	1.42	12.00	0.46	3.54	3.21	17.45	1.92
MnO	0.30	0.01	0.22	0.01	0.71	0.01	0.15	0.03	0.15	0.04
Fe_2O_3	14.01	0.05	11.85	0.69	9.44	0.02	14.51	3.81	8.25	2.26
MgO	19.32	7.50	22.32	1.34	17.80	0.62	32.13	5.51	9.63	2.76
Mg#	69.93	8.36	77.01	5.57	77.06	0.65	79.91	2.27	66.62	12.76
CaO	13.10	2.81	5.57	1.02	7.40	0.28	2.15	1.54	11.75	1.41
Na_2O	0.32	0.43	0.39	0.29	0.85	0.08	0.01	0.004	1.64	0.78
K_2O	0.10	0.06	0.13	0.06	0.14	0.01	0.24	0.23	0.24	0.22
TiO_2	0.19	0.13	0.16	0.06	0.16	0.01	0.09	0.05	0.16	0.06
P_2O_5	0.03	0.00	0.03	0.01	0.03	0.00	0.02	0.01	0.03	0.00
LOI	2.15	1.77	0.83	1.09	-0.17	0.01	5.59	4.07	0.50	1.11
Ba	29.60	18.96	20.36	4.37	49.16	0.07	38.11	13.76	96.03	69.83
Cu	1077.05	1231.71	170.38	170.05	36.18	21.46	485.40	385.94	73.74	20.35
Co	99.24	17.91	86.87	3.59	67.44	3.62	134.80	28.14	41.64	0.51
Cr	1782.5	750.24	2286.80	396.69	1493	50.91	1104.75	260.57	575.88	369
Ce	6.73	6.17	3.51	1.52	5.26	0.34	1.44	0.62	7.16	3.83
Nb	0.29	0.03	0.33	0.16	0.23	0.16	0.13	0.04	1.00	0.91
Ni	2260.20	2070.13	789.52	241.66	437.7	1.27	1907	401.64	272.92	175.33
Rb	5.21	0.30	4.46	2.76	2.99	0.33	25.64	9.82	7.35	3.59
Sr	41.75	32.17	66.03	19.72	119.55	16.05	36.92	39.68	153.95	35
Y	9.60	8.36	4.33	0.99	4.57	0.21	1.83	0.77	7.72	6.82
Zn	81.65	8.49	81.67	7.17	70.99	7.45	81.37	8.63	52.33	17.04
Zr	12.50	8.98	8.45	3.85	7.70	1.81	5.14	3.47	13.56	8.20

5.3.2. Scatter Plots

Scatter plot is a bivariate plot, which is used to evaluate the relationship between two variables. The main objective of this section is to use bivariate plots to evaluate the relationships between the major oxides/ elements and their distribution in the Platreef rocks. The relationship between elements will, therefore, provide information about the sequence of mineral fractionation and the nature of emplacement of the Platreef magma.

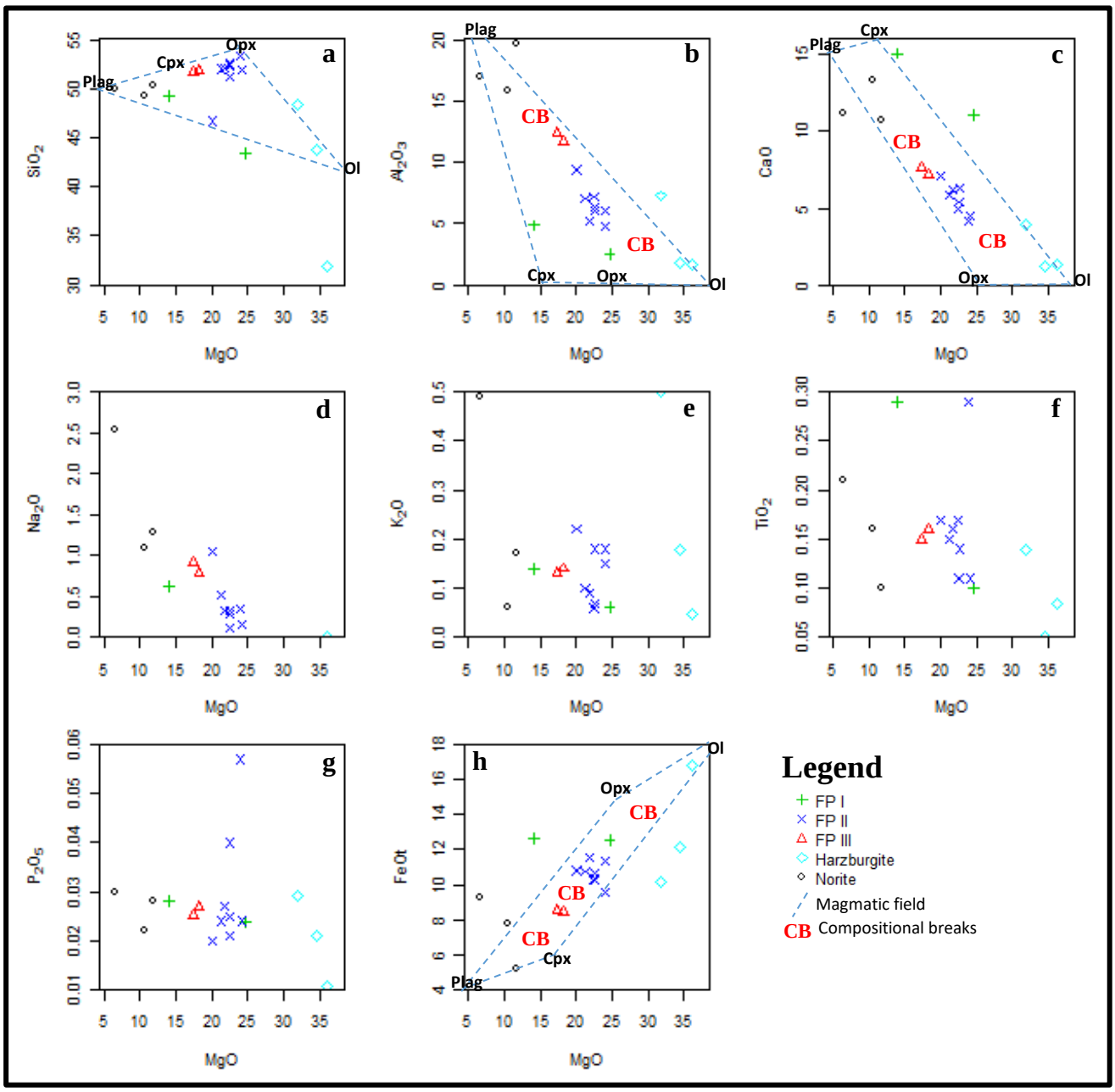

Figure 5.4: Binary Haker-type variation diagram of MgO (X-axis) plotted against oxides elements (Y-axis). The dotted line shows the magmatic field/trend with plagioclase (Plag), orthopyroxene (Opx), olivine (Ol) and clinopyroxene (Cpx). The CB indicate the compositional breaks between the Platreef rocks.

Binary Harker-type variation diagram with MgO plotted on the X-axis versus the major oxides elements in order to understand elemental fractionation between the Platreef rocks (Figure 5.4). Several evolutionary or fractionation indices can be used to determine the evolution or co-genetic nature of rocks such as Harker diagrams. In the current study, Harker diagram with MgO as Differentiation Index (DI) is preferred because the minerals that first crystallize out of the magma contain high MgO than the residual liquid.

Binary Harker-type variation diagrams show a positive correlation between MgO versus FeO and a negative correlation between MgO versus SiO_2, Al_2O_3, CaO, Na_2O, TiO_2 and P_2O_5 (Figure 5.4). In MgO versus P_2O_5 the negative correlation is visible for all the rocks except for feldspathic pyroxenites II where P_2O_5 increases at relatively constant MgO (Figure 5.4g). The negative correlation between mafic elements (MgO and Fe_2O_3) and felsic elements (SiO_2, Al_2O_3, CaO, Na_2O and K_2O) represent the decrease in mafic compositions (pyroxene and olivine) with an increase in felsic phases (plagioclase) with the stratigraphic height.

In the MgO versus SiO_2 binary diagram, most of the samples plot within the plagioclase-clinopyroxene-orthopyroxene-olivine field except for one sample of felspathic pyroxenite I and harzburgite that contains high MgO. The negative correlation between MgO and SiO_2 points to decreasing MgO as olivine and pyroxene crystallize out of the magma with increasing SiO_2 content in the residual melt (Figure 5.4a). The SiO_2 content of the Platreef rocks is relatively low with the lowest SiO_2 of 43.48 wt. % and 31.82 wt. % in sample ZF044-34 (feldspathic pyroxenite I) and ZF48-52 (serpentinised harzburgite) respectively. MgO versus SiO_2 diagram shows that SiO_2 began to increase in the early stage of crystallization at the expense of MgO due to crystallization of mafic minerals (olivine and pyroxene) and becomes almost constant in the later stage of crystallization (Figure 5.4a).

Al_2O_3 shows a negative correlation when plotted against MgO (Figure 5.4b). The negative relationship between Al_2O_3 and MgO can be attributed to the increase in plagioclase in the expense of mafic minerals such as olivine and orthopyroxene during fractional crystallization. The concentration of Al_2O_3 in rocks is primarily controlled by the abundance of plagioclase. The concentration of Al_2O_3 in the Platreef rocks varies between 1.79 wt. % - 2.54 wt. % for rocks that are depleted in plagioclase (pyroxenites and harzburgite) and between 4.8 wt. % - 19.58 wt. % for rocks that contain a significant amount of plagioclase (e.g. norite). High Al_2O_3 (11.67 wt. % - 19.58 wt. %) were found in norite rocks which contain cumulus plagioclase.

The binary Harker-type diagram for MgO versus CaO shows a negative correlation and most of the Platreef rocks plots within the olivine-orthopyroxene-clinopyroxene-plagioclase field (magmatic trend) with exception to feldspathic pyroxenite I and one sample of norite which shows a slight deviation from the magmatic trend (Figure 5.4c). Kinnard et al. (2005), have previously noted a similar trend for the Platreef rocks at Sandsloot. The fact that most of the rocks plots within the orthopyroxene-clinopyroxene-plagioclase field suggest that there was a limited effect of contamination by local footwall rocks in the Platreef rocks at Zwartfontein farm. These results are consistent with other studies that have been conducted in the Platreef (e.g. Manyeruke et al., 2005). The Platreef rocks contain relatively low CaO (1.25 wt. % - 7.59 wt. %) with exception to FP I and norite rocks which contain CaO between 10.68 wt. % - 15.09 wt. %. High CaO in FP I and norite can be attributed to the presence of Ca-rich pyroxene in the former and cumulus plagioclase in the latter.

A positive correlation exists between MgO and Fe_2O_3 (Figure 5.4h). This positive correlation is attributed to the crystallization of mafic minerals such as pyroxene and olivine. The early crystallization of mafic minerals gave rise to the formation of MgO-FeO rich rocks which include feldspathic pyroxenites (FP I, FP II and FP III) and harzburgites. The binary diagram of MgO versus FeO shows that most of the Platreef rocks plots within the olivine-orthopyroxene-clinopyroxene-plagioclase field which suggest that these rocks do not have excess or deficiency of FeO. All the feldspathic pyroxenite II and feldspathic pyroxenite III plots within the olivine-orthopyroxene-clinopyroxene-plagioclase field with slight deviation of norite, feldspathic pyroxenite I and serpentinised harzburgite (olivine-rich rock) from the magmatic field. According to Barton et al. (1986) the rocks that plot within the magmatic field have crystallized before contamination by footwall rocks.

In the studied Platreef rocks, feldspathic pyroxenites with MgO between 20 wt. % and 25 wt. % contain high Cr_2O_3 relative to low MgO rocks such as norite. Smith (2013) postulated that high MgO and Cr_2O_3 content is associated with the increase in pyroxene and chromite rich cumulates and a decrease in plagioclase content. The above is further supported by the occurrence of chromite-rich rocks, which contain cumulus chromite, with olivine, and clinopyroxene oikocryst and interstitial plagioclase at Zwartfontein farm as noted in the petrographic studies (chapter four).

The loss on ignition (LOI) is relatively low <0.5 wt. % for rocks with MgO <24 wt. % and LOI >2 wt. % for rocks with MgO >24 wt. %. This positive correlation between MgO and LOI can

be attributed to hydrothermal alteration of pyroxenes and olivine to secondary minerals (amphibole and serpentine) as noted during petrographic studies.

5.3.3. Summary

The sequence of mineral fractionation deduced from the binary Haker-type diagrams is olivine, orthopyroxene, clinopyroxene and plagioclase. Olivine and pyroxenes being the first minerals to crystalize are rich in MgO and FeO. The first rocks to crystallize from the magma such as harzburgite and pyroxenites are therefore rich in mafic elements (MgO and FeO). Plagioclase, which is characterized by high CaO and Al_2O_3 is the last mineral to crystalize and occurs as intercumulus/interstitial phase in pyroxenites and harzburgite rocks. The above indicates that plagioclase in the Platreef rocks with exception to norite; have crystallized from a trapped residual liquid. Norite and feldspathic pyroxenite III contain high CaO and Al_2O_3 which is associated with high plagioclase content.

The binary Harker-type diagrams for major oxides/elements shows that there are compositional breaks between the Platreef rocks. The compositional breaks indicate the transitional change from mafic minerals characterized by MgO and FeO to felsic minerals characterized by SiO_2, Al_2O_3, CaO, Na_2O and K_2O. The compositional breaks between the Platreef rocks is well defined where a good positive and negative relationship exist between MgO and element oxides (Figure 5.4b, c, d). The compositional breaks between norite and feldspathic pyroxenite III can be seen where MgO is between 12.5wt. % and 16.5 wt. %. The break between feldspathic pyroxenite III and feldspathic pyroxenite II occurs where MgO is 19.5 wt. % - 21 wt. % and the break between feldspathic pyroxenite II and serpentine harzburgite occurs where MgO is 26.5 wt. % to 33.5 wt. % (Figure 5.4b, c and h). The compositional breaks within the Platreef rocks indicate the change in orthopyroxene and plagioclase compositions giving evidence of multiple influxes of magma similar to those reported by Smith (2013). These results are consistent with Manyeruke (2003), where the occurrence of compositional breaks between the Platreef rocks was attributed to the formation of the Platreef in distinct sill-like bodies, converse to the intrusion of a single body. The formation of the Platreef from distinct sill-like intrusion is also supported by MgO reversals that were noted in the Platreef rocks.

5.3.4. Spider diagrams

Introduction

This section involves the use of REE plots in determining the element fractionation of light and heavy rare earth elements (LREE and HREE), as well as the behaviour of the Eu anomaly to assess the enrichment of feldspars in the Platreef rocks. Spider diagrams will be used to identify the behaviour of LILE (Sr, Rb and Ba) and HFSE (Th, U, Ce, Zr, Nb, Ti and Y) in feldspathic pyroxenites (i.e. FP I, FP II, FP III), harzburgite and norite.

According to Cox et al. (1989), different minerals may incorporate or exclude trace elements with even higher selectivity than they do for major elements. These preferences exert such a critical influence on trace elements distributions during igneous processes that their analysis can lead to constraints on the nature and composition of mineral assemblages. The distribution of trace elements is commonly used by petrologists to model the behaviour of minerals during either crystallization or partial melting (Tornos et al., 2006).

The main objective of this section was to use the trace elements to validate the results given by the major elements in characterization of the Platreef rocks in section 5.2.2. The behaviour of LREE, HREE, LILE and HFSE allowed the comparison of elemental fractionation between the Platreef rocks. Particularly the understanding of elemental fractionation between the Platreef rocks will, therefore, give an insight into the nature of contamination by footwall rocks and the possible sources of the Platreef magma.

The above was achieved by plotting REE and spider diagrams normalized to chondritic values (Sun and McDonough, 1989) and primordial mantle values (McDonough and Sun, 1995) respectively. The normalization of trace elements, for example, to primordial mantle values was to identify the original mantle concentrations before crustal contamination. Spider diagrams plot an array of trace elements on the X-axis in order of increasing incompatibility from left to right against elemental abundances on the Y-axis (Ridley, 2012).

(i) Feldspathic pyroxenite I

The REE diagrams for feldspathic pyroxenite I (Figure 5.5a) shows two distinct trends for both sample ZF044-34 and ZF044-45. The flat primitive-mantle-normalized pattern with low REE values defined by sample ZF044-34 point to a mantle source. Sample ZF044-34 also shows a substantial decrease in LREE from La to Sm while HREE remained relatively constant with a slight increase from Tm to Lu. In contrast, sample ZF044-45 shows a slightly negative trend

decreasing from Ce to Lu with a negative Eu anomaly. The high concentration of REE in sample ZF044-45 relative to ZF044-34 can be attributed to contamination by crustal materials. Sample ZF044-34 and ZF044-45 show a similar trend in LILE and HFSE except Eu which show positive anomaly in ZF044-34 and negative anomaly in ZF044-45 (Figure 5.5b). Sample ZF044-45 have relatively low $(Eu/Eu^{*})_{N}$ ratios (0.65) which account for negative Eu anomaly. In general, sample ZF044-45 is enriched in both LILE and HFSE relative to sample ZF044-34 although some HFSE have a negative anomaly.

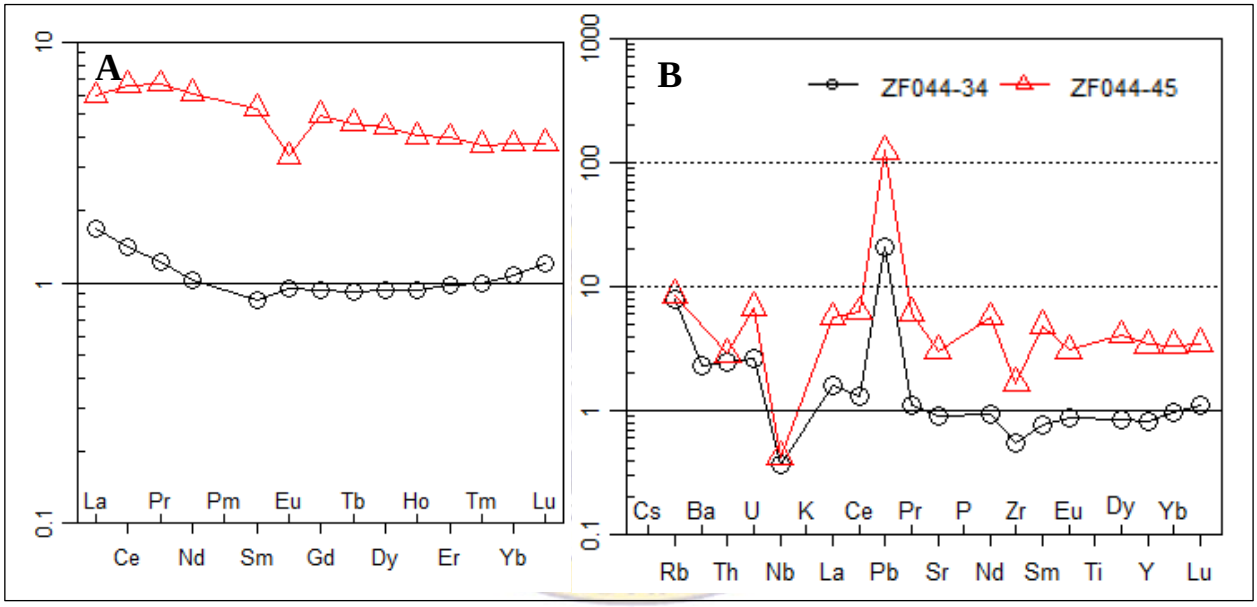

Figure 5.5: (a) REE diagram of feldspathic pyroxenite I normalized to the chondritic values of Sun and McDonough (1989). (b) Spider diagrams of feldspathic pyroxenite normalized to the primordial mantle values of McDonough and Sun (1995).

(ii) Feldspathic pyroxenite II

Feldspathic pyroxenite II is characterised by a substantial decrease in LREE with a sharp negative slope and a relatively constant HREE, which shows a slight increase from Tm to Lu (Figure 5.6a). Feldspathic pyroxenite II displays a positive Eu anomaly with exception to sample ZF044-36 and ZF048-40, which shows the absence of Eu anomaly. Feldspathic pyroxenite II, when compared to feldspathic pyroxenite I, shows a steep REE pattern whereas FP I displays a near flat REE pattern.

The spider diagrams for feldspathic pyroxenites II have similar trends with positive Rb, U, La, Pb and Sr (Figure 5.6b). Feldspathic pyroxenite II shows enrichment in large ion lithophile elements relative to high field strength elements. The large ion lithophile elements are more fractionated compared to high field strength elements that show a flat pattern. Sample ZF048-40 have $(La/Lu)_{N}$ ratio high than 3 indicating relatively high degree of fractionation compared

to other samples. Feldspathic pyroxenite II has low $(Eu/Eu^{*})_N$ ratios ranging from 0.91 to 1.31 which is consistent with low positive Eu anomaly and low feldspar content compared to other Platreef rocks.

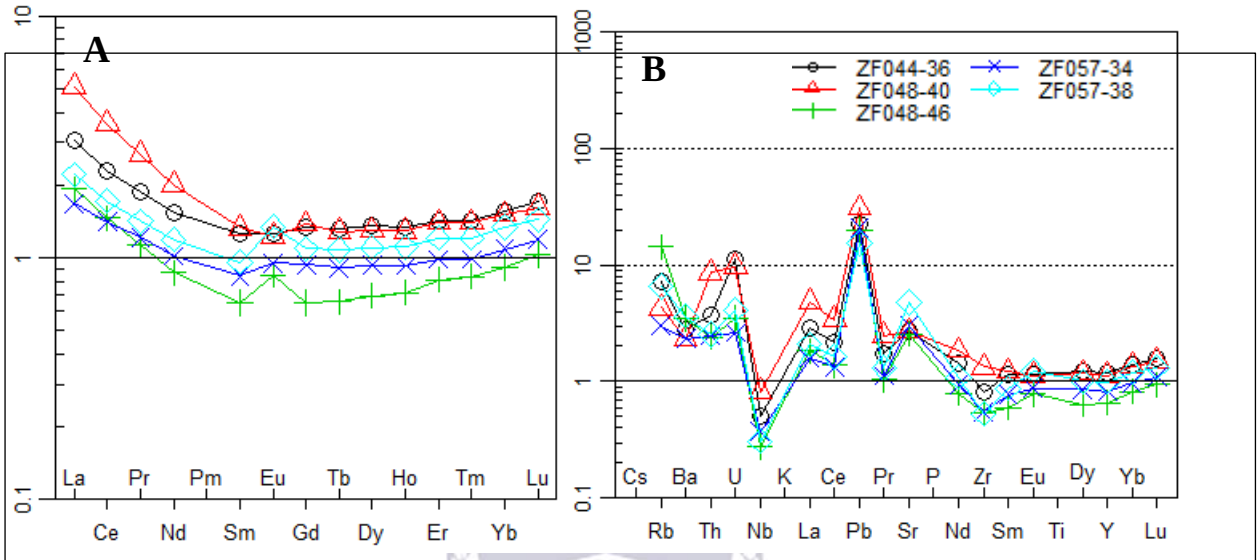

Figure 5.6: (a) REE diagram of feldspathic pyroxenite II normalized to the chondritic values of Sun and McDonough (1989). (b) Spider diagrams of feldspathic pyroxenite II normalized to the primordial mantle values of McDonough and Sun (1995).

(iii) Feldspathic pyroxenite III

Feldspathic pyroxenite III shows a similar trend with feldspathic pyroxenite II, and they are characterized by steep LREE slope and a flat HREE with a positive Eu anomaly (Figure 5.7a). When comparing FP III to FP II in terms of spider diagrams, feldspathic pyroxenite III have negative Rb anomaly and positive Ba anomaly (Figure 5.7b). The enrichment of Ba and Sr in FP III is attributed to high plagioclase content relative to FP I and FP II as noted in petrography. Feldspathic pyroxenite III displays negative HFSE anomalies for Th, Nb, Ce, Zr and Y. Trace elements in FP III show high degree of fractionation when compared to trace elements in FP II. The above is supported by high $(La/Lu)_N$ ratios that range between 2.79 to 3.50.

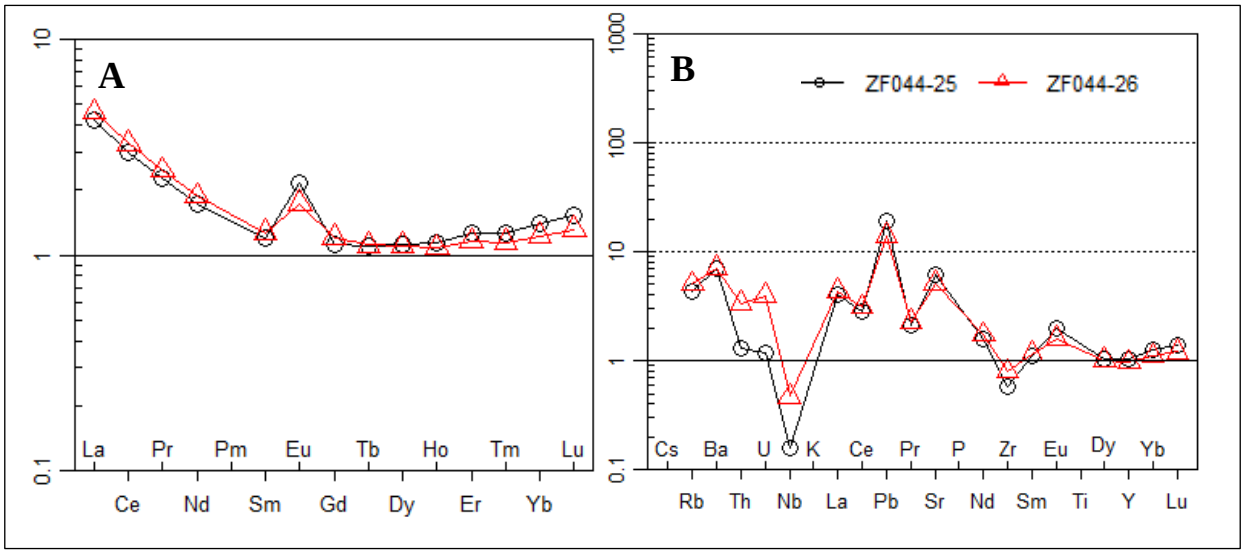

Figure 5.7: (a) REE diagram of feldspathic pyroxenite III normalized to the chondritic values of Sun and McDonough (1989). (b) Spider diagrams of feldspathic pyroxenite III normalized to the primordial mantle values of McDonough and Sun (1995).

(iv) Harzburgite

The harzburgites are characterized by a concave-upward REE pattern with a positive Eu anomaly (Figure 5.8a). Harzburgite, when compared to feldspathic pyroxenites and norite have relatively low REE concentration below 1.73. In terms of spider diagrams, harzburgite are defined by relatively high positive Rb and Pb compared to feldspathic pyroxenites and norite (Figure 5.8b). Sample ZF057-31 have high positive Sr and Eu anomaly compared to ZF057-28. The above can be explained by high intercumulus plagioclase content in ZF057-31 relative to ZF057-28. Harzburgite displays high positive LILE anomalies for Rb, Ba and Sr. However; sample ZF057-28 displays a flat Sr pattern. Harzburgite has negative HFSE anomalies displayed by Th, Nb, Ce and Y. Sample ZF057-31 shows a positive Zr anomaly whereas sample ZF057-28 shows a negative Zr anomaly. In overall, Harzburgite has relatively low large ion lithophile elements (LILE) and high field strength elements (HFSE) compared to all feldspathic pyroxenites and norite. Sample ZF057-31 have high $(La/Lu)_N$ and $(Eu/Eu^*)_N$ ratios compared to ZF057-28. High $(La/Lu)_N$ and $(Eu/Eu^*)_N$ ratios are associated with high degree of fractionation and high positive Eu anomaly respectively in sample ZF057-31.

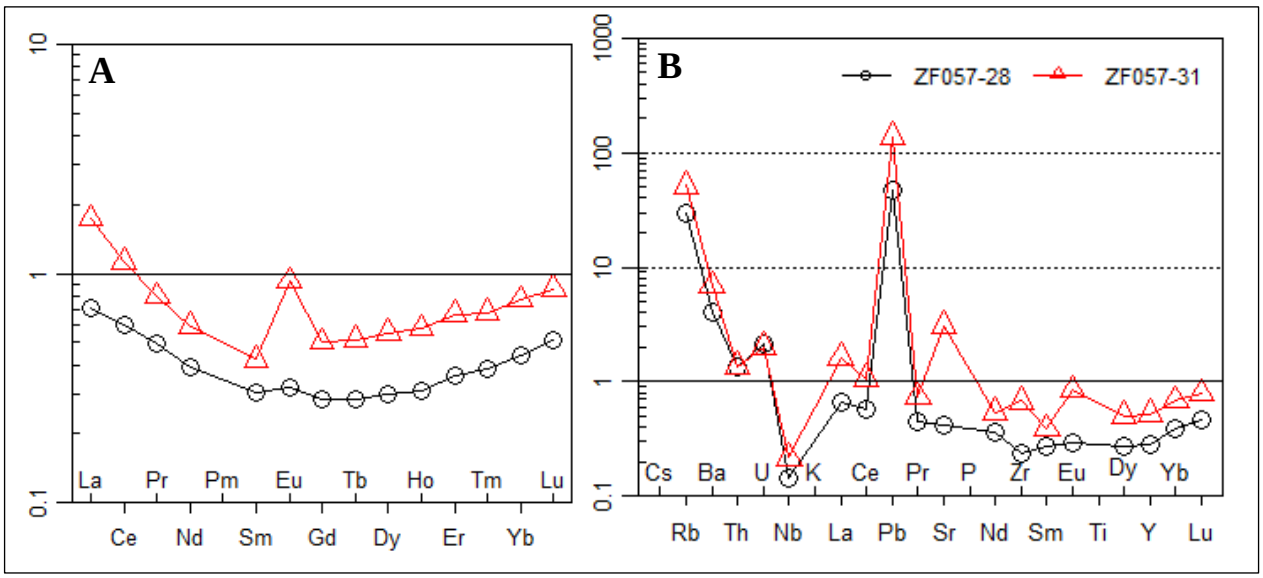

Figure 5.8: (a) REE diagram of harzburgite normalized to the chondritic values of Sun and McDonough (1989). (b) Spider diagrams of harzburgite normalized to the primordial mantle values of McDonough and Sun (1995).

(v) Norite

Norite is characterised by relatively high $(La/Lu)_N$ (4.60) and $(Eu/Eu^*)_N$ (2.01) ratios compared to other Platreef rocks. High $(La/Lu)_N$ ratios are associated with high degree of fractionation whereas high $(Eu/Eu^*)_N$ is consistent with high positive Eu anomaly and high feldspar content as noted in petrography. Norite, like other Platreef rocks are enriched in LREE and depleted HREE. Light rare earth elements show a steep slope pattern whereas heavy rare earth elements show a flat pattern with exception to sample ZF057-51, which shows a flat REE pattern (Figure 5.9a). Sample ZF057-51 contain relatively high REE with a flat Eu associated with contamination by crustal materials. Norite is enriched in LILE such as Sr, Rb, Ba and La and they show positive anomaly. HFSE are low in norite rocks and displays negative anomalies in Th, Nb, Ce, Zr and Y (Figure 5.9b).

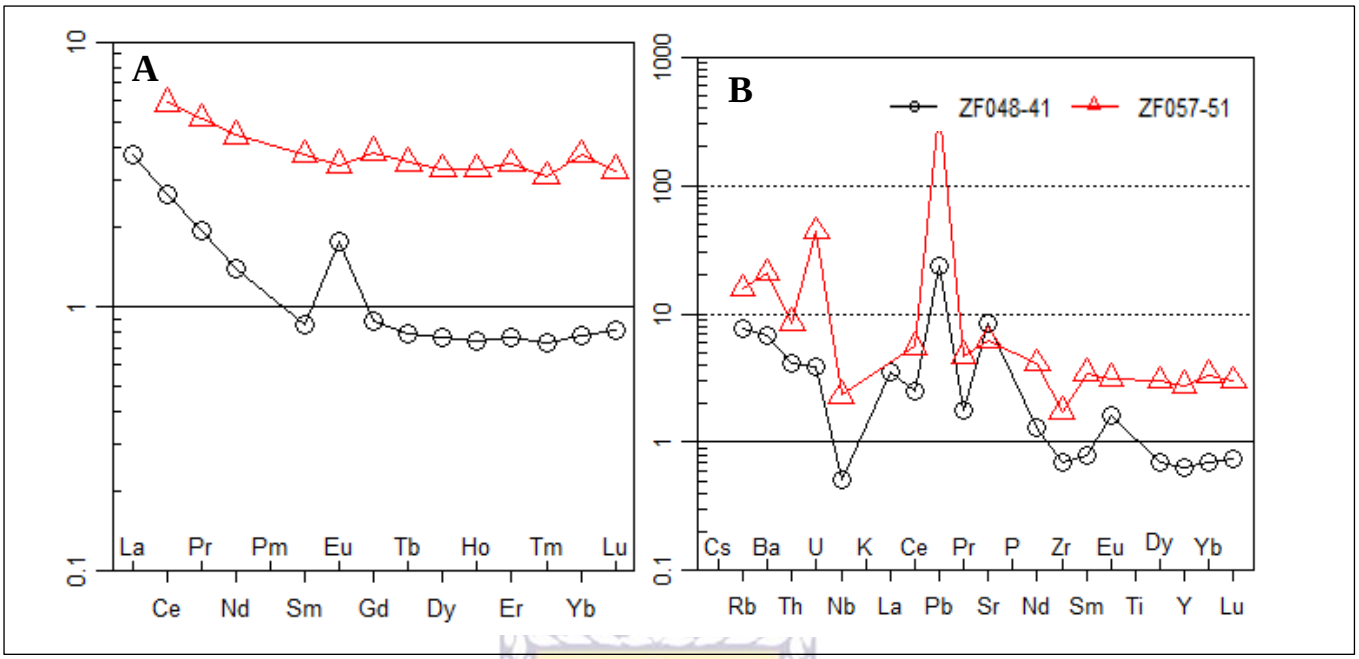

Figure 5.9: (a) REE diagram of norite normalized to the chondritic values of Sun and McDonough (1989). (b) Spider diagrams of norite normalized to the primordial mantle values of McDonough and Sun (1995).

5.3.4.1. Summary

The main objective of this section was to use spider diagrams plots in determining the element fractionation of light and heavy rare earth elements (LREE and HREE), as well as the behaviour of Eu anomaly to assess the enrichment of feldspars in the Platreef rocks. The above will assist in understanding the role of contamination by footwall rocks at Zwartfontein. Besides, to further validate the results given by the major elements in characterization of the Platreef rocks in section 5.2.2.

The Platreef rocks in the current study are characterized by high LREE fractionation with low HREE fractionation. Light rare earth elements show a steep slope fractionation pattern whereas heavy rare earth elements show a flat pattern. In contrast, sample ZF044-45 and ZF057-51 have a flat REE pattern in both LREE and HREE. Harzburgite rocks are characterized by a near U-shaped REE patterns. The occurrence of steep enriched LREE patterns, which flattens towards the HREE and a near U-shaped REE patterns, are suggested to represent contamination by crustal materials. All Platreef rocks are defined by positive Eu anomaly with varying concentrations except for sample ZF044-45 which has a negative Eu anomaly and sample ZF057-51 which show no Eu anomaly. Negative Eu anomaly in sample ZF044-45 is associated with low feldspar content (e.g. plagioclase) due to hydrothermal alteration. Feldspathic pyroxenite III and norite have high $(La/Lu)_N$ and $(Eu/Eu^*)_N$ ratios compared to feldspathic

pyroxenite I, feldspathic pyroxenite II and harzburgite. High $(La/Lu)_N$ and $(Eu/Eu^*)_N$ ratios in feldspathic pyroxenite III and norite are associated with high degree of fractionation and high feldspar content respectively. The petrographic studies have also shown high feldspar content such as plagioclase in both feldspathic pyroxenite III and norite. Feldspathic pyroxenite I, feldspathic pyroxenite II and harzburgite have low $(Eu/Eu^*)_N$ ratios ranging from 0.65 to 1.31 and this can be explained by low feldspar content in these rocks. Generally, the Platreef rocks are enriched in LILE and depleted in HFSE. The occurrence of negative HFSE anomalies such as Nb in the Platreef rocks resulted from insufficient transfer of HFSE relative to LILE. All the Platreef rocks at Zwartfotein shows strong positive Pb anomalies especially harzburgite and feldspathic pyroxenite I (sample ZF044-45). Strong positive Pb anomalies according to Manyeruke (2007) is associated with crustal contamination.

The occurrence of low REE in harzburgite is associated with high fractionation of most primitive olivine in ultramafic rocks relative to pyroxene and plagioclase. The LREE enrichment and HREE depletion in feldspathic pyroxenites and norites are associated with contamination by footwall rocks. The characterization of the Platreef based on the rare earth elements is in line with the results from the major elements in section 5.2.2.

5.4. Mass Balance

5.4.1. Introduction

Mass balance analysis is applied in geochemistry with the purpose of measuring elemental gains and losses during rocks-hydrothermal fluid interaction. It is mostly used as a quantitative method to determine the degree of interaction between the floor rocks and the magma. Elemental mass-balance changes were identified to benchmark the degree of alteration of rocks by hydrothermal and metasomatic processes. The primary purpose of performing mass-balance calculations in the current study was to identify the elements that were mobile and immobile during metasomatic processes and to further constrain if these processes have a significant influence in mineralisation of the Platreef rocks.

Mass balance calculation was done using Gresens method (1967). In the current study, the mass-balance was calculated using geochemical data kit (GCDkit) software following the Gressens method. During mass-balance analysis, immobile elements are first identified in order to calculate the gains and loss of elements during metasomatism. According to Grant (1986), elements that have a ratio of C_i^A/Ci^O in a range of 1.00 ± 0.05 are considered immobile during alteration processes. Where C_i^A is the concentration of altered rocks and Ci^O is the

concentration of the original rock. The general formula which is used to calculate the change in mass according to Gressen (1967) and Grant (1986) are shown below (equation 1 and equation 2) respectively.

$\Delta M_i = f_v(p_a/p_o)\ C_a^i - C_o^i$…….(1)

$C_a = (M_o/M_a)\ C_o$…….(2)

The mass transport function is described as the mass fraction of an element added or subtracted from the system during alteration relative to the mass of the element originally existing in the parent material. The elements added/gained during rock-fluid interaction are represented by a positive $\Delta C_i^A/C_i^O$ and they plot above the isocon/slope of immobile elements. Contrastingly, elements subtracted/lost during rock-fluid interaction are represented by a negative $\Delta C_i^A/C_i^O$, and they plot below the isocon/slope of immobile elements with $\Delta C_i^A/C_i^O = 0$.

Mass balance calculation was applied to altered serpentine harzburgite, pegmatoidal feldspathic pyroxenite and parapyroxenite relative to the original unaltered harzburgite, feldspathic pyroxenite II and feldspathic pyroxenite I respectively. Norites will not be included in the mass balance calculations because they do not show any effect of metasomatism based on both petrographic studies and geochemical data.

5.4.2. Mass balance results

(a) Harzburgite

Table 5. 2: Mass balance calculations for altered serpentine harzburgite relative to least altered harzburgite using average oxides concentrations of unaltered and altered rocks.

	Least altered	Altered	Slope data point	Gain/loss relative to C_i^o	Gain/loss Wt.% or ppm
Major elements	Harzburgite	Serp.harzbugite	C_i^A/C_i^o	$\Delta C_i^A/C_i^o$	ΔC_i
SiO_2	46.12	31.83	1.45	-0.22	-10.02
Al_2O_3	4.52	1.58	0.35	-0.60	-2.72
Fe_2O_3	12.40	18.71	1.51	0.71	8.82
MnO	0.17	0.12	0.70	-0.20	-0.03
MgO	30.16	36.08	1.19	0.36	10.77
CaO	2.59	1.28	0.50	-0.44	-1.14
Na_2O	0.01	0.00	0.29	-0.68	-0.01
K_2O	0.34	0.05	0.14	-0.84	-0.29
TiO_2	0.10	0.08	0.88	0.00	0.00
P_2O_5	0.02	0.01	0.44	-0.51	-0.01

Table 5.1 shows the average concentration of oxides elements in altered serpentine harzburgite relative to unaltered harzburgite. The slope data point and gain/loss of elements in altered serpentine harzburgite relative to unaltered harzburgite were calculated using the average oxides concentrations in the table.

Harzburgite was altered to serpentine harzburgite during fluid-rock interaction resulting in the loss of SiO_2, Al_2O_3, MnO, CaO, Na_2O, K_2O P_2O_5 and a gain in MgO and Fe_2O_3 (Figure 5.10). The table shows that the elements gained have a positive $\Delta C_i^A/C_i^o$ ranging between 0.36 to 0.71 and the elements lost have a negative $\Delta C_i^A/C_i^o$ ranging between -0.20 to -0.84. The isocon in figure 5.10 was drawn using immobile element Ti2O3 ($\Delta C_i^A/C_i^o = 0.00$) as a reference point to distinguish between gained and lost elements during metasomatism. Mass-balance results shows that the altered serpentine harzburgite are rich in MgO and Fe_2O_3 relative to the original harzburgite. This is consistent with core logging and petrographic studies where serpentine harburgite appears to be more mafic than the original harzburgite rock resembling high MgO and Fe_2O_3 in the former.

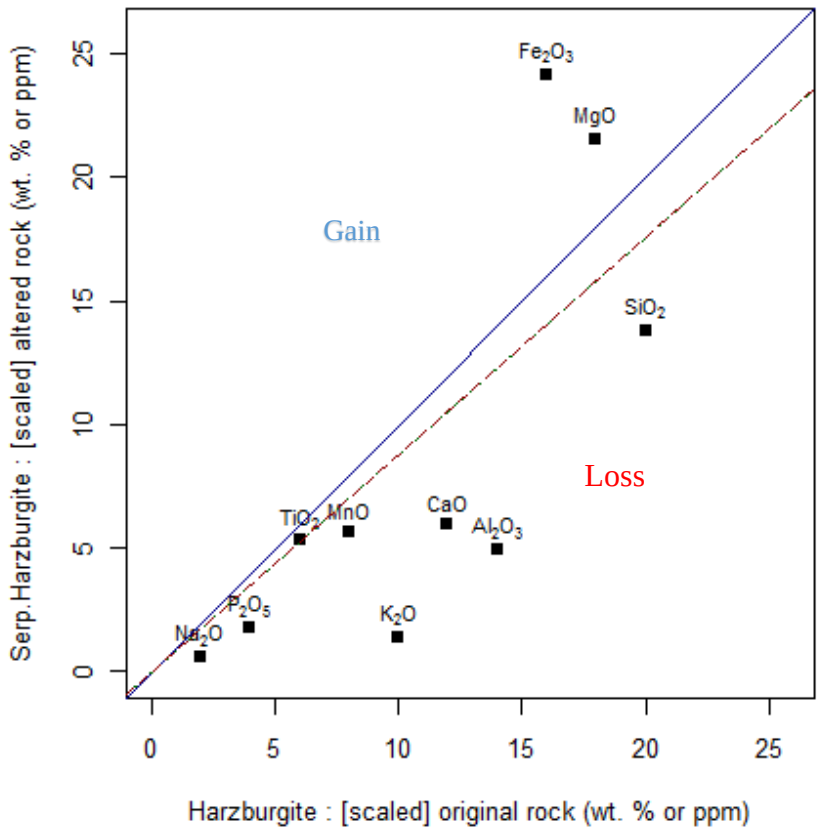

Figure 5.10: Graphical representation of enrichment-depletion of oxides elements in altered serpentine harzburgite relative to unaltered harzburgite. The isocon (red dotted line) passing through the immobile element (TiO_2) distinguish between elements gained (above the isocon) and elements lost (below the isocon) during metasomatism.

(b) Feldspathic pyroxenite I

Table 5.2: Mass balance calculations for altered parapyroxenite relative to least altered feldspathic pyroxenite I using average oxides concentrations of unaltered and altered rocks.

	Least altered	Altered	Slope data point	Gain/loss relative to C_i^o	Gain/loss Wt.% or ppm
Major elements	Feldspathic pyroxenite I	Parapyroxenite	C_i^A/C_i^o	$\Delta C_i^A/C_i^o$	ΔC_i
SiO_2	49.24	43.48	0.88	-0.14	-7.03
Al_2O_3	4.84	2.54	0.53	-0.49	-2.37
Fe_2O_3	14.04	13.97	0.99	-0.03	-0.48
MnO	0.30	0.31	1.03	0.00	0.00
MgO	14.02	24.62	1.76	0.70	9.88
CaO	15.09	11.11	0.74	-0.29	-4.30
Na_2O	0.62	0.01	0.02	-0.98	-0.61
K_2O	0.14	0.06	0.43	-0.58	-0.08
TiO_2	0.29	0.10	0.35	-0.67	-0.19
P_2O_5	0.03	0.02	0.86	-0.17	0.00

The alteration of feldspathic pyroxenite I to parapyroxenite involved significant addition of MgO and a loss in SiO_2, CaO, Al_2O_3, K_2O, TiO_2, Na_2O, Fe_2O_3 and P_2O_5 (table 5.2). MnO remained immobile during the process of metasomatism and was used as a reference point to distinguish between lost elements and gained elements (Figure 5.11). The parapyroxenite rock, which resulted from alteration of feldspathic pyroxenite I appear to be more mafic relative to the original rock due to significant gain of MgO and loss of CaO, Al_2O_3 and K_2O. The relative mass change in FP I is similar to harzburgite as both these rocks show significant loss in SiO_2, CaO, Al_2O_3, K_2O and Na_2O. However, harzburgite shows relatively high gain in Fe_2O_3 whereas in FPI Fe_2O_3 remains immobile. Hence, harzburgite appears to be more mafic relative to FPI.

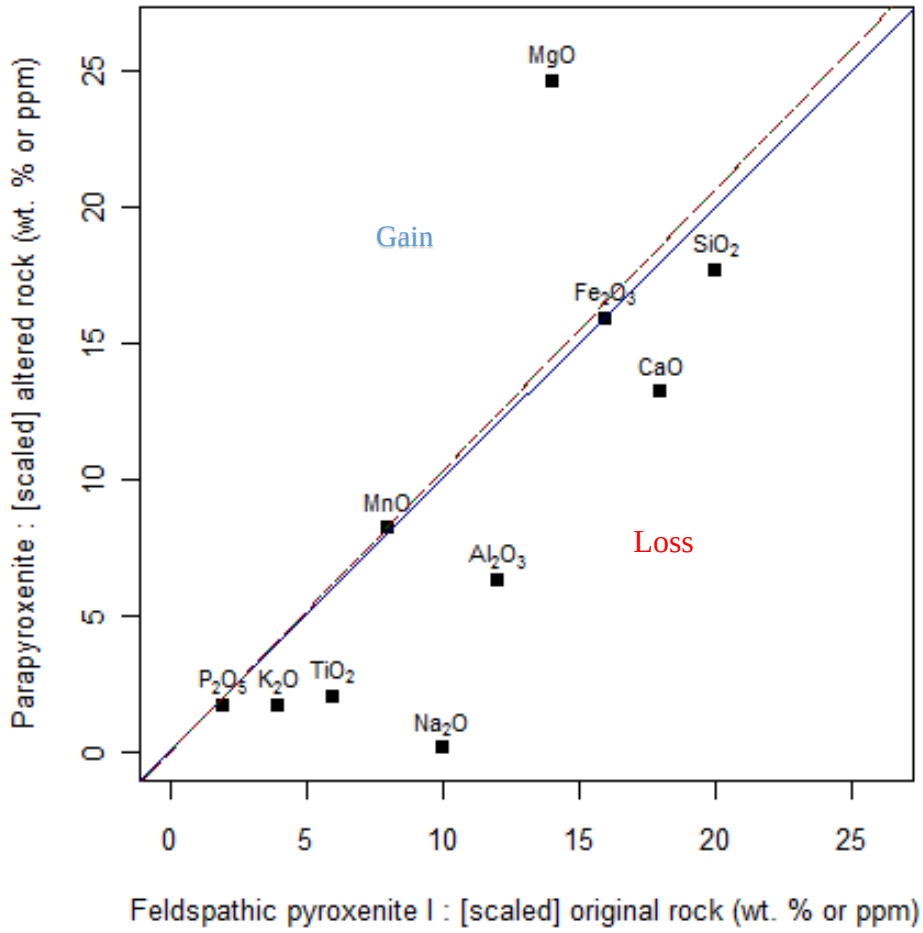

Figure 5.11: Graphical representation of enrichment-depletion of oxides elements in altered parapyroxenite relative to least altered feldspathic pyroxenite I. The isocon (red dotted line) passing through the immobile element (MnO) distinguish between elements gained (above the isocon) and elements lost (below the isocon) during metasomatism.

(c) Feldspathic pyroxenite II

Table 5. 3: Mass balance calculations for altered pegmatoidal feldspathic pyroxenite relative to least altered feldspathic pyroxenite II using average oxides concentrations of unaltered and altered rocks.

	Least altered	Altered	Slope data point	Gain/loss relative to C_i^o	Gain/loss Wt.% or ppm
Major elements	Feldspathic pyroxenite II	Pegmatoidal feldspathic pyroxenite	C_i^A/C_i^o	$\Delta C_i^A/C_i^o$	ΔC_i
SiO_2	52.18	51.59	0.99	0.00	0.00
Al_2O_3	5.88	6.22	1.06	0.07	0.41
Fe_2O_3	12.14	11.26	0.93	-0.06	-0.75
MnO	0.22	0.21	0.95	-0.04	-0.01
MgO	22.40	23.30	1.04	0.05	1.17
CaO	5.59	4.96	0.89	-0.10	-0.58
Na_2O	0.32	0.14	0.42	-0.57	-0.18
K_2O	0.12	0.16	1.33	0.35	0.04
TiO_2	0.17	0.11	0.65	-0.35	-0.01
P_2O_5	0.03	0.02	0.73	-0.26	-0.01

Table 5.3 shows the average concentration of oxides elements in altered pegmatoidal feldspathic pyroxenite relative to least altered feldspathic pyroxenite II and the graphical presentation of these data is shown in figure 5.12.

Mass-balance results indicated that the alteration of Platreef feldspathic pyroxenite II to pegmatoidal feldspathic pyroxenite involved the loss of Fe_2O_3, CaO, TiO_2, P_2O_5 and Na_2O, and gained MgO, Al_2O_3 and K_2O (Figure 5.12). SiO_2 remained immobile and was therefore used as reference to distinguish between elements gained and lost during metasomatism. Figure 5.12 shows that there was a slight mass fraction during metasomatism since all the elements plots close to the isocon with exception to Na2O which shows a significant loss. The above is also shown by the ratio of C_i^A/C_i^o in table 5.2 which ranges between 0.65 to 1.33 and relatively low value for Na2O (C_i^A/C_i^o = 0.42). In contrast to FPI, FP II shows relative mass gain in Al_2O_3 and K_2O which points to an increase in feldspar contents and more clinopyroxene relative to orthopyroxene.

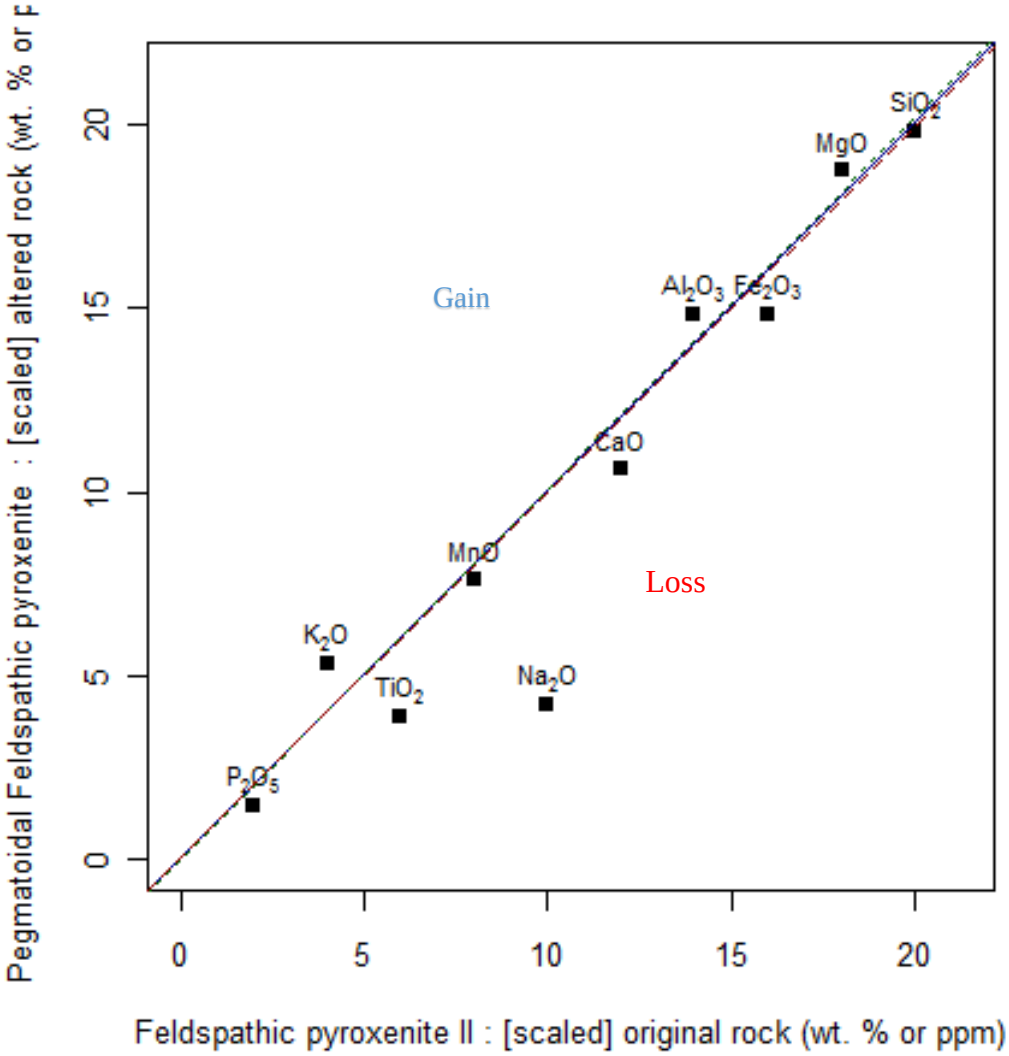

Figure 5.12: Graphical representation of enrichment-depletion of oxides elements in altered pegmatoidal feldspathic pyroxenite relative to least altered feldspathic pyroxenite II. The isocon (red dotted line) passing through immobile elements (SiO_2 and MnO) distinguish between elements gained (above the isocon) and elements lost (below the isocon) during metasomatism.

5.4.3. Summary of mass balance results (metasomatic processes)

Based on the mass balance results, the Platreef rocks were variably affected by metasomatic processes. The degree of metasomatism, however, shows fluctuation with the stratigraphic height in all the boreholes. The isocon of harzburgite (original) versus serpentinised harzburgite (altered) shows that there was significant gain in MgO and Fe_2O_3. The mass gain in MgO may

also influence the replacement of olivine to serpentine as observed during petrographic studies in sample ZF057-28 and ZF057-31. These samples also exhibit high LOI, which support the occurrence of hydrothermal alteration. Feldspathic pyroxenite I, which occurs throughout the Platreef but dominant towards the lower Platreef also show significant gain in MgO and loss in felsic elements (CaO, Al_2O_3, K_2O and Na_2O). Unlike in harzburgite, Fe_2O_3 in FP I remain immobile and defines the isocon with the slope of 0.99. However, both harzburgite and FP I appears to be ultramafic due to high concentration of MgO and Fe_2O_3. The significant loss of CaO, Al_2O_3, K_2O and Na_2O in FP I is associated with the replacement of plagioclase. Feldspathic pyroxenite II, on the other hand, shows both gain in mafic element (MgO) and felsic elements (Al_2O_3 and K_2O) and hence it appears mafic. FP II does not, however, show significant mass change compared to FP I and harzburgite. Mass balance results show that the most affected rocks by metasomatism processes are harzburgite, FP I and FP II respectively. Metasomatism of FP II was clearly noted in borehole ZF048. In petrography, FP II in borehole ZF048 was found to consist of intensively fractured orthopyroxene and laths shaped amphibole (tremolite and actinolite) reflecting replacement of orthopyroxene.

PGE and BMS mineralisation are mostly concentrated in moderately to extensively metasomatised/altered feldspathic pyroxenites and harzburgites. Considering high PGE and BMS mineralisation in altered serpentinised harzburgite, it can be suggested that hydrothermal alteration has played a role in the redistribution of mineralisation in the Platreef.

5.5. Chemostratigraphy

5.5.1. Platinum-group elements (PGE) and Base metal sulfides (BMS) mineralisation

Introduction

The platinum group elements (PGE) include osmium (Os), iridium (Ir), rhodium (Rh), ruthenium (Ru), platinum (Pt) and palladium (Pd). These elements are further subdivided into IPGE (Os, Ir and Ru) and PPGE (Rh, Pt and Pd) depending on their behaviour during crystal fractionation. The partition of IPGE in olivine during crystal fractionation is well documented (Barnes et al., 1985), whereas the PPGE behave incompatibly during olivine fractionation and they tend to remain in the silicate melt until S-saturation is reached. The platinum group elements analysis was only done for platinum and palladium which are commonly known as the commercially important PGE. Therefore, the distribution of PGE in the Platreef rocks will be determined based on these two elements. The occurrence of PGE mineralisation in the Platreef has been suggested to be associated with the occurrence of base metal sulfides (BMS) such as Ni, Cu and Zn.

The main objective of this section was to evaluate the relationship between PGE and BMS in order to understand the geochemical controls on the distributions of PGE mineralisation with the stratigraphic height. Petrography and mass balance analysis have shown that hydrothermal fluid activities /metasomatic processes affected the Platreef rocks. This section, therefore, evaluates the effect of hydrothermal fluid/metasomatism on the redistribution and decoupling of PGE from BMS in the Platreef.

The first section (section 5.4.1) focuses on the correlation between PGE (Pt and Pd) and BMS (Cu, Ni, Zn, Co) mineralisation and the second section (section 5.4.2) focuses on the distribution of PGE and BMS with the stratigraphic height. Section 5.4.2 involves identifying rocks that are highly, moderately and depleted in PGE and BMS mineralisation and their position in the stratigraphic succession.

5.5.2. Correlation between PGE and BMS

The correlation between PGE and BMS was assessed by plotting palladium and platinum against base metal sulfides elements such as Cu, Ni, Co and Zn. The primary purpose of evaluating the relationship between PGE and BMS was to determine the effectiveness of magmatic and hydrothermal processes on controlling the distribution of PGE mineralisation. Figure 5.13 shows the relationship between Pd and Cu, Ni, Co, Zn whereas figure 5.14 shows the relationship between Pt and Cu, Ni, Co, Zn. A positive correlation occurs between Pd and Cu, Ni, Co. Conversely, a weak negative correlation occurs between Pd and Zn (Figure 5.13). The negative correlation between Pd and Zn is well defined in feldspathic pyroxenite II and chromitite rocks. A high abundance of Cu, Ni and Co occur in feldspathic pyroxenite I and feldspathic pyroxenite II and they correspond with high Pt and Pd contents. The Platreef rocks are enriched in Ni relative to Cu. The above is consistent with the data reported for the Platreef rocks in Tweenfontein, Sandsloot and Overysel (Kinnaird, 2005; Hutchinson and Kinnaird, 2005; Holwell and McDonald, 2006; McCutcheon, 2012).

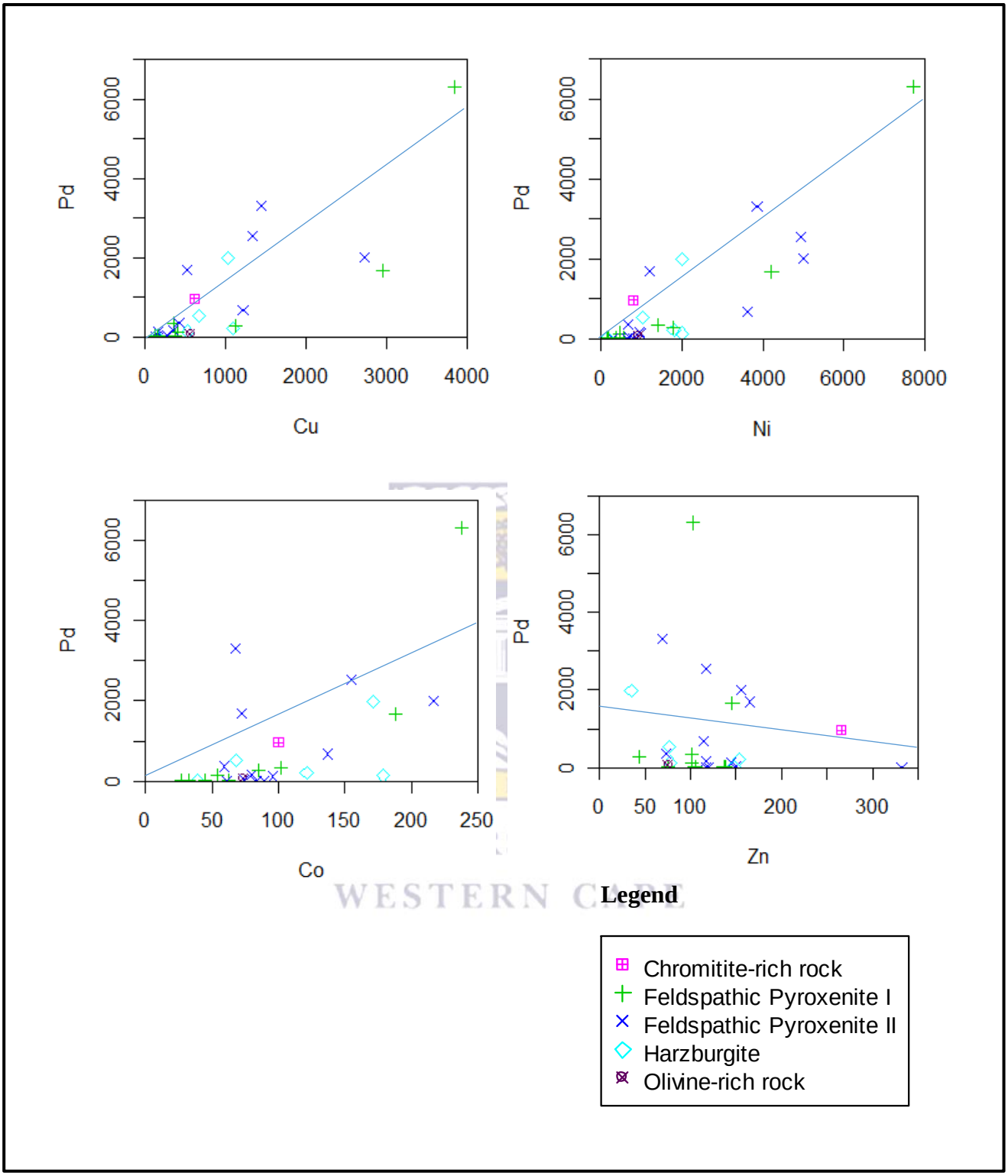

Figure 5.13: Binary plots of Pd versus Cu, Ni, Co and Zn. All plots display weak positive correlations, with exception of a non-existent correlation in Pd versus Zn.

Platinum shows a weak positive correlation with Cu, Ni, Co and a non-exixstent correlation with Zn, with exception to olivine-rich rocks which shows a negative correlation between Pt and Zn figure. A weak correlation exists between Pt and Zn due to poor compatibility relationship between these two elements.

The positive correlation between both Pd and Pt with base metal sulfides elements suggest that the distribution of PGE is controlled by sulfides liquid relative to hydrothermal alteration.

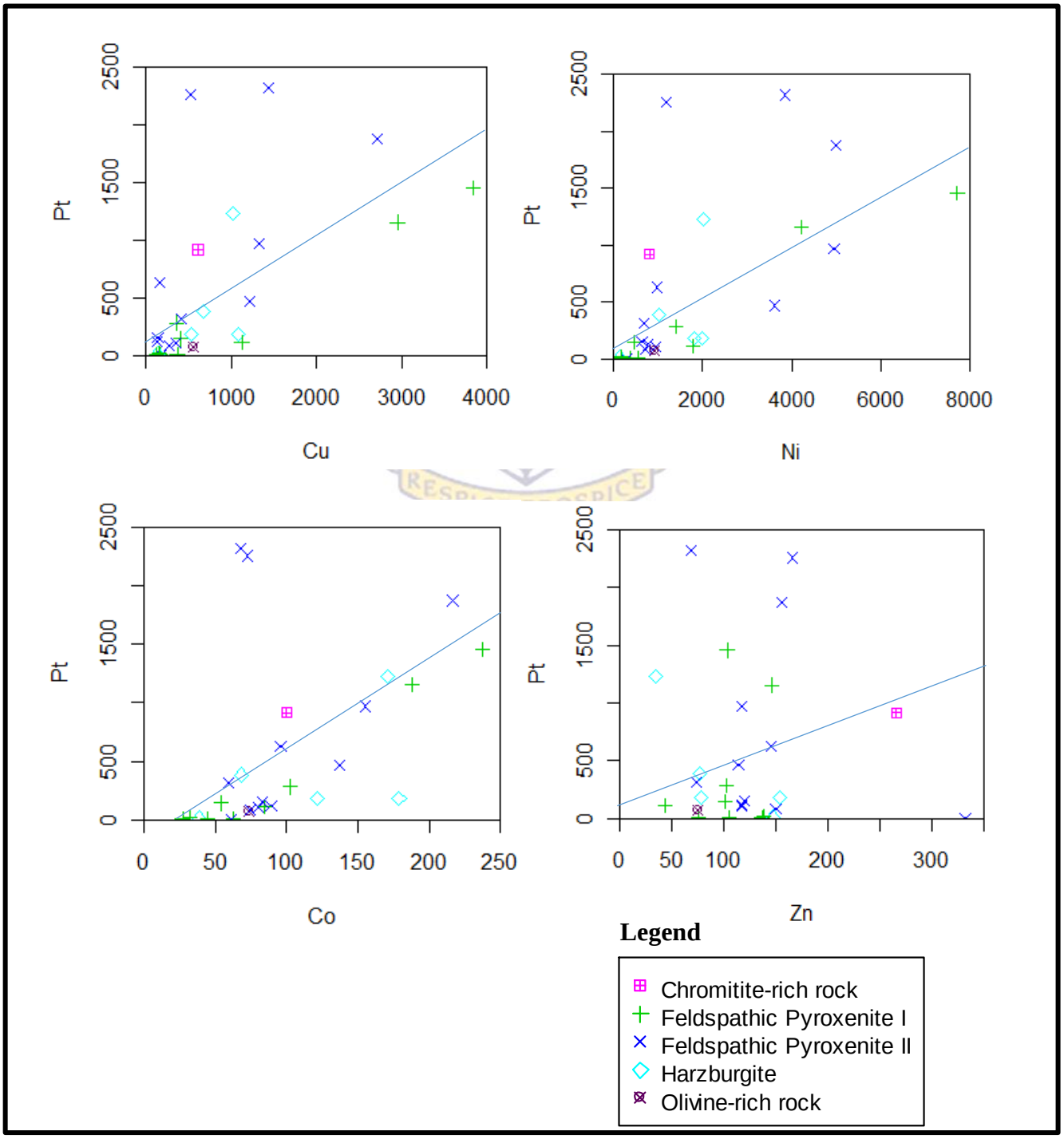

Figure 5.14: Binary plots of Pt versus Cu, Ni, Co and Zn. All plots display weak positive correlations, with exception of olivine rich rocks, which shows a negative correlation in Pt versus Zn.

5.5.3. Lithological variation and PGE-BMS mineralisation

5.5.3.1. Borehole ZF044

Borehole ZF044 underlain by dolomite consist of variable sills of feldspathic pyroxenite I, feldspathic pyroxenite II, feldspathic pyroxenite III, chromitite rich rocks and olivine-rich rocks referred to as harzburgite. Feldspathic pyroxenite I occurring towards the bottom of the Platreef (1334.48-1334.71 m) is characterized by high BMS (Ni+Cu ~ 2912.22 ppm) mineralisation with relatively low PGE (Pt+Pd ~ 390 ppb) mineralisation (Figure 5.15). The above has resulted in a negative correlation between BMS and PGE mineralisation. Chromitite rich rock occurring at 1309.6 to 1327.71 m have high PGE (Pt+Pd ~ 1879.00 ppb) mineralisation with moderately low BMS (Cu+Ni ~ 1416.98 ppm) mineralisation. PGE mineralisation in this rock can be suggested to be more associated with chromitite rather than BMS mineralisation.

Feldspathic pyroxenite I occurring at 1281.6 – 1309.6 m is intensively mineralised in both BMS (Ni+Cu ~ 5292.69 ppm) and PGE (Pt+Pd ~ 5633.00 ppb) mineralisation (Figure 5.15). Overlying this FP I, is a weakly mineralised (low BMS and PGE) feldspathic pyroxenite II occurring at 1242.7 to 1280 m. Feldspathic pyroxenite II (1242.7 to 1280 m) is overlain by moderately mineralised olivine-rich harzburgite occurring at 1221.58 to 1242.7 m.

Feldspathic pyroxenite I occurring in the upper Platreef shows an abrupt upwards increase in BMS (Cu+Ni ~ 11554.00 ppm) and PGE (Pt+Pd ~7774.00 ppb) mineralisation. This rock contains high BMS and PGE mineralisation compared to the rest of the Platreef rocks encountered in borehole ZF044. In general, BMS and PGE mineralisation in borehole ZF044 are intensively concentrated in feldspathic pyroxenite I. In overall, there is a good positive correlation between BMS and PGE mineralisation in borehole ZF044.

Pt/Pd ratio is relatively constant (0.85) in the middle of the Platreef, but relatively low at the top and bottom of the Platreef averaging to 0.32. Low Pt/Pd ratio at the top and bottom of the Platreef is associated with high Pd relative to Pt.

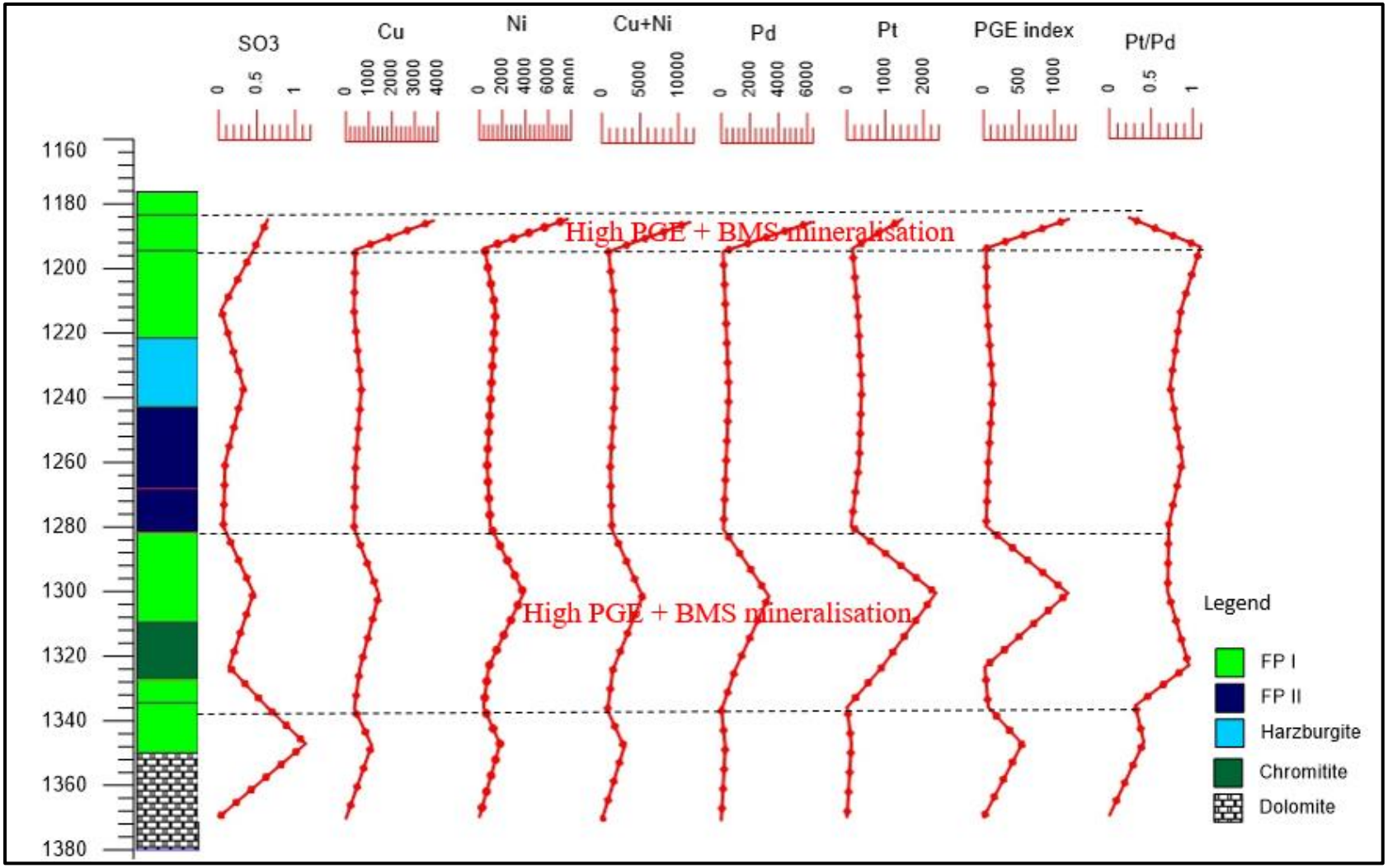

Figure 5.15: Chemostratigraphic profile showing geochemical variations of BMS (Ni, Cu, and SO_3) and PGE (Pt, Pd) in borehole ZF044. BMS is expressed in ppm and PGE in ppb.

5.5.3.2. Borehole ZF048

Borehole ZF048 underlain by Archean granite gneiss footwall rocks shows that rocks located at the bottom and top of the Platreef have higher Pt and Pd concentrations compared to the middle Platreef (Figure 5.16). The bottom and top-loaded Ni-Cu-PGE mineralisation were also noted at Turfspruit and Macalacaskop farms (Hutchison and Kinnaird, 2005). The bottom-loaded PGE-BMS mineralisation is hosted in olivine-rich rock occurring at a depth of 1564.32 to 1570.52 m. This rock is highly mineralised with both PGE (Pt+Pd ~3230 ppb) and BMS (Ni+Cu ~2999.45 ppm). In terms of PGE mineralisation, Pd (2000 ppb) is dominant over platinum (1250 ppb), and Pt/Pd ratio is < 1. There is a good positive correlation between PGE and BMS.

The top-loaded PGE-BMS mineralisation is hosted in feldspathic pyroxenite II occurring at the depth of 1416.53 to 1507.18 m. This rock is extensively mineralised with both BMS (6838.17 ppm) and PGE (3510 ppb) compared to the. Palladium is also dominant in FP II compared to Pt, and Pt/Pd ratio is approximately 0.4. There is a good positive correlation between SO_3, BMS (Ni+Cu) and PGE (P+Pd).

The middle Platreef shows variable PGE and BMS mineralisation. Olivine rich rock occurring at a depth of 1552.80 to 1562.63 m shows a negative correlation between BMS and PGE resulting from high BMS (2437.39 ppm) and low PGE (310 ppb) mineralisation (Figure 5.16). This negative correlation between PGE and BMS is well preserved in altered feldspathic pyroxenites II. The negative correlation between PGE and BMS was explained by Holwell and McDonald (2006) to represent the effect of hydrothermal fluid having added PGE content and removed sulfides. Also, the negative correlation between PGE and BMS was explained as the result of crystallization of rocks from S-undersaturated magma where sulfur was relatively low to scavenge PGE from the magma. Feldspathic pyroxenite II occurring at a depth of 1513.50 to 1544.32 m shows an upward decrease in SO_3 and an increase in Cu.

On the other hand, Ni, Pd and Pt are variably distributed and does not show a consistent trend. This feldspathic pyroxenite II is moderately mineralised in PGE where Pt is dominant over Pd resulting in high Pt/Pd ratio > 1 (Figure 5.16). Feldspathic pyroxenite I occurring at 1507.18 to 1513.50 m shows relatively high SO_3 and Cu with low Ni, P and Pd. This has resulted in a negative correlation between BMS and PGE in feldspathic pyroxenite I.

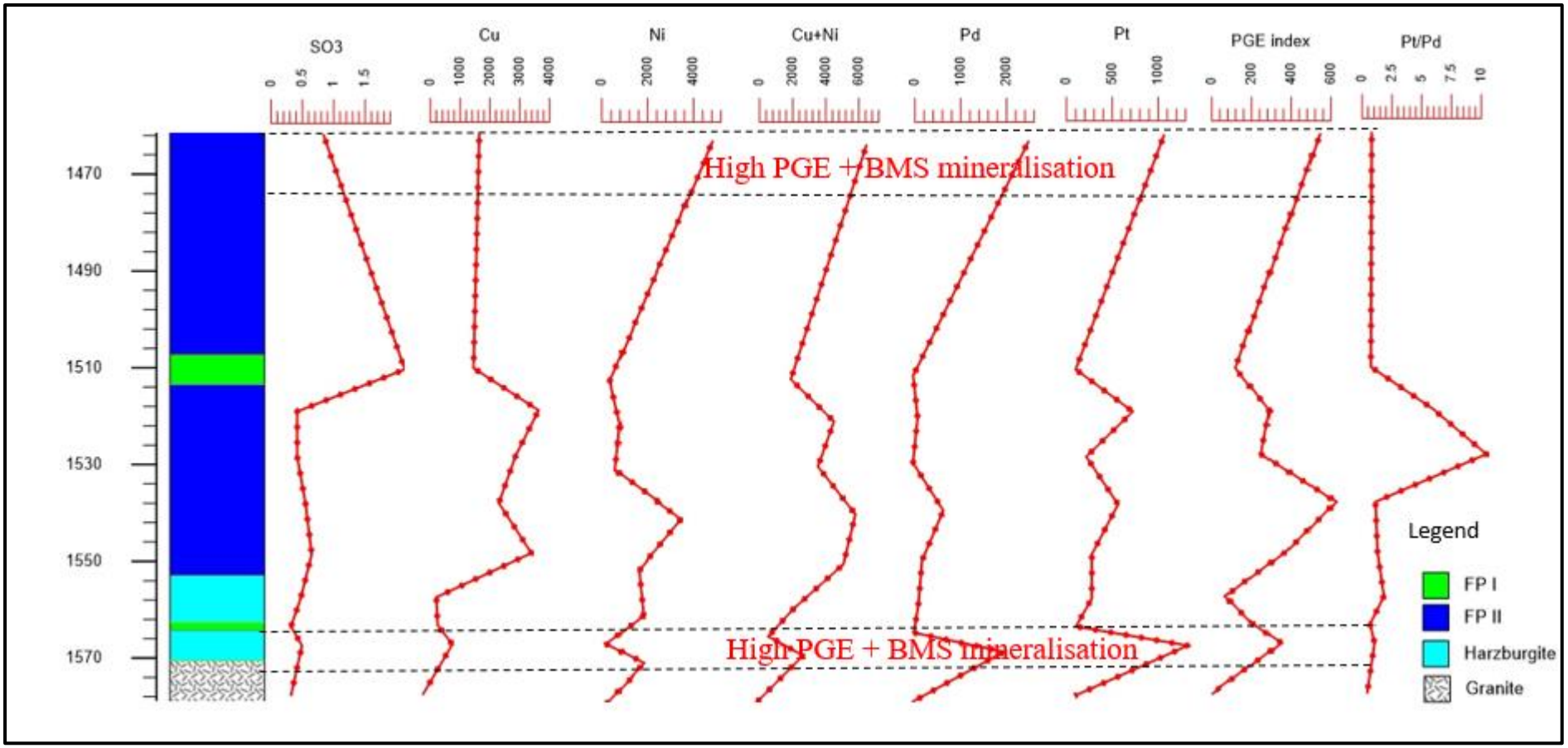

Figure 5. 16: Chemostratigraphic profile showing geochemical variations of BMS (Ni, Cu, and SO_3) and PGE (Pt, Pd) in borehole ZF048. BMS is expressed in ppm and PGE in ppb.

5.5.3.3. Borehole ZF057

Borehole ZF057 is dominated by variable sills of feldspathic pyroxenite I, feldspathic pyroxenite II and olivine-rich rock referred to as harzburgite in the current study. These rocks show variable PGE and BMS mineralisation along the stratigraphic height. The upper Platreef comprises of two sills of feldspathic pyroxenite II and feldspathic pyroxenite I occurring at 1283.15-1291.08 m and 1291.08-1316.12 m respectively (Figure 5.17). These rocks show high PGE (Pt+Pd) and BMS (Ni+Cu) mineralisation with PGE concentration of 3870 ppb in FP II and 2830 ppb in FP I. The concentration of BMS mineralisation is 7707.98 ppm in FP II and 7163.55 in FP I. High PGE and BMS mineralisation was also noted in FP II occurring at a depth of 1444.05-1458.77 m (Figure 5.17). The concentration of PGE in this rock is similar to that of FP II occurring at the top of the Platreef but with relatively low BMS mineralisation. Serpentinised harzburgite occurring at a depth of 1280.47-1289.60 m and 1303.28-1303.46 m also shows high PGE and BMS mineralisation. Rocks occurring at the bottom of the Platreef (FP I and harzburgite) between 1458.77 to 1499.21 m and those occurring in the middle of the Platreef between 1316.15 to 1427.43 m (FP II and harzburgite) are weakly mineralised in both PGE and BMS.

Pt and Pd in borehole ZF057 show a strong positive correlation with Ni throughout the succession. Conversely, Pt and Pd show a positive correlation with Cu and SO_3 from the depth of 1492.17 m to 1291.08 m and changes to a negative correlation at 1291. 08 m due to the decrease in Cu and SO_3 (Figure 5.17). The decoupling of Cu and SO_3 from Pt, Pd and Ni can be attributed to remobilization of Cu and SO_3 as a result of hydrothermal processes or late-stage magmatic processes (Armitage et al. 2002). Despite the decoupling of Cu and SO_3 at the depth of 1291. 08 m in borehole ZF057, the trend of SO_3, BMS, PGE index are mirror images of PGE (Pt+Pd).

Pt/Pd ratio in borehole ZF057 is relatively high compared to borehole ZF044 and ranges between 0.69 – 2 average to 1.3. High Pt/Pd ratio (~2) were found in FP I and FP II rocks which contain relatively high Pt compared to Pd at the depth of 1343.13, 1427.43 and 1492.17 m. The ratio of Pt/Pd is, however, expected to be low in the Platreef due to high Pd concentration relative to Pt concentration.

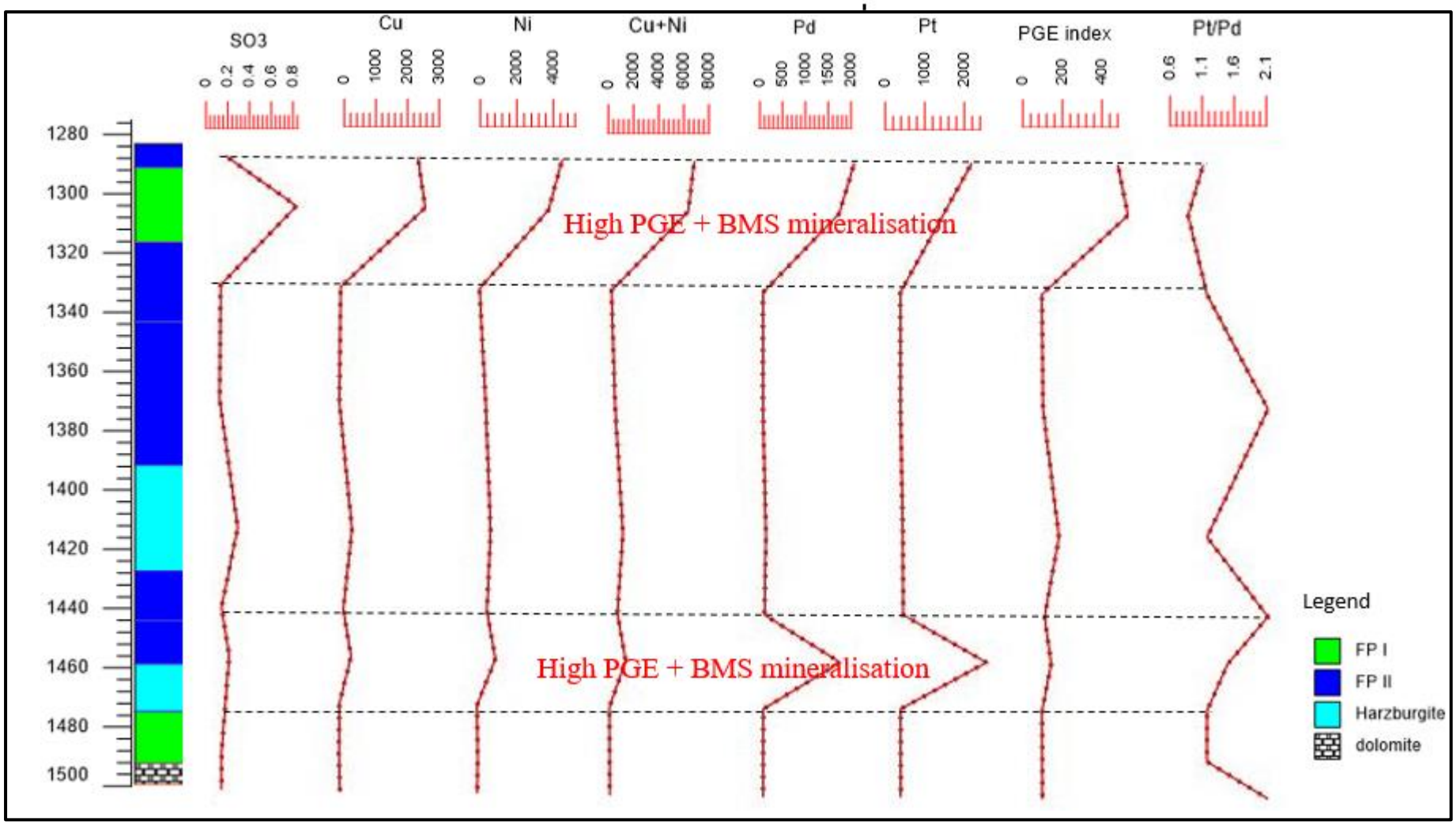

Figure 5. 17: Chemostratigraphic profile showing geochemical variations of BMS (Ni, Cu, SO_3) and PGE (Pt, Pd) in borehole ZF057. BMS is expressed in ppm and PGE in ppb.

5.5.3.4. Summary

The chemostratigraphic profiles show that BMS (SO_3+Cu+Ni) and PGE (Pt+Pd) mineralisation are variably distributed throughout the Platreef at Zwarftfontein. Middle and top-loaded PGE and BMS mineralisation were noted in borehole ZF044 and ZF057 underlain by dolomite footwall rocks. Whereas in borehole ZF048 underlain by granite, high BMS and PGE mineralisation occurs at the bottom, middle and top of the Platreef. In borehole ZF044 BMS and PGE mineralisation are concentrated in feldspathic pyroxenite I and harzburgite, whereas in borehole ZF057 mineralisation is hosted in feldspathic pyroxenite I, feldspathic pyroxenite II and harzburgite. In borehole ZF048, high BMS and PGE mineralisation is hosted in feldspathic pyroxenite II and olivine-rich rock. In general, high BMS and PGE mineralisation occurs in moderately to extensively altered FP I, FP II and harzburgite. There is overall a good positive correlation between BMS and PGE mineralisation in the Platreef at Zwartfontein. However, there is a negative correlation between BMS and PGE mineralisation in places. This negative correlation may have resulted from hydrothermal redistribution of either BMS and/or PGE mineralisation.

Based on the positive correlation between PGE mineralisation and BMS it can be postulated that the distribution of PGE mineralisation in the Platreef at Zwartfontein was dominantly controlled by immiscible sulfides liquids with minor redistribution by hydrothermal fluids/metasomatic processes where negative correlation occurs. These results are inconsistent with the ones reported by Hutchison and Kinnaird (2005) in the southern portion of the Platreef (Turfspruit and Macalacaskop farm). Hutchison and Kinnaird (2005) on their study of multistage genesis of Ni-Cu-PGE noted that the correlation between PGE and BMS is weak but a good correlation exists between Ni and Cu. They further explained the weak correlation between PGE and BMS as a result of decoupling of Ni and Cu from Pt and Pd due to late-stage metasomatic alteration of silicate minerals and remobilisation of PGE.

5.6. Isotope Geochemistry

5.6.3. Introduction

There are still controversies regarding the magma source and whether the Platreef was formed from single or multiple magma pulses. According to Maier et al. (2000), Kinnard et al. (2005) and Pronost et al. (2008) the Platreef comprise of a series of sill-like intrusions which are geochemically distinct. The fact that the Platreef package is underlain by a variety of rock types ranging from Transvaal Supergroup in the south to Archean granite gneiss in the north also makes it difficult to constrain its petrogenesis. Kinnaird (2005), Sharman-Harris et al. (2005) and Penniston-Dorland et al. (2008) provided strong evidence that shows the effects of floor rocks on the nature and style of mineralisation in the Northern limb specifically the Platreef. The possible magma source that has been suggested for the Platreef include primitive mantle components, SCLM (including depleted and metasomatized components), lower crustal components and host country rocks, as well as fluids produced by dehydration of the enclosing metapelites and carbonates (Wilson et al., 2017).

The main objective of doing Sr-Nd isotope analysis in the current study is to investigate the petrogenesis of the Platreef pyroxenite rocks. In particular, the crystallization age, the parental magma source and further constraining the role of crustal contamination in the formation of both the Platreef pyroxenites and PGE mineralisation. Also, Sr-isotope was further used to investigate the formation of the Platreef from multiple magma pulses.

The Platreef rocks were analysed for Sr-Nd isotopes at the University of Cape Town using ICP-MS following the methods outlined in chapter four. The concentration of Sr, Rb, Nd and Sm were also measured using ICP-MS and expressed as parts per million (ppm) (Table 5.4).

Table 5. 4: Rb-Sr and Sm-Nd isotopic data for the Platreef rocks at Zwatfontein.

Sample ID	Rock types	Rb	Sr	Nd	Sm	$(^{87}Sr/^{86}Sr)m$	$(^{87}Sr/^{86}Sr)i$	$(^{143}Nd/^{144}Nd)m$	$(^{143}Nd/^{144}Nd)i$	εNd
ZF044-25	FP III	2,753	130,9	2,163	0,486	0.710909	0.709101	0.511460	0.509618	-6.91
ZF044-26	FP III	3,224	108,2	2,337	0,516	0.710831	0.708271	0.511452	0.509642	-6.43
ZF044-34	FP I	5,000	19,00	1,271	0,341	0.723661	0.701017	0.512107	0.509907	-1.23
ZF044-36	FP II	4,525	56,10	1,914	0,507	0.715709	0.708773	0.511848	0.509677	-5.75
ZF044-45	FP I	5,418	64,50	7,653	2,149	0.719137	0.711912	0.511918	0.509616	-6.94
ZF048-40	FP II	2,721	56,71	2,503	0,540	0.711993	0.707869	0.511379	0.509611	-7.05
ZF048-41	Norite	4,812	178,7	1,746	0,347	0.710961	0.708646	0.511249	0.509619	-6.88
ZF048-46	FP II	9,018	53,77	1,081	0,264	0.722180	0.707750	0.511578	0.509576	-7.73
ZF048-52	Harzburgite	3,38	15,385	0,9145	0,1475	0.733320	0.714398	0.511153	0.509831	-2.73
ZF057-28	Harzburgite	18,69	8,861	0,486	0,122	0.881729	0.697427	0.511638	0.509580	-7.64
ZF057-31	Harzburgite	32,58	64,97	0,737	0,171	0.742560	0.699330	0.511438	0.509536	-8.51
ZF057-34	FP II	1,906	62,75	1,271	0,341	0.711829	0.709218	0.511866	0.509666	-5.96
ZF057-38	FP II	4,152	100,8	1,483	0,389	0.709929	0.706389	0.511875	0.509725	-4.81
ZF057-46	FPII	13,33	85,545	2,81	0,85	0.722690	0.709283	0.511576	0.509096	-17.14
ZF057-51	Norite	9,885	129,205	5,54	1,525	0.716290	0.709712	0.511852	0.509595	-7.35

5.6.4. Crystallization age of the Platreef rocks

This section focuses on identifying the crystallisation age of minerals which record the magmatic age of the rocks. Rb-Sr dating method was used in identifying the age of igneous rocks in the Platreef. The above involved the use of $^{87}Sr/^{86}Sr$ isotopic ratios, $^{87}Rb/^{86}Sr$, concentration of Rb and Sr measured. The isocon was generated by plotting measured $^{87}Sr/^{86}Sr$ versus $^{87}Rb/^{86}Sr$ using GCDkit software. The age of the rocks was determined first by calculating the slope of the isocon and then substitute the value of the slope in equation 1. In equation 1, *t* represents the time (age), *m* represent the slope of the isocon and ƛ is the constant value $1.42*10^{-11}$.

$$t = \frac{1In\,(m+1)}{ƛ} \quad \ldots\ldots\ldots\ldots\ldots\ldots\ldots\ldots (1)$$

Rb and Sr are relatively mobile, and they can be removed or added to the rock during the influx of fluids or related thermal events. The above can result in errors when calculating the age of the rocks. Therefore, Sm-Nd dating method was used to validate the age calculated from Rb-Sr method. The Sm-Nd method, compared to Rb-Sr method, is more effective in dating rocks since both Sm and Nd are immobile and cannot be affected by thermal influx of fluid. The method followed when calculating the age of the rocks from Sm-Nd data is the same as the method followed when using Rb-Sr data including the use of equation 1.

There are a few assumptions that needs to be made prior to calculating the crystallisation age of the rocks. Firstly, the age of the rocks calculated from both Rb-Sr and Sm-Nd methods is considered correct if all the samples plot on or close to the isochron. The above shows that Rb/Sr and Sm/Nd ratio has not been modified by fractionation after separation from the mantle source. Secondly, the isotopic composition of the rocks is either depleted mantle or CHUR. Lastly, it is further assumed that all the rocks have crystallized from the mantle in a single event.

Crystallization age of the Platreef rocks using the Rb-Sr method

Rb/Sr is petrogenetically informative, mainly when used in association with Sr isotopes (Buchanan et al., 2004). Variation in Rb/Sr can be used to identify if plagioclase were formed entirely from trapped liquids as intercumulus phase to mafic/ultramafic cumulus minerals or occurs as cumulus phase (Wilson et al., 2017). In this section, Rb/Sr was used in association with initial Sr isotope to plot an isocon, which was further employed to calculate the crystallisation age of the Platreef rocks.

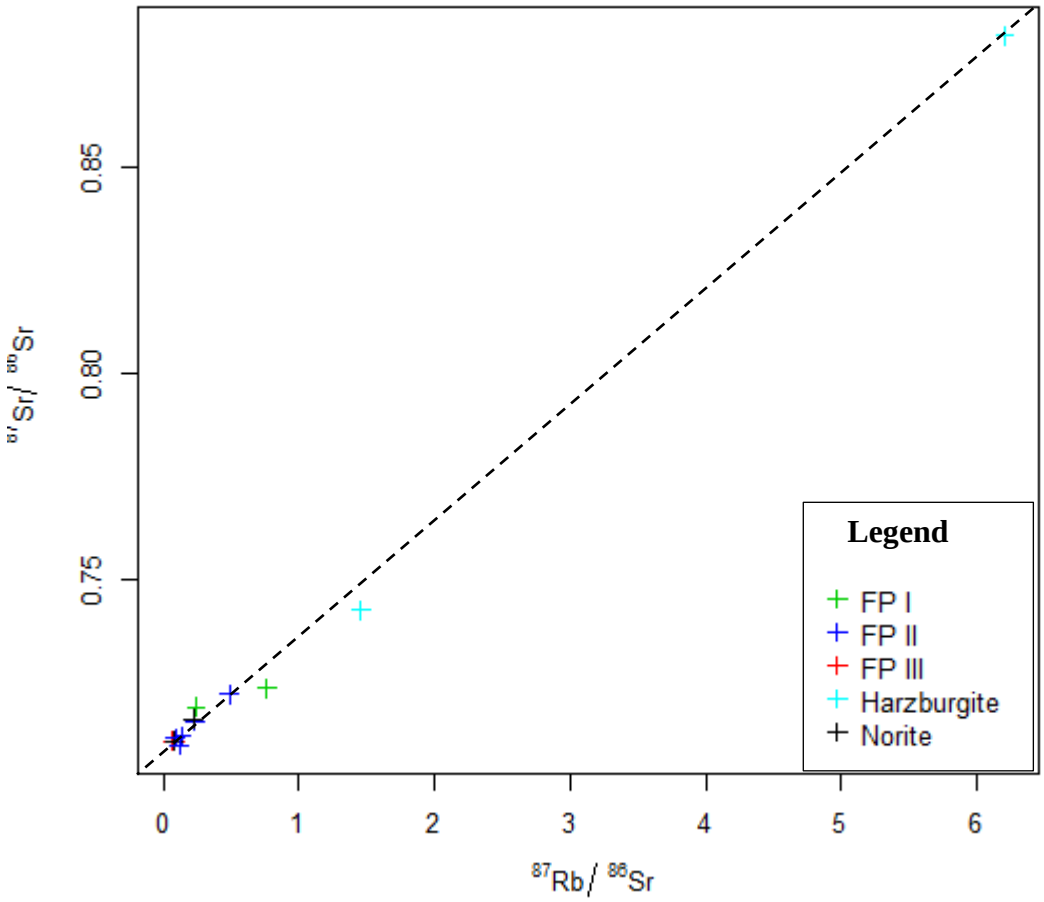

Figure 5. 18: Plot of $^{87}Rb/^{86}Sr$ vs $(^{87}Sr/^{86}Sr)_m$ for all analysed samples of the Platreef, where subscript m represent measured $^{143}Nd/^{144}Nd$. The data are from table 5.4.

The estimated initial $^{87}Sr/^{86}Sr$ value of the magma from which the rocks have crystallised is 0.700 calculated directly from figure 5.18. All the rock samples are plotting on and close to the isochron (Figure 5.18). The above suggests that all the requirements listed in section 5.6.2 for calculating the crystallisation age of the rocks from the isocon were fulfilled. The Rb-Sr dating method constrained a crystallisation age of 1.5 Ga for the Platreef rocks with the initial ratio ($^{87}Sr/^{86}Sr$) of 0.700.

5.6.4.4.Crystallization age of the Platreef rocks using Sm-Nd method

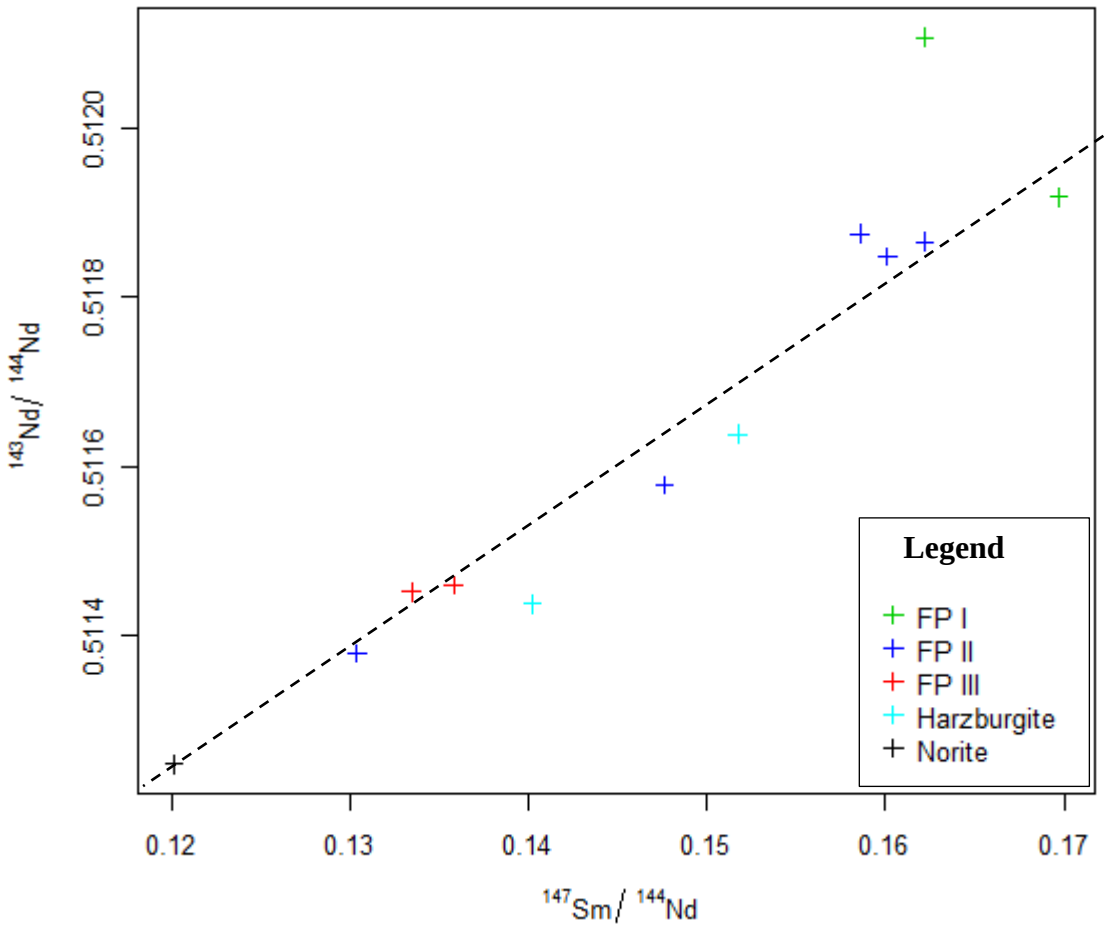

Figure 5. 19: Plot of $^{157}Sm/^{144}Nd$ vs $(^{143}Nd/^{144}Nd)_m$ for all analysed samples of the Platreef, where subscript m represent measured $^{143}Nd/^{144}Nd$. The data are from table 5.4.

Sm-Nd isotope data for all the Platreef rocks are listed in Table 5.4. The Platreef rocks have $(^{143}Nd/^{144}Nd)_m$ that ranges from 0.511249 ± 0.000014 to 0.512107 ± 0.000009. The estimated initial $^{143}Nd/^{144}Nd$ value of the magma from which the rocks have crystallised is 0.509536 calculated directly from figure 5.19. All the rock samples plot on and close to the isochron with the exception to sample ZF044-34 which have the highest $(^{143}Nd/^{144}Nd)_m$ of 0.512107. The calculated age shows that the suite of the Platreef rocks crystallized at 2.05 Ga with the initial ratio $^{143}Nd/^{144}Nd$ of 0.509536.

When comparing the crystallisation age of the Platreef rocks calculated from Sm-Nd and Rb-Sr dating method, it essential to highlight that the calculated age from Rb-Sr (1.5 Ga) is lower than the one calculated is from Sm-Nd (2.05 Ga). The different crystallisation age for the Platreef rocks may be due to disturbance of Rb-Sr system during crustal contamination and

hydrothermal fluid activities. Since the Rb-Sr define the younger age of 1.5 Ga, this age is interpreted to represent the time at which the Rb–Sr isotopic systematics of the Platreef rocks were disturbed by hydrothermal alteration.

5.6.5. Strontium (Sr) variation in the Platreef

This section reports the Sr isotopic compositions of the ultramafic/mafic rocks in order to evaluate the isotopic variations across the stratigraphy of the Platreef and potential occurrence of isotope distinct magmas and the extent of crustal contamination.

The Platreef rocks show significant variation in the initial $(^{87}Sr/^{86}Sr)_i$ values ranging from 0.697427 to 0.714398. The Platreef rocks occurring towards the bottom of the Platreef close to the contact with the footwall rocks have high initial $(^{87}Sr/^{86}Sr)_i$ values compared to the rest of the rocks in the upper stratigraphic succession (Figure 5.20). Harzburgite rock in contact with the granite footwall in borehole ZF048 have high initial $(^{87}Sr/^{86}Sr)_i$ of 0.714398 compared to feldspathic pyroxenite I (0.710397) and norite (0.709712) in contact with dolomite in borehole ZF044 and ZF057, respectively (Figure 5.20). The general overall decrease in the initial $(^{87}Sr/^{86}Sr)_i$ in all boreholes with the stratigraphic height reflect progressive increase in the involvement of primitive mantle melt and lower contribution of crustal materials. The preceding is exceptional to feldspathic pyroxenite III occurring at the top of the Platreef in borehole ZF044 which shows an abrupt increase in the initial $(^{87}Sr/^{86}Sr)_i$ associated with high plagioclase content as evidenced in petrographic studies.

The Platreef rocks intersected by borehole ZF048 have a high initial $(^{87}Sr/^{86}Sr)_i$ ranging between 0.707150 and 0.714389 with an average of 0.709666. The initial $(^{87}Sr/^{86}Sr)_i$ ratios decrease from 0.714398 in harzburgite which is in direct contact with the footwall granite to 0.707750 in feldspathic pyroxenite II. The preceding is followed by reversals with a peak in norite and a decrease in feldspathic pyroxenite from 0.708646 to 0.707869 (Figure 5.20 a).

The Platreef rocks intersected by borehole ZF044 have initial $(^{87}Sr/^{86}Sr)_i$ ranging between 0.711912 and 0.701017 with an average of 0.707814. The initial $(^{87}Sr/^{86}Sr)_i$ ratios decreases from 0.711912 at a depth of 1228.14 m to 0.708773 at a depth of 1186.58 m. An abrupt decrease in $(^{87}Sr/^{86}Sr)_i$ ratios from 0.708773 to 0.701017 was noted at a depth of 1186.58 m to 1184.58 m. The above was followed by a sharp increase in $(^{87}Sr/^{86}Sr)_i$ from 0.701017 to 0.709101 in feldspathic pyroxenite occurring towards the top of the Platreef (Figure 5.20 b).

The Platreef rocks intersected by borehole ZF057 have initial $(^{87}Sr/^{86}Sr)_i$ ranging between 0.697427 and 0.709712 with an average of 0.705227. The initial $(^{87}Sr/^{86}Sr)_i$ ratios decrease with the stratigraphic height from 0.709712 to 0.697427, and an abrupt increase to 0.709218 was noted, forming a peak value at a depth of 1324.13 m (Figure 5.20 c).

The variations and reversals in $(^{87}Sr/^{86}Sr)_i$ ratios with the stratigraphic height in the Platreef is consistent with the formation of the Platreef rocks from multiple influxes of magma with contrasting Sr-isotopic ratios and significant variations of contamination by footwall rocks supported by high initial $(^{87}Sr/^{86}Sr)_i$ ratios. It is however, important to note that the results are not showing clear indication of formation of the Platreef from multiple magma influxes due to limited Sr-isotope data presented.

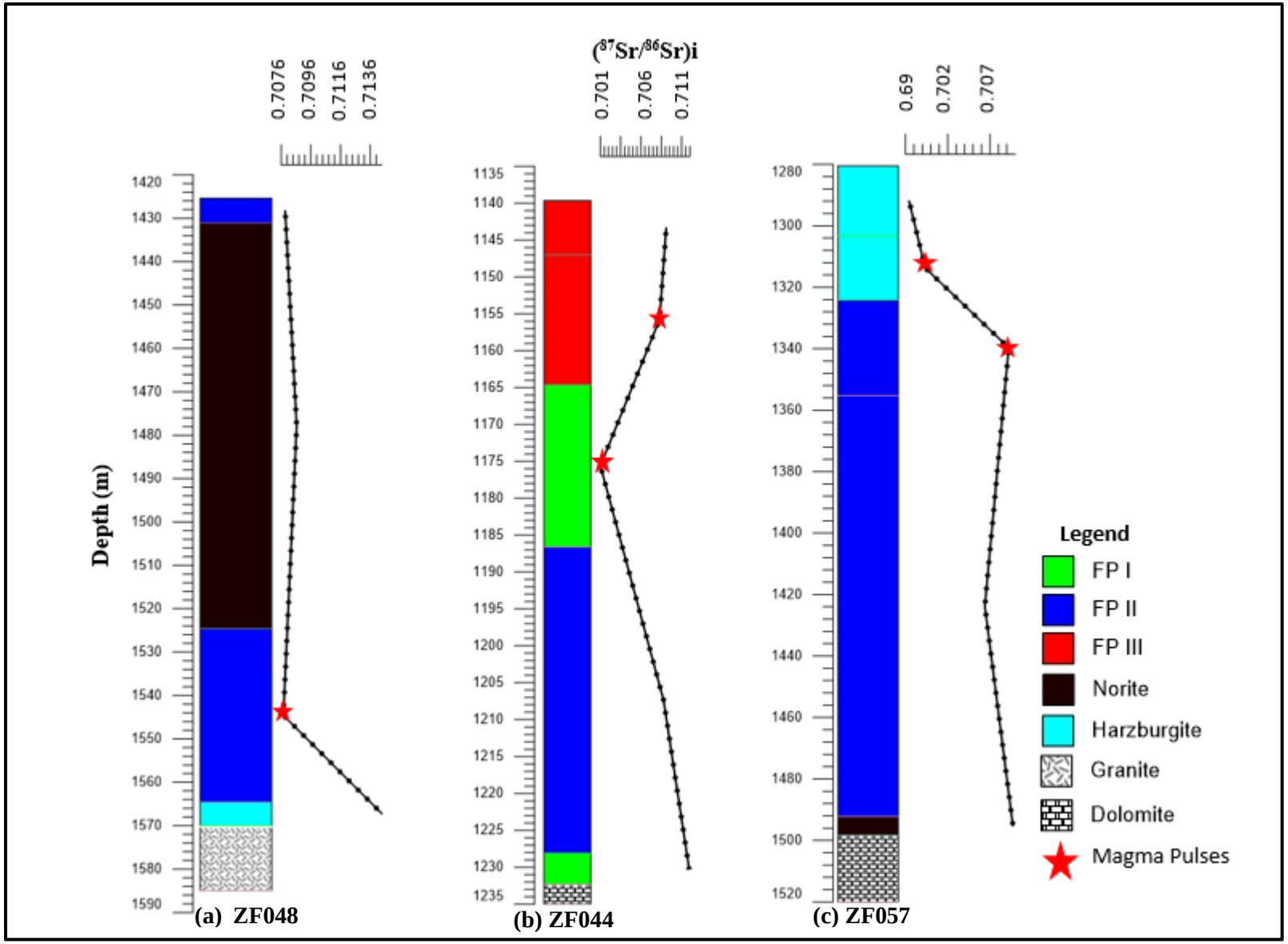

Figure 5. 20: The initial $(^{87}Sr/^{86}Sr)_i$ ratios for the Platreef rocks calculated at 2060 Ma plotted against depths for borehole ZF048, ZF044 and ZF057.

5.6.6. Determining the Platreef magma source from Sr-Nd isotope data

The previous sections were focused on determining the age of the Platreef rocks and evaluating the variation in strontium (Sr) isotope in the Platreef rocks with stratigraphic height. The variations in the initial $(^{87}Sr/^{86}Sr)_i$ with the stratigraphic height confirms that the Platreef was formed as an open system with the influx of multiple sill-like magma intrusions and a considerable variation in contamination caused by footwall rocks. This section aims at determining the magma sources and reservoirs that were involved in the formation of the Platreef.

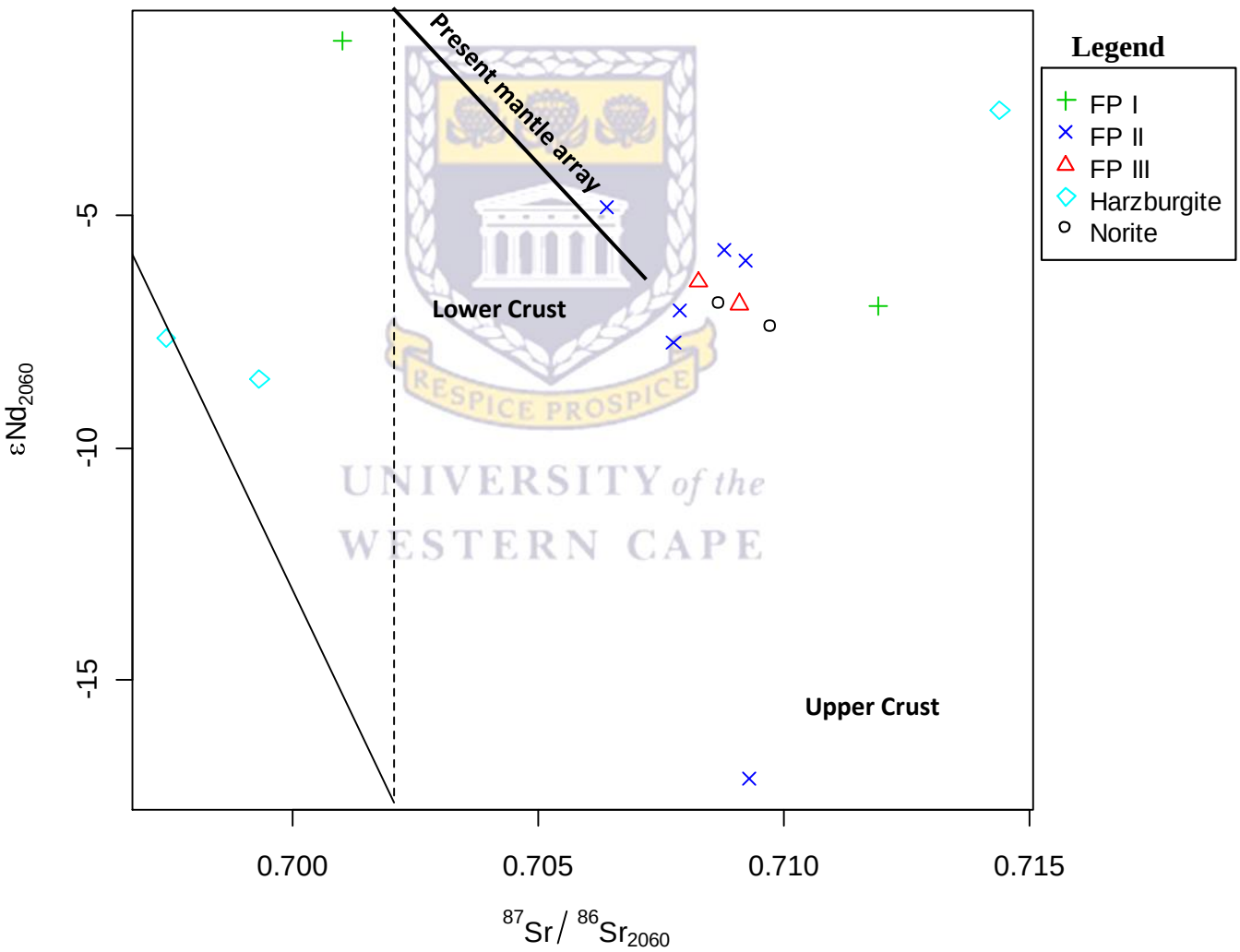

Figure 5. 21: Plot of εNd_{2060} versus $^{87}Sr/^{86}Sr_{2060}$ for all the analysed Platreef rocks. The dotted line represents the boundary between primitive mantle (left) and evolved/contaminated mantle (right).

The analysed Platreef rocks have shown negative εNd_{2060} which ranges from -1.23 to -17.14 with $^{87}Sr/^{86}Sr_{2060}$ that ranges from 0.697 to 0.721. The Platreef rocks plot close to the mantle array on the lower crustal field with exception to harzburgite rocks and feldspathic pyroxenite II (sample ZF057-46) (Figure 5.21). Harzburgite rocks (sample ZF0-28 and ZF057-31) plot on the primitive mantle field (left) with low $(^{87}Sr/^{86}Sr)_{2060}$ that ranges from 0.697 to 0.699 and negative εNd_{2060} that ranges from -7.64 to -8.51. The low initial $(^{87}Sr/^{86}Sr)_{2060}$ isotopic ratios in these harzburgite rocks and high negative εNd_{2060} suggest that contamination by lower crust have occurred but did not affect the $(^{87}Sr/^{86}Sr)_i$. These harzburgites were formed from a primitive mantle source as evidenced by low initial $(^{87}Sr/^{86}Sr)_{2060}$ and more primitive olivine with high Mg# (>80). Feldspathic pyroxenite II (sample ZF057-46) have a negative εNd_{2060} value of -17.14 and initial $(^{87}Sr/^{86}Sr)_i$ of 0.7093 consistence with contamination by upper crust materials (Figure 5.21). Sample ZF044-34 have low initial $(^{87}Sr/^{86}Sr)_{2060}$, high $(^{143}Nd/^{144}Nd)_{2060}$ and εNd value of -1.23 compatible with formation from a primitive mantle source. The fact that the Platreef rocks exhibit negative εNd value ranging between -1.23 and -17.14 implies that they have crystallized from primitive mantle-derived magma with significant crustal contamination. The preceding is also supported by high initial $(^{87}Sr/^{86}Sr)_{2060}$ with the average of 0.707811.

CHAPTER SIX

6. DISCUSSION, CONCLUSIONS AND RECOMMENDATIONS

6.1. DISCUSSION

6.5.3. Introduction

The aim of this study is to advance understanding of the petrogenesis of the Platreef at Zwartfontein, which will assist mining companies in locating areas of high PGE mineralisation. This study mainly focused on investigating whether the Platreef was formed from multiple sill-like intrusion or single magma intrusion. Similar studies were conducted in the Northern limb by Mangwegape et al. (2016), where Sr-isotope data on plagioclase was used to understand the stratigraphy and petrogenesis of the Northern limb. Kruger et al. (1994) explained the formation of the Bushveld in the Western Limb from differentiation and integration stages based on Sr-isotope data. Differentiation stage occurs in the upper Main Zone and Upper Zone where Sr-isotope remain relatively constant. Integration stage, on the other hand, occurs in the Lower Zone, Critical Zone and lower Main Zone where Sr-isotope is heterogeneous. The fluctuations in Sr-isotopes from the Lower Zone to lower Main Zone is associated with multiple sill-like intrusion of the magma (Kruger et al., 1994). Most of the previous work (e.g. Pronost et al., 2008; Mitchell and Scoon, 2012) in the investigation of the formation of the Platreef was focused on using petrography and whole-rock geochemical data. The current study carries a different approach with the use of Sr-Nd isotope data that brings a new perspective to the Platreef at Zwartfontein.

The current study uses new Sr-Nd isotope data, petrography and whole-rock geochemical data to understand the petrogenesis of the Platreef at Zwartfontein. The discussion of the results is outlined as follows:

- The lithologies of the Platreef at Zwartfontein
- Hydrothermal fluid activity and PGE-BMS mineralisation
- Evidence of crustal contamination in the Platreef
- The Platreef magma source

All these aspects will contribute directly and indirectly towards the investigation and understanding of the formation of the Platreef either from multiple or single magma pulses.

6.5.4. The lithologies of the Platreef at Zwartfontein

The Platreef is underlain by a variety of floor rocks, from the Transvaal Supergroup in the south to Archean granite gneiss in the north. The variation in the footwall rocks has affected the lithology and mineralisation of the Platreef (Pronost et al., 2008). Several studies (e.g. Harris and Chaumba, 2001; Manyeruke, 2007; Pronost et al., 2008) have been done to understand the lithology, stratigraphy and mineralisation in the Platreef with varying floor rocks. However, this remains controversial due to post-crystallisation processes, which have variably affected the Platreef lithology and mineralisation. The main objective of this section is to discuss the lithology and stratigraphy of the Platreef at Zwartfontein based on the results given in the preceding chapters and compare them to some previous works in the Platreef. The above will assist in understanding the types of Platreef lithologies and their position in the stratigraphic succession including their relationship to PGE-BMS mineralisation.

The lithology and stratigraphy of the Platreef are complex and cannot be correlated along the strike even on a small scale (Kinnaird et al., 2007). White (1994) divided the stratigraphy of Platreef into A-, B- and C-reefs in an upward succession. Where A-reef contains little mineralisation, B-reef is extensively mineralised, and C-reef is barren. The Platreef at Zwartfontein is dominated by feldspathic pyroxenite which is classified into feldspathic pyroxenite I (FP I), feldspathic pyroxenite II (FP II) and feldspathic pyroxenite III (FP III) based on texture, mineralogy and PGE-BMS mineralisation. FP I, FP II and PF III is comparable to A-, B- and C-reefs respectively in terms of PGE-BMS mineralisation. The classification of the Platreef into A-, B- and C-reefs was solely based on mineralogy (Holwell, 2006) and thought to follow a systematic stratigraphic sequence. These reefs were noted in the northern farms of Overysel, Drenthe (Viljoel and Schurmann, 1998) and Tweenfontein (White, 1994). Mitchell and Scoon (2012) proposed that the Platreef can instead be divided into PU1, PU2 and PU3, considering that the Platreef does not follow a simple upwards-younging sequence. PU1 was formed through repeated intrusion of gabbroic magma and is characterised by dominance of fine-grained gabbronorite-websterite with minor feldspathic orthopyroxenite. PU2 is characterised by dominance of harzburgite formed from intrusion of ultramafic magma. The partial melting and recrystallization of PU1 due to the intrusion of ultramafic magma has resulted in the formation of PU3 dominated by coarse-grained pyroxenites, gabbronorite and minor harzburgite.

The stratigraphy of the Platreef at Zwartfontein is complex and rock layers do not follow a consistency sequence. Therefore, it is difficult to subdivide the Platreef into A-, B- and C-reefs. Instead, the Platreef at Zwartfontein can be divided into lower, middle and upper Platreef consisting of FP I, FP II and FP III, respectively. The lower Platreef is characterised by dominance of FP I, harzburgite intercalated with chromitite, norite and dolomite xenoliths. Harzburgite in the lower Platreef correlates to PU2 harzburgite formed from crystallisation of ultramafic magma. The middle Platreef is characterised by dominance of FP II with minor FP I intercalated with serpentinite, norite, orthopyroxenite, parapyroxenite and dolomite xenoliths. The upper Platreef is characterised by dominance of FP III, with minor serpentinite intercalated with parapyroxenite.

The Platreef at Zwartfontein consists predominantly of variety of feldspathic pyroxenites interlayered with harzburgite, orthopyroxenite, norite and metasomatic rocks such as parapyroxenite and serpentinite.

(i) Feldspathic pyroxenites I

Feldspathic pyroxenite I are medium- to fine-grained rocks consisting of orthopyroxene (70 vol. %), clinopyroxene (10 vol. %), olivine (15 vol. %) and plagioclase (5 vol. %). Orthopyroxene and olivine occur as cumulus phases enclosed within clinopyroxene oikocryst and plagioclase occurring on grain boundaries exhibiting a poikilitic texture. Feldspathic pyroxenite I contain erratic BMS mineralisation such as pyrite, chalcopyrite and pentlandite. Accessory minerals include biotite and quartz. Some of the feldspathic pyroxenite I intersected by borehole ZF048 contain quartz which is associated with contamination by felsic melts.

(ii) Feldspathic pyroxenites II

Feldspathic pyroxenites II are coarse-grained rocks consisting of orthopyroxene (85-70 vol. %), clinopyroxene (5-25 vol. %) and plagioclase (10-5 vol. %). Feldspathic pyroxenites II is the dominant rock in the Platreef containing relatively high PGE-BMS mineralisation and is equivalent to B-reef defined by White (1994). Most of the feldspathic pyroxenites II shows a poikilitic texture where orthopyroxene and clinopyroxene occur as cumulus phases enclosed in plagioclase oikocryst. Feldspathic pyroxenite II intersected by borehole ZF048 displays an interlocking texture, extensively fractured and large orthopyroxene crystals compared to that intersected by borehole ZF044 and ZF057 where the footwall is Malmani dolomite. Geochemically, feldspathic pyroxenite II are characterised by relatively high values in MgO, Fe_2O_3 and Si_2O with lower values in CaO, Al_2O_3, Na_2O, K_2O and LOI.

(iii)Feldspathic pyroxenites III

Feldspathic pyroxenites III are barren and equivalent to C-reef defined by White (1994). These rocks consist of orthopyroxene (65-60 vol. %), clinopyroxene (15 -25 vol. %) and plagioclase (20-15 vol. %). Feldspathic pyroxenites III occurring in the upper Platreef contain high plagioclase compared to FP I and FP II, and it occurs towards the top of the Platreef. Contrary to FP I and FP II, the FP III contain high values in CaO, Al_2O_3 and Sr associated with high plagioclase content.

(iv) Harzburgite

Harzburgite is dominant towards the bottom in the lower Platreef at Zwartfontein. Harzburgite consists predominantly of olivine (75-65 vol. %), which occurs as chadacrysts enclosed in orthopyroxene (25-30 vol. %) and clinopyroxene (< 5 vol. %) oikocrysts. In borehole ZF057, some harzburgites were also noted towards the top in the upper Platreef. The occurrence of harzburgite towards the top of the Platreef may be attributed to an intrusion of new primitive magma after crystal fractionation of pre-existing magma. Scoon and de Klerk (1987) described the unexpected occurrence of olivine cumulate in cyclic unit between the UG1 chromitite and the Bastard Reef, as a result of new magma influx. Olivine in harzburgite is moderate to extensively altered to serpentine; hence this rock is also referred to as serpentinized harzburgite in the current study. Kinnard (2005) also noted the occurrence of serpentine harzburgite enriched in chromite at Turfspruit, but absent at Overysel (Holwell and McDonald, 2006). Cronje (2017) reported some variable degree of serpentinisation at Zwartfontein where some harzburgite were altered beyond recognition, and others still maintain primary magmatic textures. Previously, there was a debate as to whether the olivine in Platreef harzburgite originated from magmatic or non-magmatic processes. Kinnard et al. (2010), Mitchell and Scoon (2012) based on geochemical data supported that harzburgite rocks at Akanani are of magmatic origin. Harris and Chaumba (2001) explained that magmatic harzburgite are characterised by elevated values in Cr, Co and Fe. Therefore, harzburgite rocks identified in the current study are of magmatic origin based on elevated values in Cr, Co and Fe with an average value of 1280 ppm, 128 ppm and 15 wt. % respectively. Serpentinite harzburgite is the host of high PGE-BMS mineralisation at Zwartfontein, which is consistent with the results reported by Cronje (2017) at Zwartfontein. Some harzburgite (sample ZF057-37) contain cumulus chromite which occurs as chadacrysts within olivine and orthopyroxene. Petrography has shown that chromite at Zwartfontein occurs as disseminated, angular grains in harzburgite. Holwell and McDonald (2006) also noted the presence of chromite at Sandsloot and Overysel. Holwell and McDonald (2006) described the occurrence of chromitite as crucially important

in understanding the style of PGE mineralisation in the Platreef. Mitchell and Scoon (2012) reported the occurrence of chromitite stringers and layers at Akanani, which are associated with harzburgite. Harzburgite, as compared to other Platreef rocks, contain relatively low LREE, HREE and $(La/Lu)_N$ ratios which support low degree of fractionation and low effect of crustal contamination.

(v) Parapyroxenite

Parapyroxenite were formed from modified pyroxenites as a result of contact metamorphism with Malmani dolomite-calcsilicates. According to Harris and Chaumba (2001), parapyroxenites are rocks that seem to be a 'mélange of variably recrystallised pyroxenites and calc-silicates rocks'. Parapyroxenite was intersected by borehole ZF044 and ZF057 at various depths and contained massive and disseminated sulphildes mineralisation such as chalcopyrite, pentlandite and pyrite. Harris and Chaumba (2001) explained the economic occurrence of sulfides mineralisation in parapyroxenite rocks as evidence of high degree of fluid-rock interaction in the Platreef. Parapyroxenite at Zwartfontein is characterized by olivine (50-60 vol. %), clinopyroxene (35-30 vol. %) and orthopyroxene (15-10 vol. %). Parapyroxenite is sometimes referred to as clinopyroxenite due to predominance of clinopyroxene content over orthopyroxene. Parapyroxenite intersected by borehole ZF057 at a depth of 1403 m, shows gradational contact with calc-silicate and contain significant veins of altered olivine to serpentine, similarly to what was noted by Harris and Chaumba (2001) in Sandsloot.

(vi) Norite

Norite at Zwartfontein are characterised by cumulus plagioclase enclosed in orthopyroxene oikocryst and intercumulus clinopyroxene. In terms of rare earth elements, norite shows similar trends with feldspathic pyroxenites except that the former has high positive Eu anomalies and high $(Eu/Eu^*)_N$, which reflect high plagioclase content. Norite occurs as interlayers between the feldspathic pyroxenites and they are barren. Norite rocks from the current study are similar to those reported at Overysel by Pronost et al. (2008).

6.5.5. Hydrothermal fluid activity and PGE-BMS mineralisation

The source of hydrothermal fluid and its effect on the PGE mineralisation in the Platreef have yet to be fully explained (Harris and Chaumba, 2001). Harris and Chaumba (2001) reported magmatic source of hydrothermal fluids at Sandsloot farm and supported by Holwell and McDonald (2006) that these fluids are more prevalent at Sandsloot where the footwall is dolomite as opposed to the granitic footwall at Overysel. The composition and temperature of hydrothermal fluids in the Platreef vary throughout the Platreef. Hydrothermal fluids in the Platreef, as explained by Pronost et al. (2008), can be subdivided into (1) magmatic fluids and (2) meteoric fluids. The former is responsible for deuteric alteration resulting in the formation of quartzo-feldspathic veins dominantly found in ZF048 at Zwartfontein, while meteoric fluids are responsible for a low-temperature alteration of minerals to serpentine veins, which are dominantly occurring in borehole ZF044 and ZF057. Hydrothermal quartzo-feldspathic veins at Zwartfontein were intersected by borehole ZF048 at various depths where the thickest veins occur at the depths of 85.50 – 87.72 m and 549.46 – 556.8 m. These quartzo-feldspathic veins consist dominantly of 80% of quartz with texture that ranges from graphic to spotted texture. Armitage et al. (2002) also reported hydrothermal quartzo-feldspathic veins at Sandsloot, where they appear to be coarse-grained and dominated by quartz and feldspar minerals with some aggregates of low temperature minerals such as calcite.

From the current study, the corroboration to the occurrence of hydrothermal fluid in Zwartfontein is exhibited by the replacement of primary minerals such as orthopyroxene, olivine and plagioclase by low-temperature minerals such as amphibole, serpentine and sericite respectively (as seen in petrography). The substantial occurrence of secondary minerals at Zwartfontein was observed in samples from borehole ZF044 and ZF057 where the floor rock is dolomite in contrast to granite floor rock in ZF048. These findings are consistent with those reported by Harris and Chaumba (2001). More evidence of hydrothermal fluid activity is shown by fracturing on orthopyroxene filled with talc and opaque minerals. Although mineral alteration by hydrothermal fluid activity has occurred in the Platreef rocks at Zwartfontein, primary minerals still maintain their original state suggesting relatively weak to moderate hydrothermal effect. The occurrence of quartz as interstitial phase in feldspathic pyroxenites I (sample ZF048-40) and feldspathic pyroxenite II (sample ZF044-45) can be evidence of contamination by felsic melts that arose from partial melting of Archean granite (Barton et al., 1986).

The effects of hydrothermal fluid activity in the development and alteration of Ni-Cu-PGE mineralisation remains an unresolved subject in research. Kinnard et al. (2005) suggested that hydrothermal fluid activities are responsible for decoupling of PGEs from base metal sulfides and trigger their redistribution. In contrary, most authors (e.g. Klemd et al., 2016) argue against the effect of hydrothermal fluid activity in the decoupling of PGEs from base metal sulfides (BMS). Klemd (2016) noted a good correlation between PGE and BMS in both Sandsloot and Overysel underlain by dolomite and granite, respectively. The Pt:Pd ratios (1:1) of the studied rocks are inconsistence with the redistribution of PGE by hydrothermal fluid activities. McCallum et al. (1976) and Wood (2002) emphasised that Pt:Pd ratios would be expected to be lower as a result of the decoupling of mobile Pd from Pt. The strong correlation between PGE and BMS at Zwartfontein in the current study rules out the effect of hydrothermal fluid in the decoupling of PGE from BMS, consequently, not in support of the redistribution of PGE mineralisation. Therefore, based on these results, it can be suggested that the distribution of PGE mineralisation at Zwartfontein was controlled by sulphide mineralisation as opposed to hydrothermal fluid activity and metasomatic processes. Manyeruke et al. (2005) noted good correlation between PGE and BMS at Townland and associated it to significant control by segregating sulphide liquid. Holwell and McDonald (2006) also noted a strong correlation between PGE and BMS at Overysel suggesting the predominance of sulfides liquid in the distribution of PGE mineralisation consistent with orthomagmatic deposits.

In contrast, hydrothermal fluid activity has played a significant role in the redistribution of PGE mineralisation in areas where the footwall consist of shales such as Turfspruit, Macalacaskop (Hutchinson and Kinnaird, 2005) and dolomite at Sandsloot (Holwell and McDonald, 2006). The weak correlation between BMS and PGE is therefore due to decoupling process during hydrothermal alteration. These results are consistent with those reported by Armitage et al. (2002), who concluded that the redistribution of PGE mineralisation in Sandsloot where the footwall is dolomite was influenced by hydrothermal fluid activity. Armitage et al. (2002) further suggested that mineralisation at Sandsloot cannot be of orthomagmatic origin only. The interaction of the Platreef magma with a variety footwall rocks has affected the style of Ni-Cu-PGE mineralisation in the Platreef (Holwell, 2006). Despite the alteration of style and distribution of PGE mineralisation by footwall rocks and hydrothermal fluids, the primary Platreef Ni-Cu-PGE mineralisation is of magmatic origin (Holwell, 2006).

Several studies (e.g. Mountain and Wood, 1988; Smith, 2013) have shown that high concentration of As, Sb, Bi and Te plays a significant role in restricting the remobilization of

PGE by hydrothermal alteration. PGE mineralisation in the current study (Zwartfontein 814 LR) seems to be controlled by sulphide liquid. Armitage et al. (2002) noted that PGE mineralisation in the southern portion of Zwartfontein 818 LR and Sandsloot where footwall is dominantly dolomite, PGE mineralisation are associated with platinum-group minerals (PGM) and in part with late-stage magmatic-hydrothermal fluid as compared to sulfides. The hydrothermal fluid activity also played a role in the distribution of Ni-Cu-PGE mineralisation into dolomite footwall rocks at Sandsloot and Zwartfontein (e.g. Armitage et al., 2002; Holwell et al., 2006; Holwell and Jordaan, 2006). However, this is not consistent with the results from the current study and those reported at Sandsloot (Klemd et al., 2016). The results reported in the current study support predominance of sulphide liquid of magmatic origin in the distribution of PGE mineralisation with minor hydrothermal fluid in places.

6.5.6. Evidence of crustal contamination in the Platreef

Contamination in the Platreef have been previously divided into two stages namely; (1) first-stage contamination event and (2) second-stage contamination event (Ihlenfeld and Keays 2011). The first-stage contamination event is referred to crustal contamination at the staging chamber before the emplacement of the Platreef, whereas second-stage contamination event is referred to the contamination of the Platreef magma by local footwall rocks during the emplacement. The effect of crustal contamination in the Platreef has been the interest to several authors (e.g. Harris and Chaumba (2001); Holwell and McDonald (2005) and Pronost et al., (2008)) although some questions remain unanswered. This section, therefore, aims at discussing evidence of the effect of contamination in the Platreef type PGE mineralisation based on the petrography, whole-rock geochemistry and isotope geochemistry.

Contamination of the Platreef rocks by local footwall rocks have been a subject of research (e.g. Holwell and McDonald, 2007; Ihlenfeld and Keays, 2011). Contamination of the Platreef magma by local footwall rocks at Zwartfontein is exhibited by the occurrence of calc-silicate xenoliths where the footwall is dolomite (borehole ZF044 and ZF057). The significant occurrence of calc-silicate in the Platreef was also reported by Harris and Chaumba (2001) at Sandsloot farm where they account for 18% contamination of the Platreef magma. According to Viljoen (2016), contamination by calc-silicate may result in the dilution of PGE mineralisation grade rather than enhancing sulfur saturation of the Platreef magma.

The Platreef has variable heterogeneity along the strike in terms of the thickness, mineralogy, texture and distribution of PGE mineralisation as explained by Armitage et al. (2002) that it is

the reflection of variable footwall rocks along strike. The distribution of PGE mineralisation in the Platreef also depend on the type of the footwall rocks. Chemostratigraphic profiles from the current study show that high PGE mineralisation in borehole ZF048 occurs at the contact with the granite footwall rocks and at the top of the Platreef package. In contrast, high PGE mineralisation in borehole ZF044 and ZF057 occur respectively at 52.88 m and 48.12 m above the contact with dolomite footwall rocks. The occurrence of top-loaded PGE mineralisation at Zwartfontein was noted in all the boreholes (ZF044, ZF048 and ZF057). Holwell et al. (2007) suggested that the footwall rocks play an important role in the distribution and abundance of PGE mineralisation in the Platreef. Besides, Viljoen and Schurmann (1998) noted that the variation in PGM in the Platreef is associated with the change in the footwall rocks along strike. The dolomite footwall in Sandsloot is known to contain high-grade PGE mineralisation compared to areas where the footwall rocks are mainly Archean granite (e.g. Overysel). Pronost et al. (2008) explained the influence of assimilation of dolomite in the Platreef as key to high PGE mineralisation. The above was seen at Zwartfontein in boreholes underlain by dolomite (ZF044 and ZF057) where high PGE mineralisation is hosted in feldspathic pyroxenites (FP I and FP II), serpentinites and parapyroxenites. However, precise understanding of linkage and relationship between PGE mineralisation and dolomite is to date not clarified.

In terms of Chondrite-normalized rare earth elements (REE) patterns, the Platreef rocks at Zwartfontein show similar trends to the previous results reported at Townlands by Manyeruke et al. (2005) and Overysel (Howell and McDonald, 2006). The Platreef rocks usually are known to exhibit a positive Eu anomaly unless when affected by crustal contamination. The Platreef rocks at Zwartfontein have a positive Eu anomaly, with exception to sample ZF044-34 which have a negative Eu anomaly and relatively high REE values. McDonald et al. (2005) explained the occurrence of the negative Eu anomaly as a result of contamination by dolomite of the Malmani Formation. Holwell and McDonald (2006) also reported the occurrence of highly fractionated feldspathic pyroxenites enriched in REE at Overysel, and attributed this to contamination derived from partial melting of footwall gneisses. Crustal contamination in the Platreef rocks is also supported by pronounced depletion in Nb, Ta and high positive Pb anomalies consistent with the results reported by Hutchison & Kinnaird (2005).

Strontium (Sr) and neodymium (Nd) isotopes can be used as tracers to determine the nature and extent of contamination. The initial $^{87}Sr/^{86}Sr$ values of a primitive mantle magma are approximately 0.703 (Kruger, 1994), and higher values are associated with crustal contamination. Considering the results from Sr-Nd isotopes, contamination in the Platreef have

occurred both prior and post crystallisation. The initial $^{87}Sr/^{86}Sr$ values of the Platreef pyroxenites are high (0.660 to 0.714) and above the range of primitive mantle magma. This is attributed to the contamination of the Platreef magma by in-depth crustal materials before emplacement. Platreef rocks in direct contact with the floor rocks (Archean granite in borehole ZF048 and dolomite in borehole ZF044 and ZF057) have high initial ($^{87}Sr/^{86}Sr$)i ratio compared to other rocks in the stratigraphic height.

Similarly, Barton et al. (1986) noted high initial ($^{87}Sr/^{86}Sr$) in A-reef compared to the overlaying B- and C-reefs. According to Kruger (1994), the difference in these initial ratios shows a decreasing influence of crustal contamination in the Platreef magma with the stratigraphic height. The base of the Platreef exhibit high initial ($^{87}Sr/^{86}Sr$)i in borehole ZF048 (0.714398) underlain by Archean granite relative to borehole ZF044 and ZF057 underlain by dolomite with initial ($^{87}Sr/^{86}Sr$)i of 0.710397 and 0.709712 respectively. Platreef rocks also show high contamination by crustal/footwall rocks after crystallisation. The above is supported by high ($^{87}Sr/^{86}Sr$)m and relatively low values ($^{143}Nd/^{144}Nd$)m of the pyroxenites rocks which ranges in-between 0.709929-0.881729 and 0.511452-0.512107, respectively.

Based on the chemostratigraphic results which show that high PGE mineralisation are concentrated on the lower Platreef exhibiting high initial ($^{87}Sr/^{86}Sr$)i ratios confirm that contamination by crustal/footwall rocks has played a role on concentration of PGE mineralisation in the Platreef.

6.5.7. The Platreef magma source

The Platreef rocks analysed in the current study shows significant variation in the initial $(^{87}Sr/^{86}Sr)_i$ ratios ranging between 0.660 and 0.714 calculated at 2.06 Ga. According to Kruger (1994), the parental magma that gave rise to the formation of the RLS has the initial values that range between 0.705 - 0.709. Although some of the Platreef rocks have an initial $(^{87}Sr/^{86}Sr)_i$ ratio as low as 0.660 and as high as 0.714, most of the Platreef rocks have initial $(^{87}Sr/^{86}Sr)i$ ratio within the RLS range. Barton et al. (1986) suggested that the parental magma to the Platreef have an initial Sr_i comparable to that of the Merensky Reef (0.7066-0.7074, Kruger & Marsh, 1982), with the Platreef rocks overlying dolomite in the Southern Sector (Sr_i = 0.7054) and early formed orthopyroxene (Sr_i = 0.7079) representing the closest approximates for the isotopic composition of the "truly magmatic" Platreef magma.

The chemostratigraphic plots of initial $^{87}Sr/^{86}Sr$ versus depth show a considerable variation in $(^{87}Sr/^{86}Sr)i$ with stratigraphic succession in all the boreholes. The variation in the initial $(^{87}Sr/^{86}Sr)i$ ratio of the Platreef rocks is suggested to represent crystallization of these rocks from different magma source and multiple magmas pulses with contrasting $(^{87}Sr/^{86}Sr)i$ compositions. Sharpe et al. (1986) and Hutton and Schweitzer (1995) suggested that the different magma composition resulted from progressive contamination of the magma by crustal components during the emplacement. Based on high initial Sr-isotope ratios observed in the Platreef rocks, it is essential to highlight that crustal contamination initially occurred in the staging chamber before crystallisation.

The formation of the Platreef from sill-like intrusion is also supported by Mg# reversals, which were observed throughout the stratigraphic succession in all the boreholes. The compositional breaks shown by major and trace elements in Zwartfontein rocks were explained by Manyeruke et al. (2005) to represent distinct sill-like intrusion of Platreef magma rather than single body. The Platreef sills are discriminated from each other by differences in Mg#, $(^{87}Sr/^{86}Sr)_i$, $(^{143}Nd/^{143}Nd)_i$ and Pd:Pt ratios. Holwell (2006) reported some evidence supporting the intrusion of the Platreef at Zwartfontein as a single magma body but emplaced as multiple magma series (Kinnard, 2005). Mitchell and Scoon (2012) conducted a study on the formation of the Platreef from multiple, non-sequential magma replenishment. In their study, Mitchell and Scoon (2012) concluded that the Platreef was formed from multiple sill-like intrusions.

Although most of the Platreef rocks shows that contamination occurred in the staging chamber, sample ZF044-34, ZF057-28 and ZF057-31 have a relatively low initial $(^{87}Sr/^{86}Sr)i$ ratio ranging between 0.660 and 0.701 showing crystallization of these rocks from primitive mantle magma. These rocks, however, contains high measured $(^{87}Sr/^{86}Sr)m$ isotope in the present day with an average of 0.72582. The above suggests that significant contamination resulted from hydrothermal alteration post-crystallization. The effect of hydrothermal alteration was also noted during petrographic studies by the occurrence of hydrothermal veins and secondary minerals such as sericite, chlorite, tremolite and actinolite.

The progressive decrease in $(^{87}Sr/^{86}Sr)i$ in borehole ZF057 from 1492.17 to 1355.24 m reflect the progressive addition of primitive mantle magma. The abrupt increase in $(^{87}Sr/^{86}Sr)i$ from 1355.24 to 1324.13 m (sample ZF057-34) is associated with contamination of the magma by crustal materials. The addition of primitive magma at a depth of 1303.28 m resulted in the decrease of $(^{87}Sr/^{86}Sr)i$. These fluctuations in Sr-isotopes with the stratigraphic height were

also observed in borehole ZF044 and ZF048 representing multiple, sill-like magma intrusions. The initial ($^{87}Sr/^{86}Sr$)i ratio does not, however, show a consistent increase or decrease with the stratigraphic height but instead, it shows reversals and fluctuations. Kruger, (2005) explained the fluctuations and reversals in initial ($^{87}Sr/^{86}Sr$)i as a result of multiple influxes of magma with different isotopic composition and referred this to an open system integration stage.According to Wilson et al. (2017), this represents interplay between multiple ingression of mafic/ultramafic magma, melt separation, and country-rock contamination. The occurrence of chromitite in the lower Platreef supports the interplay between primitive ultramafic magma and evolved magmatic fluids.

The possible magma source for the Bushveld rocks includes primitive mantle source, evolved mantle source and lower/upper crustal source (Wilson et al., 2017). Based on the results in the current study, the Platreef magma source does not point out to a single source but shows the interplay of multiple magma sources, which includes depleted mantle magma source and crustal magma source. The occurrence of relatively high ($^{143}Nd/^{144}Nd)_i$ ratios (0.509907) and low ($^{87}Sr/^{86}Sr$)i ratio (0.701017) in sample ZF044-34 confirms derivation from a primitive mantle source. Contrastingly, the occurrence of relatively low ($^{143}Nd/^{144}Nd)_i$ ratios, high ($^{87}Sr/^{86}Sr$)i ratios and negative $Nd_{(2060)}$ in most of the Platreef rocks confirms derivation from subcontinental lithospheric mantle or depleted mantle source with high crustal contribution. Buchanan et al. (2004) suggested that another possible explanation for this is the formation of the rocks from a hybrid mixture of mantle and crustal derived melt. The general decrease in ($^{87}Sr/^{86}Sr$)i ratios with the stratigraphic height in the Platreef especially in borehole ZF057 supports the progressive replenishment of a more primitive mantle magma (Kruger, 1994). According to Wilson et al. (2017), a subcontinental lithospheric mantle source with contribution of crustal materials is defined by flat REE patterns and low Mg#. In the current study, this was observed in sample ZF044-45 and ZF057-51, which contain high REE, flat REE patterns and low Mg# of 64 and 52, respectively, compatible with SCLM and crustal contamination.

6.2. CONCLUSIONS

The current study aims at improving the understanding of petrogenesis of the Platreef by determining whether the Platreef was formed from multiple or single magma pulses. The above also involved the evaluation of geological processes that were involved during the formation of the Platreef such as fractionation, crustal contamination and hydrothermal fluids.

Based on the results from detailed petrography, whole-rock geochemical data and isotope geochemistry conducted in the current study, the following conclusions are made:

- Petrographic studies, which were complemented by whole-rock geochemical data have shown that the Platreef at Zwartfontein consists of multiple sills of pyroxenite, feldspathic pyroxenite, orthopyroxenite, norite and harzburgite. These rocks are intercalated with parapyroxenite and serpentinite referred to as metasomatic rocks. Calc-silicate xenoliths occur throughout the stratigraphic succession in borehole ZF044 and ZF057 underlain by dolomite. On the other hand, granite xenoliths were found in borehole ZF048 underlain by granite. Lithologically and stratigraphically, the Platreef at Zwartfontein is significantly heterogeneous and more complicated due to high degree of contamination by footwall rocks. Feldspathic pyroxenites are the most dominant rocks in the Platreef and were subdivided into FP I, FP II and FP III based on their mineralogical, textural and geochemical variations.

  Lower Platreef

  The Lower Platreef is dominated by feldspathic pyroxenites I which consist of orthopyroxene (70-60 vol. %), clinopyroxene (10-15 vol. %), olivine (15-10 vol. %) and plagioclase (5 vol. %). In terms of the major elements, feldspathic pyroxenite I is characterized by high MgO, Fe_2O_3, CaO, LOI and low Al_2O_3, Si_2O, Na_2O and K_2O. Spider diagrams have shown that feldspathic pyroxenite I are enriched in LREE relative to HREE. This is exceptional to sample ZF044-45 which have relatively high LREE and HREE due to contamination. The lower Platreef is moderately to extensively mineralised with PGE-BMS mineralisation.

Middle Platreef

The Middle Platreef is dominated by feldspathic pyroxenites II which consist of orthopyroxene (85-70 vol. %), clinopyroxene (5-25 vol. %) and plagioclase (10-5 vol. %). Feldspathic pyroxenite II, in terms of major elements is characterized by high MgO, Fe_2O_3 and low CaO, Al_2O_3, Na_2O, K_2O and LOI. Feldspathic pyroxenite II are characterized by a strong decrease in LREE with a sharp negative slope and a relatively constant HREE. Feldspathic pyroxenite II has low $(Eu/Eu^*)_N$ ratios ranging from 0.91 to 1.31 which is consistent with low positive Eu anomaly and low feldspar content compared to other Platreef rocks. The middle Platreef is extensively mineralised with PGE-BMS mineralisation compared to lower and upper Platreef.

Upper Platreef

The Upper Platreef is dominated by feldspathic pyroxenites III consisting of orthopyroxene (65-60 vol. %), clinopyroxene (15 -25 vol. %) and plagioclase (20-15 vol. %). High plagioclase content in feldspathic pyroxenite III was corroborated by high CaO and Al_2O_3, coupled with low Fe2O3 and MgO. Feldspathic pyroxenite III shows a similar trend with feldspathic pyroxenite II, and they are characterized by steep LREE slope and a flat HREE with positive Eu anomaly. Trace elements in FP III show high degree of fractionation when compared to trace elements in FP II. This is supported by high $(La/Lu)_N$ ratios that range between 2.79 to 3.50 in feldspathic pyroxenite. In terms of PGE-BMS mineralisation, the upper Platreef is barren.

- The Platreef rocks show a high degree of fractionation patterns enriched in LREE relative to HREE. REE shows an increase with stratigraphic height in borehole ZF048 where the footwall is granite and a progressive decrease in borehole ZF044 and ZF057 where the footwall is dolomite. The above is attributed to high contamination of the Platreef rocks in borehole ZF044 and ZF057 by dolomite at great depth. The predominance of magmatic olivine, orthopyroxene and clinopyroxene with minor plagioclase at the bottom of the Platreef and their decrease with increasing plagioclase with stratigraphic height reflect a normal fractionation trend from lower to upper Platreef. The positive Eu anomalies in the Platreef rocks reflect the significant role of plagioclase in partitioning of REE between cumulate assemblages and magma.

- Contamination by crustal materials occurred as two stages (1) in the staging chamber prior to intrusion and (2) after crystallisation of the Platreef magma. Variably high initial $^{87}Sr/^{86}Sr$ ratios in the Platreef pyroxenites represent the first stage of contamination in the staging chamber. The occurrence of secondary minerals in the Platreef rocks, such as quartz, biotite and high measured $^{87}Sr/^{86}Sr$ ratios ranging between 0.701 and 0.880 represents the second stage of contamination by siliceous materials after crystallization. The Platreef rocks at Zwartfontein contain relatively high negative εNd values consistent with contamination by local footwall rocks. The significant contamination by crystal materials occurred after crystalization as evidenced by relatively high measured $(^{87}Sr/^{86}Sr)_m$ and low $(^{143}Nd/^{144}Nd)_m$ values in the Platreef rocks.

- PGE mineralisation is variably distributed in the Platreef with high concentration occurring at the base and the top of the Platreef package. PGE mineralisation are hosted in feldspathic pyroxenites, harzburgite and in metasomatic rocks such as parapyroxenite and serpentinite. Hydrothermal fluid activities have played a minor role in the redistribution and decoupling of PGE and BMS in the Platreef. Hydrothermal fluid-rock interaction has variably affected the Platreef rocks. Feldspathic pyroxenite intersected by borehole ZF048 were extensively affected by hydrothermal fluids as evidenced by complete alteration of plagioclase, the occurrence of talc, fractures and hydrothermal veins. Borehole ZF044 and ZF057 which are underlain by dolomite, are moderate to extensively affected by hydrothermal fluids resulting in the occurrence of serpentinite rocks towards the top of the Platreef. The Platreef rocks at Zwartfontein were affected by both magmatic fluids responsible for formation of quartzo-feldspathic veins in borehole ZF048 and meteoric water responsible for serpentinisation in borehole ZF044 and ZF057. Although hydrothermal fluids have affected the Platreef rocks, their contribution to the redistribution of PGE mineralisation is insignificant. Based on the good positive correlation between PGE and BMS it can be said that the redistribution of PGE in the Platreef at Zwartfontein were predominantly controlled by sulfides liquid.

- The calculated age for the Platreef rocks based on Rb-Sr dating method is $\pm$ 1.5 Ga. The Sm-Nd dating method has yielded a crystallisation age of 2.05 Ga consistent with

the crystallisation age previously suggested for the Bushveld Complex (2.06 Ga). The poorly constrained age for the Platreef rocks calculated from Rb-Sr dating method is consistence with post-crystallisation hydrothermal fluid alterations.

- In conclusion, the Platreef was formed from multiple, sill-like intrusion of magma with different initial $^{87}Sr/^{86}Sr$ isotope ratios, which varies between 0.690207 and 0.714398. This is also supported by the occurrence of Mg# reversals, reversed differentiation trend and compositional breaks throughout the stratigraphic succession in the Platreef. These results are consistent with the ones reported by Kinnard *et al.,* (2005) at Overysel. The initial $^{87}Sr/^{86}Sr$ ratios are variably high supporting contamination in the staging chamber and multiple parental magma sources. The formation of the Platreef rocks does not point out to a single magma source but instead it includes primitive mantle source, subcontinental lithospheric mantle (SCLM) and crustal source. The parental magma source for most of the Platreef rocks is dominantly primitive mantle source with high contribution of crustal materials as supported by high initial $^{87}Sr/^{86}Sr$ and high negative $\varepsilon Nd_{(2060)}$ values. Very few samples (ZF057-28, ZF057-31 and ZF044-34) were formed from uncontaminated primitive mantle magma source with initial $^{87}Sr/^{86}Sr$ ratio of <0.7011, which is within the range of primitive mantle magma values (<0.7030).

6.3. Recommendations

Petrogenesis of the Platreef is complicated and even after detailed petrography and geochemical studies presented in the current study, there are some gaps that remained unanswered. The question about the exact contacts between the Platreef sills and the detailed stratigraphy reamain unaswered. It is, therefore, recommended that further studies must done on the petrogenesis of the Platreef, which will involve detailed Sr-Nd isotope data taken on a small scale.

REFERENCES

Armitage, P.E.B., McDonald, I., Edward, J.S. & Manby, G.M. (2002). Platinum-group element mineralisation in the Platreef and calc-silicate footwall at Sandsloot, Potgietersrus District, South Africa, vol. 307, pp. 36-45.

Armitage, P.E.B., McDonald, I. & Tredoux, M. (2007). A geological investigation of the Waterberg hydrothermal platinum deposit, Mookgophong, Limpopo Province, South Africa, *Applied Earth Science (Transactions of the Institute of Mining and Metallurgy)*, vol. 116, pp. 113–129.

Barnes, S-J., Naldrett, A.J. & Gorton, M.P. (1985). The origin of the fractionaton of platinum group elements in terrestrial magmas, *Chemical geology*, vol. 53 (3-4), pp. 303-323.

Barnes, S-J. & Maier, W.D. (2002). Platinum-group element distributions in the Rustenberg Layered Suite of the Bushveld Complex, South Africa. The Geology, Geochemistry, Mineralogy and Mineral Beneficiation of Platinum-Group Elements. Edited by L.J. Cabri, Canadian Institute of Mining, *Metallurgy and Petroleum***,** Special vol. 54, pp.431-458.

Barton, J.M., Cawthorn, R.G. & White, J. (1986). The role of contamination in the evolution of the Platreef of the Bushveld Complex, vol. 81, pp. 1096-1104.

Buchanan, D.L., Nolan, J., Sudaby, P., Rouse, J.E., Viljoen, M.J. & Davenport, J.W.J. (1981). The genesis of sulphide mineralisation in a portion of the Potgietersrus Limb of the Bushveld Complex: *Econominc Geology*, vol. 76, pp. 568–579.

Buchanan, P.C., Reimold, W.U., Koeberl C. & Kruger, F.J. (2004). Rb-Sr and Sm-Nd isotopic compositions of the Rooiberg Group, South Africa: early Bushveld-related volcanism, *Lithos*, vol. 29, pp. 373-388.

Cameron, E. N. (1978). The Lower Zone of the Eastern Bushveld Complex in the Olifants River Trough, *Journal of Petrology*, vol. 19, pp. 437-462.

Cawthorn, R.G. (1999). Platinum-group element mineralisation in the Bushveld Complex—a critical reassessment of geochemical models, *South African Journal of Geology*, vol. 02, pp. 268–281.

Cawthorn, R.G. & Webb, S.J. (2001). Connectivity between the western and eastern limbs of the Bushveld Complex: *Tectonophysics*, vol. 330, pp. 195-209.

Cawthorn, R.G., Lee, C.A., Schouwstra, R.P. & Mellowship, P. (2002). Relationship between PGE and PGM in the Bushveld Complex, *The Canadian Mineralogist*, vol. 40, pp. 311-328

Cawthorn, R.G. (2005). Pressure fluctuations and formation of the PGE-rich Merensky and chromitite reefs, Bushveld Complex, *Mineralium Deposita*, vol. 40, pp. 231–235.

Cawthorn, R.G. (2010). Geological interpretations from the PGE distribution in the Bushveld Merensky and UG2 chromitite reefs. *The 4th International Platinum Conference, Platinum in transition 'Boom or Bust',* The Southern African Institute of Mining and Metallurgy.

Cox, K.G., Bell, J.D. & Pankhurst, R.J. (1993). The Interpretation of Igneous Rocks. Chapman and Hall, pp. 358.

Cronje, L.J. (2017). An evaluation of chromiferous layers and their host rocks in the Platreef on the Turfspruit and Zwartfontein properties; A comparative study with the main Bushveld Complex, MSc thesis, University of Witwatersrand.

Eales, H.V., Botha, W.J., Hattingh, P.J., De klerk, W.J., Maier, W.D. & Odgers, A.T.R. (1993). The mafic rocks the Bushveld Complex: a review of emplacement and crystallization and mineralisation, in the light of recent data, *Journal of Earth Sciences*, vol. 16 (1-2), pp. 121-142.

Everitt, B.S., Landau, S. & Leese, M. (2001). Cluster Analysis, Fourth edition, Arnold, pp. 10-50.

Finch, H. (2005).Comparison of distance measures in cluster analysis with dichotomous data, *Journal of Data Science*, vol. 3 (1), pp. 85-100.

Friendly, M. &Denis, D. (2005). The early origins and development of the scatterplots, *Journal of the History of the Behavioral Sciences*, vol. 41 (2), pp. 103-130.

Gain, S.B. & Mostert, A.B. (1982). The geological setting of the platinoid and base metal sulphide mineralisation in the Platreef of the Bushveld Complex in Drenthe, north of Potgietersrus: *Economic Geology*, vol. 77, pp. 1395–1404.

Gain, S.B. & Mostert, A. (1982). The geological setting of the platinoid and base metal sulfide mineralisation in the Platreef of the Bushveld Complex in Drenthe, north of Potgietersrus, *Economic Geology*, vol. 77 (6), pp. 1395-1404.

Grant, J.A. (1986). The isocon diagram - a simple solution to Gresens'equation for metasomatic alteration, *Economic Geology*, vol. 81, pp. 1976-1982.

Gresens, R.L. (1967). Composition-volume relationships of metasomatism, *Chemical Geology*, vol. 2, pp. 47-65.

Harris, C. & Chaumba, J.B. (2001). Crustal contamination and fluid-rock interaction during the formation of the Platreef, northern lobe of the Bushveld Complex, South Africa, *Journal of Petrology*, vol. 42, pp. 1321–1347.

Harris, C., Pronost, J.J.M., Ashwal, L.D. & Cawthorn, R.G. (2005). Oxygen and hydrogen isotope stratigraphy of the Rustenburg Layered Suite, Bushveld Complex: Constraints on crustal contamination: *Journal of Petrology*, vol. 46, pp. 579-601.

Holwell, D.A. (2006). The role of magmatism, contamination and hydrothermal processes in the development of Platreef mineralisation, Bushveld Complex, South Africa. Unpublished Ph.D thesis, Wales, Cardiff University, pp. 260-285.

Holwell, D.A. & McDonald., I. (2006). Petrology, geochemistry and the mechanisms determining the distribution of platinum-group element and base metal sulphide mineralisation in the Platreef at Overysel, northern Bushveld Complex, South Africa: Miner Deposita, vol. 41, pp. 575-595.

Holwell, D.A. & Jordaan, A. (2006). Three-dimensional mapping of the Platreef at the Zwartfontein South mine: implications for the timing of magmatic events in the northern limb of the Bushveld Complex, South Africa, *Applied Earth Science (Transactions of the Institute of Mining and Metallurgy B)*, vol. 115, pp. 41-48.

Holwell, D.A. & McDonald, I. (2006). Petrology, geochemistry and the mechanisms determining the distribution of platinum-group element and base metal sulfide mineralisation in the Platreef at Overysel, northern Bushveld Complex, South Africa, *Mineralium Deposita*, vol. 41, pp. 575-598.

Holwell, D.A. & McDonald, I. (2007). Distributions of platinum-group elements in the Platreef at Overysel, northern Busveld Complex: a combined PGM and LA-ICP-MS study, *Contributions to Mineralogy and Petrology*, vol. 154, pp. 171–190.

Holwell, D.A., Boyce, A.J. & McDonald, I. (2007). Sulfur isotope variation within the Platreef Ni-Cu-PGE deposits: genetic implication for the origin of sulfide mineralisation: *Economic Geology*, vol. 102, pp. 1085-1109.

Hutchinson, D. & Kinnaird, J.A. (2005). Complex multistage genesis for the Ni-Cu-PGE mineralisation in the southern region of the Platreef, Bushveld Complex, South Africa, *Applied Earth Science (Transactions of the Institute of Mining and Metallurgy B)*, vol. 114, pp. 208-223.

Hutton, C.J. & Schweitzer JK. (1995). Evidence for synchronous extrusive and intrusive bushveld magmatism, *Journal of African Earth Sciences*, vol. 21, pp. 579-594.

Ihlenfeld, C. & Keays, R.R. (2011). Crustal contamination and PGE mineralisation in the Platreef, Bushveld Complex, South Africa: evidence for multiple contamination events and transport of magmatic sulfides: *Miner Deposita*, vol. 46, pp. 813–832.

Irvine, T.N. (1975). Crystallization sequences in the Muskox intrusion and other layered intrusions—II. Origin of chromitite layers and similar deposits of other magmatic ores, *Geochimica et Cosmochimica Acta*, vol. 39, pp. 991-1020.

Keays, R.R. & Lightfoot, P. (2010). Crustal sulfur is required to form magmatic Ni-Cu sulfides deposits: evidence from chalcophile elements signatures of Siberian and Deecan trap basalt, *Mineral deposita*,vol. 45, pp. 241-257.

Kinnard, A.J., Hutchison, D. & Schurmann, L. (2005). Petrology and mineralisation of the Platreef: northern limb of the Bushveld Complex, South Africa: *Mineralium Deposita*, vol. 40, pp. 476-481.

Kinnaird, A.J. (2005). Geochemical evidence for multiphase emplacement in the southern Platreef, *Applied Earth Science (Transactions of the Institute of Mining and Metallurgy B)*, vol. 114, pp. 225-241.

Klemd, R., Junge, M., Oberthur, T., Herdrich, T., Schouwstra, R. & Roberts, J. (2016). Platinum-group elements concentrations in base-metal sulfides from the Platreef, Mogalakwena platinum mine Bushveld Complex, South Africa, *geological society of South Africa*, vol. 119 (4), pp. 623-638.

Kruger, F.J. & Marsh, J.S. (1982). Significance of 87Sr/86Sr ratios in the Merensky cyclic unit of the Western Bushveld Complex. Vol. 298, pp. 53-55.

Kruger, F.J., Armstrong, R.A. & Walraven, F. (1990). A chronostratigraphic framework for the north-central Kaapvaal craton, the Bushveld Complex and the Vredefort structure, vol. 171, pp. 23-48.

Kruger, F.J. (1994). The Sr-isotopic stratigraphy of the western Bushveld Complex, *South African Journal of Geology*, Vol. 94, pp. 393-398.

Kruger, F.J. (2005). Filling the Bushveld Complex magma chamber: lateral expansion, roof and floor interaction, magmatic unconformities and the formation of giant chromitite, PGE and Ti-V-magnetite deposits: *mineralium deposita*, vol. 40, pp. 449-469.

Kruger, F.J. (2010). The Merensky and Bastard cyclic units and the Platreef of the Bushveld Complex: Consequences of Main Zone magma influxes and dynamics. The 4th International Platinum Coference, Platinum in transition "Boom or Bust", *The South African Institute of mining and metallurgy*, pp. 2-5.

Lesher, C.M. & Keays, R.R. (2002). Komatiite-associated Ni-Cu-(PGE) deposits: Geology, mineralogy, geochemistry and genesis, *Canadian Institute of Mining, Metallurgy and Petroleum*, Special vol.54, pp. 579-618.

Li, C. & Naldrett, A.J. (1993). Sulfide capacity of magma: A quantitative model and its application to the formation of the sulfide ores at Sudbury, *Economic Geology*, vol. 88, pp. 1253-1260.

Lightfoot, P.C. & Keays, R.R. (2005). Siderophile and chalcophile metal variations in flood Basalts from the Siberian Trap, Noril'sk Region: Implications for the origin of Ni-Cu-PGE sulfides ores, *Economic geology*, vol. 100 (3), pp. 439-462.

Luolavirta, K. (2018). Magmatic evolution of the Kevitsa igneous complex, northern Finland and its relation to the associated Ni-Cu-(PGE) mineralisation, *University of Oulu*, vol. 37 pp.7-37.

Maier, W.D., Arndt, N.T. & Curl, E.A. (2000). Progressive crustal contamination of the Bushveld Complex: evidence from Nd isotopic analysis of the cumulate rocks, *Contrib Mineral petrol*, vol. 140, pp. 316-327.

Mandende, H. (2014). Geochemical and petrographic characteriation of Platreef pyroxenites package P1, P2, P3 and P4 units at the Akanani Prospect area, Bushveld complex, South Africa, MSc thesis, University of the Western Cape, pp. 160-170.

Mangwegape, M., Roelofse, F., Mock, T. & Carlson, R.W. (2016). The Sr-isotopic stratigraphy of the Northern Limb of the Bushveld Complex, South Africa, *Journal of African Earth Sciences*, vol. 113, pp. 95-110.

Manyeruke, T.D. (2003). The petrology and geochemistry of the Platreef on the farms Townlands, near Potgietersrus, northern Bushveld Complex. Unpublished M.Sc. thesis, Pretoria, South Africa, *University of Pretoria*, pp. 36-70.

Manyeruke, T.D., Maier, W.D. & Barnes, S.J. (2005). Major and Trace Element Geochemistry of the Platreef on the farm Townlands, northern Bushveld Complex, *South African Journal of Geology*, vol. 108, pp. 381-396.

Manyeruke, T.D. (2007). Compositional and lithological variation of the Platreef on the farm Nonnewerth, Northern lobe of the Bushveld Complex: Implications on the origin of platinum group elements (PGE) mineralisation. Ph.D thesis, *University of Pretoria*, pp. 92-120.

Marsh, B. D. (2006). Dynamics of magmatic systems, *Elements*, vol. 2, pp. 287-292.

McCallum, M.E., Loucks, R.R., Carlson, R.R., Cooley, E.F. & Doerge, T.A. (1976). Platinum metals associated with hydrothermal copper ores of the New Rambler mine, Medicine Bow Mountains, Wyoming, *Economic Geology*, vol. 71, pp. 1429-1450.

McCandless, T.E. & Ruiz, J. (1991). Osmium isotopes and crustal sources for platinum-group mineralisation in the Bushveld Complex, South Africa, *Geology*, vol. 19, pp. 1225-1228.

McCutcheon, S.C. & Kinnaird, J.A. (2011). Platinum-group mineral assemblages in the Platreef at Tweefontein [abstract]. Platreef Workshop, 4th, Mokopane, South Africa, 14th-16th January 2011, Abstracts.

McCutcheon, S.C. (2012). Platinum-group mineral assemblages in the Platreef at Tweefontein, northern Bushveld Complex, South Africa, MSc thesis, *University of Witwatersrand*, pp. 20-80.

McDonald, I., Holwell, D.A. & Armitage, P.E.B. (2005). Geochemistry and mineralogy of the Platreef and ‘‘Critical Zone’’ of the northern lobe of the Bushveld Complex, South Africa: implications for Bushveld stratigraphy and the development of PGE mineralisation, vol. 40, pp. 526-549.

McDonough, W.F. & Sun, S.S. (1995). The composition of the earth, *Chemical Geology*, vol. 120, pp. 223-253.

Mitchell, A.A. & Scoon, R.N. (2012). The Platreef of the Bushveld Complex, South Africa: A new hypothesis of multiple, non-sequential, magma replenishment based on the observations at Akanani Project, north-west of Mokopane, vol. 115, 4, pp. 535-550.

Molyneaux, T. G. (1974). A geological investigation of the Bushveld Complex in Sekhukhuneland and part of the Steelpoort valley, *South African Journal of Geology*, vol. 77, pp. 329- 338.

Mountain, B.W. & Wood, S.A. (1988). Chemical controls on the solubility, transport, and deposition of platinum and palladium in hydrothermal solutions: a thermodynamic approach, *Economic Geology*, vol. 83, pp. 492-510.

Mungall, J.E., Andrews, D.R.A., Cabri, L.J., Sylvester, P.J. & Tubrett, M. (2005). Partitioning of Cu, Ni, Au, and platinum-group elements between monosulfide solid solution and sulphide melt under oxygen and sulfur fugacities, *Geochimica et Cosmochimica Acta*, vol. 69, pp. 4349-4360.

Mungall, J.E. & Naldrett, A.J. (2008). Ore deposits of the platinum-group elements, *Article in elements*, vol. 4 (4), pp. 253-258.

Naldrett, A.J. & Barnes, S.J. (1986). The behaviour of platinum group elements during fractional crystallization and partial melting with special reference to the composition of magmatic sulfide ores, *Forschritte der Mineralogie*, vol. 74, pp. 113-133.

Nell, J. (1985). The Bushveld metamorphic aurole in the Potgietersrus area; evidence for a two-stage metamorphic event, *Eonomic geology*, vol. 80, No.4, pp. 1129-1152.

Penniston-Dorland, S.C., Wing, B.A., Nex, P.A.M., Kinnaird, J.A., Farquhar, J., Brown, M. & Sharman, E.R. (2008). Multiple sulfur isotopes reveal a magmatic origin for the Platreef platinum group element deposit, Bushveld Complex, South Africa. *Geology*, vol. 36, pp. 979-982.

Penniston-Dorland, S.C., Mathez, E.A., Wing, B.A., Farqhar, J. & Kinnaird, J.A. (2012). Multiple sulfur isotopes evidence for surface-derived sulfur in the Bushveld Complex, *Earth and Planetary Science Letters*, vol. 337-338, pp.236-242.

Pronost, J., Harris, C. & Pin, C. (2008). Relationship between footwall composition, crustal contamination, and fluid–rock interaction in the Platreef, Bushveld Complex, South Africa. *Mineralium Deposita*, vol. 43, pp. 825-848.

Ridley, J. (2013). Ore deposit geology, *Cambrige University prees*, pp. 253-258.

Ripley, E.M., Park, Y.R., Li, C. & Naldrett, A.J. (1999). Sulfur and oxygen isotopic evidence of country rock contamination in the Voisey's Bay Ni–Cu–Co deposit, Labrador, Canada, *Lithos*, vol. 47, pp. 53-68.

Scoon, R.N. & De Klerk, W.J. (1987). The relationship of olivine cumulates and mineralisation to cyclic units in part of the critical zone of the western Bushveld Complex, *Canadian mineralogist*, vol. 25, pp. 57-77.

Sharman-Harris, E.R., Kinnaird, J.A., Harris, C. & Horstmann, U.E. (2005). A new look at sulfide mineralisation of the northern limb, Bushveld Complex: a stable isotope study: *Applied Earth Science*, vol. 114, pp. 252–263.

Sharpe, M.R., Evensen, N.M. & Naldrett, A.J. (1986). Sm/Nd and Rb/Sr evidence for liquid mixing, magma generation and contamination in the Eastern Bushveld Complex. *Geological Society of South Africa, Geocongress 1986, abstract, Johannesburg*, pp. 621-624.

Smith, J.W., Holwell, D.A. & McDonald, I. (2013). The mineralogy and petrology of platinum-group element-bearing sulphide mineralisation within the Grasvally Norite–Pyroxenite–Anorthosite (GNPA) member, south of Mokopane, northern Bushveld Complex, South Africa, *Applied Earth Science*, vol. 120 (4), pp. 158-174.

Sun, S.S. & McDonough, W.F. (1989). Chemical and isotopic systematics of oceanic basalts; implications for mantle composition and processes. In: Magmatism in the ocean basins. Saunders, A.D. and Norry, M.J. (Editors), *Geological Society of London, London*. 42: pp. 313-345.

Tawanda, D., Manyeruke, T.D. & Maier, W.D. (2005). Major and trace elements geochemistry of the Platreef on the farm Townlands, northern Bushveld Complex, *Geology society of South Africa*, pp. 381-396.

Templ, M., Filzmoser, P. & Reimann, C. (2008).Cluster analysis applied to regional geochemical data: problems and possibilities, *Applied Geochemistry*, vol. 23, no. 8, pp. 2198-2213.

Tornos, F., Galindo, C., Casquet, C., Pevida, L.R., Martinez, C., Martinez, E., Velasco, F. & Iriondo, A. (2006). The Aguablanca Ni-(Cu) sulphide deposits, SW Spain: geologic and

geochemical controls and relationship with a midcrustal layered mafic complex, *Minerallium Deposita*, vol. 41 (8), pp. 737-769.

Van der Merwe, M. (1976). The layered sequence of the Potgietersrus limb of the Bushveld Complex, *Economic Geology*, vol. 71 (7), pp. 1337-1351.

Viljoen, M.J & Schürmann, L.W. (1998). Platinum-group metals. In: Wilson MGC, Anhaeusser CR (eds) The mineral resources of South Africa. *Council for Geoscience, Pretoria*, pp. 532-568.

Viljoen, M. (2016). The Bushveld Complex: Host to the world's largest platinum, chromium and vanadium resources, vol. 30, pp. 239-251.

Wagner, P.A. (1929). The Platinum deposits and mines of South Africa, Struick, London, pp. 325-338.

Walvaren, F., Armstrong, R.A. & Kruger, F.J. (1990). A chronostratigraphic framework for the north-central Kaapvaal craton, the Bushveld Complex and the Vredefort structure, *Tectonophysics*, vol. 171, pp. 23-48.

White, J.A. (1994). The Potgietersrus prospect–geology and exploration history XVth CMMI congress, *Johannesburg SAIMM*, vol. 3, pp. 173–181.

Wilson, A.H. & Chunnett, G. (2006). Trace Element and Platinum Group Element Distributions and the Genesis of the Merensky Reef, Western Bushveld Complex, South Africa, *Journal of Petrology*, vol. 47, pp. 2369-2403.

Wilson, A.H., Zeh, H., Gerdes, A. (2017). In situ Sr isotope in plagioclase and trace elements systematics in the lower part of the Eastern Bushveld Complex: Dynamic process in an evolving magma chamber, *Journal of Petrology*, vol.58 (2), pp. 327-360.

Winch, J. (2011). The importance of drilling too deep a Platreef prospective: Abstract of 4th Platreef Workshop Mokopane, 14th – 16th January 2011, *University of Witwatersrand*.

Wood, S.A. (2002). The aqueous geochemistry of the platinum–group elements with applications to ore deposits. In: Cabri LJ (ed) The Geology, Geochemistry, Mineralogy and Mineral Beneficiation of Platinum–Group Elements, *Canadian Institute of Mining, Metallurgy and Petroleum*, Special vol. 54, pp. 211-249.

Yudovskaya, M.A. & Kinnaird, J.A., 2010. Chromite in the Platreef (Bushveld Complex, South Africa): occurrence and evolution of its chemical composition, *Mineralium Deposita*, vol. 45 (4), pp. 369-391.

Yudovskaya, M.A., Kinnaird, J.A., Naldrett, A.J., Mokhov, A.V., McDonald, I. & Reinke, C. (2011). Facies variation in PGE mineralisation in the Central Platreef of the Bushveld Complex, South Africa, *The Canadian Mineralogist*, vol. 49, pp. 1349-1384.

Yudovskaya, M.A., Kinnard, J.A., Sobolev, A.V., Kuzmin, D.V., McDonald, I. & Wilson, A.H. (2013). Petrogenesis of the Lower Zone Olivine-Rich Cumulates beneath the Platreef and their correlation with recognized occurrences in the Bushveld Complex: *Economic Geology*, vol. 108, pp. 1923-1952.

APPENDICES

APPENDIX I

Modal compositions of the Platreef rocks from X-Ray Diffraction (XRD) analysis

Sample	Petrology	Clinopyroxene	Orthopyroxene	Plagioclase	Olivine	Serpentine	Amphibole	Chlorite	Quartz
ZF044-19	Norite	20	22	50	-	-	3	3	tc
ZF044-25	FP III	15	36	49	-	-	-	-	-
ZF044-26	FP III	16	26	58	-	-	-	-	-
ZF044-34	FP I	49	5	-	18	23	5	-	-
ZF044-36	FP II	21	35	42	-	tc	-	-	-
ZF044-45	FP I	43	32	23	-	tc	-	-	tc
ZF048-40	FP II	30	30	38	-	-	-	tc	2
ZF048-41	Norite	13	44	41	-	-	-	2	-
ZF048-42	FP II	29	25	33	-	-	10	3	-
ZF048-46	FP II	31	25	31	-	-	10	4	-
ZF057-28	Harzburgite	32	30	-	-	36	2	-	-
ZF057-31	Harzburgite	32	29	32	-	3	2	2	-
ZF057-34	FP II	31	25	43	-	-	tc	tc	-
ZF057-38	FP II	30	27	43	-	-	-	-	-
ZF057-43	FP II	31	27	42	-	-	tc	-	-

APPENDIX II

Whole-rock geochemical data for the Platreef rocks

Summary of the procedure followed during bulk chemistry analysis by XRF for major and trace elements.

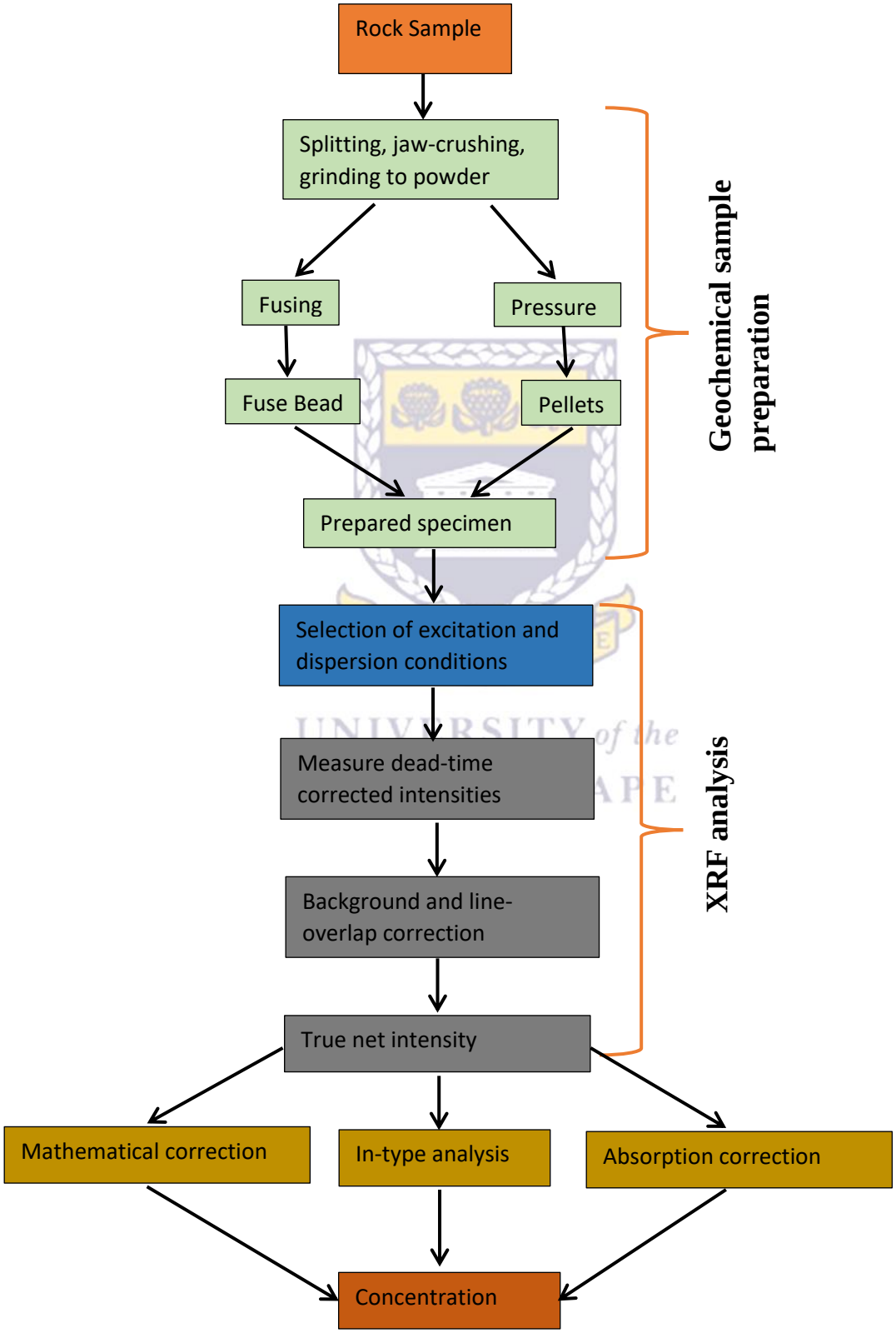

Major elements

Sampled ID	From	To	Petrology	Farm	SiO2	Al2O3	Fe2O3	MnO	MgO	Mg#	CaO	Na2O	K2O	TiO2	P2O5	LOI
ZF044-19	740.21	740.32	Norite	Zwartfontein	49.3	15.85	8.65	0.185	10.6	68.59	13.34	1.09	0.06	0.16	0.022	0.53
ZF044-25	1139.65	1139.79	FP III	Zwartfontein	51.63	12.32	9.45	0.167	17.36	76.60	7.59	0.91	0.13	0.15	0.025	-0.17
ZF044-26	1146.98	1147.21	FP III	Zwartfontein	51.89	11.67	9.42	0.175	18.23	77.52	7.2	0.79	0.14	0.16	0.027	-0.16
ZF044-34	1184.58	1184.3	FP I	Zwartfontein	43.48	2.54	13.97	0.309	24.62	75.84	11.11	<0.01	0.06	0.1	0.024	3.4
ZF044-36	1186.58	1186.76	FP II	Zwartfontein	52.04	5.2	12.84	0.243	21.77	75.13	6.21	0.32	0.09	0.16	0.027	0.38
ZF044-45	1228.14	1228.33	FP I	Zwartfontein	49.24	4.84	14.04	0.3	14.02	64.02	15.09	0.62	0.14	0.29	0.028	0.89
ZF048-40	1425.39	1425.58	FP II	Zwartfontein	52.52	7.21	11.43	0.199	22.43	77.76	4.96	0.32	0.06	0.17	0.04	0.25
ZF048-41	1431.11	1431.33	Norite	Zwartfontein	50.36	19.58	5.82	0.107	11.77	78.28	10.68	1.29	0.17	0.1	0.028	-0.62
ZF048-42	1462.36	1462.62	FP II	Zwartfontein	51.26	6.35	11.87	0.221	22.5	77.15	5.44	0.12	0.18	0.11	0.021	1.36
ZF048-46	1524.58	1524.8	FP II	Zwartfontein	51.92	6.09	10.64	0.204	24.1	80.14	4.48	0.15	0.15	0.11	0.024	1.56
ZF048-52	1564.32	1564.52	Harzburgite	Zwartfontein	31.827	1.584	18.709	0.121	36.078	77.46	1.281	0.003	0.048	0.084	0.011	10.079
ZF057-28	1280.47	1280.66	Harzburgite	Zwartfontein	43.82	1.79	13.54	0.164	34.48	81.94	1.25	<0.01	0.18	0.05	0.021	4.5
ZF057-31	1303.28	1303.46	Harzburgite	Zwartfontein	48.42	7.25	11.27	0.179	25.83	80.33	3.93	<0.01	0.5	0.14	0.029	2.19
ZF057-34	1324.13	1324.3	FP II	Zwartfontein	52.34	6.02	11.46	0.221	22.57	77.82	6.34	0.29	0.07	0.14	0.025	-0.04
ZF057-38	1355.24	1355.43	FP II	Zwartfontein	51.99	7.03	11.92	0.214	21.22	76.03	5.87	0.52	0.1	0.15	0.024	0.48
ZF057-43	1410.55	1410.76	FP II	Zwartfontein	53.27	4.8	12.59	0.215	23.94	77.21	4.11	0.35	0.18	0.29	0.057	-0.36
ZF057-46	1444.05	1444.22	FP II	Zwartfontein	46.659	9.382	12.012	0.220	20.034	74.82	7.141	1.050	0.220	0.170	0.020	2.991
ZF057-51	1492.17	1492.29	Norite	Zwartfontein	50.010	16.927	10.294	0.170	6.513	52.99	11.215	2.531	0.490	0.210	0.030	1.591

Trace and Rare earth elements

Sample ID	Petrology	Li	Sc	V	Cr	Co	Ni	Cu	Zn	Rb	Sr	Y	Zr	Nb	Ba	La	Ce	Pr	Nd	Sm	Eu	Tb	Gd	Dy	Ho	Er	Tm	Yb	Lu	Hf	Ta	Pb	Th	U
ZF044-25	FP III	5,627	22,81	129,8	1529	64,88	436,8	51,35	65,73	2,75	130,9	4,73	6,41	0,11	49,11	2,73	5,02	0,57	2,16	0,49	0,33	0,11	0,61	0,76	0,17	0,55	0,09	0,62	0,10	0,21	0,02	1,36	0,11	0,03
ZF044-26	FP III	9,402	23,25	133,8	1457	70	438,6	21	76,26	3,22	108,2	4,42	8,97	0,34	49,21	2,97	5,51	0,63	2,34	0,52	0,27	0,11	0,66	0,74	0,16	0,51	0,08	0,54	0,10	0,27	0,03	0,99	0,28	0,08
ZF044-34	FP I	3,651	29,48	118,3	2313	86,57	796,4	206,1	87,65	5,00	19,00	3,69	6,15	0,27	16,19	1,10	2,36	0,31	1,27	0,34	0,15	0,09	0,51	0,63	0,14	0,43	0,07	0,48	0,08	0,21	0,04	1,47	0,21	0,06
ZF044-36	FP II	3,538	33,62	144,7	2753	88,30	608	57,87	88,48	4,53	56,10	5,36	9,23	0,36	19,73	1,98	3,83	0,47	1,91	0,51	0,19	0,13	0,73	0,91	0,19	0,62	0,10	0,69	0,12	0,30	0,03	1,58	0,32	0,24
ZF044-45	FP I	10,51	41,28	200,9	1252	111,9	3724	1948	75,64	5,42	64,50	15,51	18,85	0,31	43	3,88	11,09	1,69	7,65	2,15	0,52	0,45	2,69	2,98	0,61	1,76	0,25	1,66	0,26	0,76	0,18	8,79	0,25	0,14
ZF048-40	FP II	4,897	28,73	132,1	1745	92,20	1204	451,5	76,31	2,72	56,71	5,09	14,86	0,59	16,15	3,31	6,01	0,68	2,50	0,54	0,19	0,13	0,75	0,87	0,19	0,61	0,10	0,67	0,11	0,42	0,05	2,19	0,73	0,20
ZF048-41	Norite	4,311	15,29	74,25	837	42	396,9	88,13	40,28	4,81	178,7	2,90	7,77	0,36	46,65	2,42	4,45	0,49	1,75	0,35	0,27	0,08	0,48	0,51	0,11	0,33	0,05	0,34	0,06	0,22	0,04	1,67	0,35	0,08
ZF048-46	FP II	10,90	26,01	113,7	2553	83,55	665,1	37,95	72,17	9,02	53,77	2,98	6,04	0,19	24,34	1,25	2,45	0,29	1,08	0,26	0,13	0,07	0,35	0,47	0,11	0,36	0,06	0,40	0,07	0,19	0,02	1,40	0,20	0,07
ZF057-28	Harzburgie	3,617	14,11	51,24	1289	154,7	1623	212,5	75,26	18,69	8,86	1,28	2,69	0,10	28,38	0,46	1,01	0,13	0,49	0,12	0,05	0,03	0,16	0,20	0,05	0,16	0,03	0,19	0,04	0,08	0,02	3,28	0,11	0,05
ZF057-31	Harzburgie	7,142	16,42	187,3	921	114,9	2191	758,3	87,47	32,58	64,97	2,37	7,60	0,16	47,84	1,12	1,88	0,20	0,74	0,17	0,14	0,05	0,27	0,37	0,09	0,29	0,05	0,34	0,06	0,28	0,02	9,73	0,12	0,04
ZF057-34	FP II	3,651	29,48	118,3	2313	86,57	796,4	206,1	87,65	1,91	62,75	3,69	6,15	0,27	16,19	1,10	2,36	0,31	1,27	0,34	0,15	0,09	0,51	0,63	0,14	0,43	0,07	0,48	0,08	0,21	0,04	1,47	0,22	0,06
ZF057-34	FP II	4,021	28,18	121,3	2073	83,77	674,1	98,41	83,75	4,15	100,5	4,52	5,93	0,27	25,39	1,40	2,88	0,31	1,47	0,34	0,25	0,19	0,51	0,73	0,14	0,53	0,07	0,58	0,18	0,21	0,04	1,08	0,22	0,06
ZF057-38	FP II	4,023	28,10	121,2	2070	83,72	674,1	98,48	83,74	4,15	100,8	4,52	5,93	0,22	25,38	1,43	2,88	0,36	1,48	0,39	0,21	0,11	0,59	0,74	0,17	0,53	0,08	0,59	0,10	0,21	0,04	1,08	0,22	0,07
ZF057-51	Norite		30,165	172,3	315	41,28	148,945	59,345	64,38	9,89	129,21	12,54	19,36	1,65	145,41	4.74	9,87	1,30	5,54	1,53	0,53	0,35	2,09	2,22	0,49	1,52	0,21	1,65	0,22	0,71	0,13	28,80	0,73	0,92

APPENDIX III

Normalised trace elements concentration data for the studied Platreef rocks from GCDkit

Sample ID	LaN	CeN	PrN	NdN	SmN	EuN	GdN	TbN	DyN	HoN	ErN	TmN	YbN	LuN	Eu/Eu	LaN/YbN	LaN/SmN	CeN/YbN	CeN/SmN	EuN/YbN	Sum_REE
ZF044-25	4.216	2.998	2.268	1.73	1.197	2.169	1.125	1.091	1.122	1.141	1.251	1.265	1.395	1.515	1.869	3.023	3.522	2.15	2.504	1.555	14.31
ZF044-26	4.586	3.288	2.465	1.87	1.271	1.734	1.206	1.111	1.104	1.081	1.153	1.147	1.227	1.309	1.4	3.739	3.609	2.68	2.587	1.413	15.109
ZF044-34	1.674	1.411	1.213	1.017	0.84	0.948	0.936	0.909	0.933	0.926	0.984	0.985	1.082	1.191	1.069	1.548	1.994	1.305	1.68	0.877	7.937
ZF044-36	3.054	2.285	1.866	1.531	1.249	1.26	1.338	1.313	1.349	1.329	1.425	1.426	1.565	1.706	0.974	1.952	2.446	1.461	1.83	0.805	12.388
ZF044-45	5.983	6.621	6.673	6.122	5.293	3.351	4.96	4.586	4.417	4.06	4.023	3.721	3.755	3.779	0.654	1.593	1.13	1.763	1.251	0.892	37.642
ZF048-40	5.106	3.59	2.677	2.002	1.33	1.227	1.373	1.283	1.297	1.289	1.397	1.397	1.512	1.618	0.908	3.376	3.839	2.373	2.699	0.811	16.658
ZF048-41	3.728	2.657	1.933	1.397	0.855	1.753	0.886	0.788	0.763	0.738	0.763	0.735	0.773	0.809	2.015	4.822	4.362	3.437	3.109	2.267	11.685
ZF048-46	1.927	1.46	1.122	0.865	0.65	0.851	0.651	0.657	0.697	0.718	0.811	0.838	0.914	1.029	1.308	2.109	2.964	1.597	2.245	0.931	7.336
ZF057-28	0.711	0.6	0.496	0.389	0.3	0.318	0.285	0.283	0.3	0.309	0.358	0.382	0.44	0.515	1.087	1.617	2.368	1.364	1.997	0.723	3.092
ZF057-31	1.733	1.12	0.795	0.59	0.421	0.922	0.502	0.515	0.552	0.577	0.662	0.676	0.766	0.853	2.006	2.261	4.115	1.461	2.659	1.203	5.765
ZF057-34	1.674	1.411	1.213	1.017	0.84	0.948	0.936	0.909	0.933	0.926	0.984	0.985	1.082	1.191	1.069	1.548	1.994	1.305	1.68	0.877	7.937
ZF057-38	2.205	1.718	1.413	1.186	0.958	1.344	1.092	1.081	1.101	1.107	1.208	1.206	1.336	1.441	1.314	1.651	2.302	1.286	1.793	1.006	9.65
ZF057-51		5.89	5.134	4.432	3.756	3.425	3.833	3.5	3.294	3.299	3.47	3.096	3.741	3.265	0.903			1.574	1.568	0.915	27.507

APPENDIX IV

Platinum group elements (Pt+Pd) and base metal sulfides (BMS) data for the Platreef rocks at Zwartfontein measured in ppb

BOREHOLE ZF044

Borehole	Sample ID	Depth from (m)	Depth to (m)	Lithology	SO3	Cu	Ni	Cu+Ni	Au	Pd	Pt	Pd+Pt	Pt/Pd	Co	Zn	Cu/Zn	Ni/Co	PGE index
ZF044	32	1176.2	1183.38	FP I	0.64	3838.68	7715.32	11554.00	117.00	6317.00	1457.00	7774.00	0.231	237.37	102.95	37.29	32.50	1211.99
ZF044	34	1183.38	1194.45	FP I	0.47	405.92	459.21	865.13	12.00	129.00	141.00	270.00	1.093	54.02	101.51	4.00	8.50	33.99
ZF044	39	1194.45	1221.58	FP I	0.03	357.72	1398.89	1756.60	33.00	325.00	280.00	605.00	0.862	102.12	101.79	3.51	13.70	48.14
ZF044	43	1221.58	1242.7	Harzburgite	0.33	671.02	1018.70	1689.72	129.00	526.00	384.00	910.00	0.730	67.92	76.81	8.74	15.00	131.02
ZF044	47	1242.7	1268.18	FP II	0.08	419.64	672.12	1091.76	47.00	361.00	316.00	677.00	0.875	59.50	72.97	5.75	11.30	64.96
ZF044	51	1268.18	1281.6	FP II	0.06	353.93	955.87	1309.80	73.00	153.00	109.00	262.00	0.712	79.89	117.26	3.02	11.96	36.11
ZF044	53	1281.6	1309.6	FP I	0.46	1440.62	3852.07	5292.69	293.00	3314.00	2319.00	5633.00	0.700	67.67	68.74	20.96	56.93	1192.99
ZF044	55	1309.6	1327.35	Chromitite	0.14	611.59	805.40	1416.98	32.00	962.00	917.00	1879.00	0.953	99.92	265.52	2.30	8.06	18.57
ZF044	57	1327.35	1334.48	FP I	0.63	368.03	363.99	732.02	<5	16.00	5.00	21.00	0.313	26.91	74.99	4.91	13.53	66.38
ZF044	58	1334.48	1350	FP I	1.13	1123.05	1789.17	2912.22	45.00	276.00	114.00	390.00	0.413	84.67	43.57	25.78	21.13	544.71

BOREHOLE ZF048

Borehole	Sample ID	Depth from (m)	Depth to (m)	Lithology	SO3	Cu	Ni	Cu+Ni	Au	Pd	Pt	Pd+Pt	Pt/Pd	Co	Zn	Cu/Zn	Ni/Co	PGE index
ZF048	39	1416.53	1507.18	FP II	0.52	1891.46	4946.71	6838.17	129.42	2535.89	970.68	3506.57	0.38	154.86	117.36	16.12	31.94	514.82
ZF048	44	1507.18	1513.50	FP I	1.82	1697.91	561.66	2259.57	5.00	16.03	5.00	21.03	0.31	62.73	136.38	12.45	8.95	111.48
ZF048	45	1513.50	1524.58	FP II	0.10	3882.67	986.03	4868.70	36.47	113.48	628.17	741.64	5.54	95.86	144.94	26.79	10.29	275.55
ZF048	46	1524.58	1532.14	FP II	0.10	3117.20	780.70	3897.89	5.00	12.11	121.09	133.20	10.00	89.12	116.98	26.65	8.76	233.44
ZF048	47	1532.14	1544.32	FP II	0.23	2549.10	3615.45	6164.55	104.73	672.71	467.27	1139.98	0.69	136.94	113.90	22.38	26.40	590.90
ZF048	48	1544.32	1552.80	FP II	0.33	3640.92	1798.82	5439.74	36.29	209.68	181.45	391.13	0.87	121.13	153.30	23.75	14.85	352.70
ZF048	49	1552.80	1562.63	Harzburgite	0.15	448.95	1988.44	2437.39	12.05	128.51	180.72	309.24	1.41	178.92	77.97	5.76	11.11	64.00
ZF048	51	1562.63	1564.32	Pegmatite	0.00	494.60	402.56	897.16	5.00	32.13	8.03	40.16	0.25	35.79	28.58	17.31	11.25	194.66
ZF048	52	1564.32	1570.52	Harzburgite	0.18	987.47	2011.98	2999.45	245.23	1993.97	1230.15	3224.12	0.62	171.07	34.82	28.36	11.76	333.51

BOREHOLE ZF057

Sample ID	Depth from (m)	Depth to (m)	Petrology	SO3	Cu	Ni	Cu+Ni	Au	Pd	Pt	Pd+Pt	Pt/Pd	Co	Zn	Cu/Zn	Ni/Co	PGE index
29	1283.15	1291.08	FP II	0.06	2717.64	4986.34	7703.98	355.56	2000.00	1874.75	3874.75	0.94	216.52	155.60	17.47	23.03	402.22
30	1291.08	1316.115	FP I	0.81	2950.98	4212.57	7163.55	328.99	1673.02	1155.47	2828.49	0.69	187.80	145.80	20.24	22.43	454.00
33	1316.115	1343.13	FP II	0.01	179.91	285.78	465.69	<5	5.00	5.00	10.00	1.00	61.25	331.82	0.54	4.67	2.53
36	1343.13	1391.66	FP II	0.00	137.57	638.52	776.09	<5	5.00	10.00	15.00	2.00	83.23	119.86	1.15	7.67	8.81
40	1391.66	1427.43	Harzburgite	0.19	552.15	914.58	1466.73	15.90	71.57	71.57	143.14	1.00	73.16	74.60	7.40	12.50	92.53
44	1427.43	1444.05	FP II	0.02	267.05	706.45	973.50	12.12	40.40	80.81	121.21	2.00	74.43	149.84	1.78	9.49	16.92
46	1444.05	1458.77	FP II	0.10	518.84	1192.13	1710.97	186.61	1691.68	2259.63	3951.32	1.34	72.65	165.50	3.13	16.41	51.44
47	1458.77	1474.74	Harzburgite	0.06	138.18	141.76	279.94	<5	12.22	12.22	24.44	1.00	38.86	147.34	0.94	3.65	3.42
50	1474.74	1492.17	FP I	0.02	120.27	183.11	303.38	<5	5.00	5.00	10.00	1.00	44.73	104.77	1.15	4.09	4.70
51	1492.17	1499.29	FP I	0.02	154.12	158.22	312.34	<5	8.13	16.26	24.39	2.00	32.18	138.02	1.12	4.92	5.49

APPENDIX V

Strontium (Sr) and Neodymium (Nd) isotope data for the Platreef rocks at Zwartfontein.

Sample ID	Petrology	Rb (ppm)	Sr (ppm)	Nd (ppm)	Sm (ppm)	87Sr/86Sr	(87Sr/86Sr)i	143Nd/144Nd	(143Nd/144Nd)i	εNd
ZF044-25	FP III	2,753	130,9	2,163	0,486	0.710909	0.709101	0.511460	0.509618	-6.91
ZF044-26	FP III	3,224	108,2	2,337	0,516	0.710831	0.708271	0.511452	0.509642	-6.43
ZF044-34	FP I	5,00	19,00	1,271	0,341	0.723661	0.701017	0.512107	0.509907	-1.23
ZF044-36	FP II	4,525	56,10	1,914	0,507	0.715709	0.708773	0.511848	0.509677	-5.75
ZF044-45	FP I	5,418	64,50	7,653	2,149	0.719137	0.711912	0.511918	0.509616	-6.94
ZF048-40	FP II	2,721	56,71	2,503	0,540	0.711993	0.707869	0.511379	0.509611	-7.05
ZF048-41	Norite	4,812	178,7	1,746	0,347	0.710961	0.708646	0.511249	0.509619	-6.88
ZF048-46	FP II	9,018	53,77	1,081	0,264	0.722180	0.707750	0.511578	0.509576	-7.73
ZF057-28	Harzburgie	18,69	8,861	0,486	0,122	0.881729	0.697427	0.511638	0.509580	-7.64
ZF057-31	Harzburgie	32,58	64,97	0,737	0,171	0.742560	0.699330	0.511438	0.509536	-8.51
ZF057-34	FP II	1,906	62,75	1,271	0,341	0.711829	0.709218	0.511866	0.509666	-5.96
ZF057-38	FP II	4,152	100,8	1,483	0,389	0.709929	0.706389	0.511875	0.509725	-4.81
ZF057-51	Norite	9,885	129,205	5,54	1,525	0.716290	0.709712	0.511852	0.509595	-7.35

i = Initial ($^{87}Sr/^{86}Sr$) and ($^{143}Nd/^{144}Nd$) were calculated at 2060 Ma

m = measured

Crystallisation age calculations:

In order to determine the age of the rocks, the slope of the isochron is calculated using a gradient formula and the coordinates are taken from two points that plots on the isochron. The coordinates of sample ZF057-46 (0.5; 0.722690) and ZF057-28 (7.8; 0881729) were used to calculate the slope as shown below.

$$m = \frac{\Delta\, 87Sr/86Sr}{\Delta 87Rb/86Sr}$$

$$= \frac{0.881729 - 0.722690}{7.8 - 0.5}$$

$$= 0.0218$$

The slope of the isochron and the constant value of $1.42*10^{-11}$ are substituted in equation 1.

$$t = \frac{1In\,(m+1)}{\lambda}$$

$$= \frac{1In\,(0.0218+1)}{1.42*10-11}$$

$$= 1.5 \text{ Ga}$$